UNIVERSITY OF CALIFORNIA
RIVERSIDE

Transcriptomic Profiling of *Arabidopsis* Abscisic Acid Sensitivity and Receptor Function

A Dissertation submitted in partial satisfaction
of the requirements for the degree of

Doctor of Philosophy

in

Plant Biology

by

Zenan Xing

March 2023

Dissertation Committee:
Dr. Sean Cutler, Chairperson
Dr. David Nelson
Dr. Thomas Girke

The Dissertation of Zenan Xing is approved:

_____

_____

_____

Committee Chairperson

University of California, Riverside

Acknowledgements

Foremost, I would like to express my sincere gratitude to my supervisor, Dr. Sean Cutler for his continuous support and guidance in my Ph.D. study and research. He has been a patient, motivated, enthusiastic researcher with immense knowledge.

I am really grateful to the other two members of the dissertation committee, Dr. David Nelson and Dr. Thomas Girke, for their encouragement and great insights and perspectives during this long journey.

I would also like to thank the members of my qualifying exam, Dr. Thomas Eulgem, Dr. Yanran Li, Dr. David Nelson, Dr. Patricia Springer, and Dr. Jikui Song for their encouragement and insightful comments. And I'd also like to appreciate the help and guidance from the professors in my guidance committee, Dr. Sean Cutler, Dr. Xuemei Chen, and Dr. Linda Walling.

I also want to thank all the lab mates past and present in our lab, they have helped me a lot through this journey toward my Ph.D. I want to sincerely thank Sang-youl Park, Aditya Vaidya, Dezi Elzinga, and James Eckhardt for their help and guidance in my work. Sang, Adi, and Dezi taught me almost all the techniques in the lab. Sang generated all the mutants and their corresponding complementation lines for my work, and James helped me a lot in the seedling establishment experiments. And also, many thanks to other members for always being there to discuss data and provide ideas for my research.

I also want to thank all my friends. I'd like to thank Yan Zhu, she has been a wonderful friend since we were in high school. I also want to thank my friends in college, Wei Li, Dan Zhang, and others who supported me and comfort me during this time. I also want to thank my friends here in Riverside. Han Qu for her accompany and encouragement since we

met in the orientation. I would also like to thank Ye Xu, Lusheng Fan, Baoye He, Kristina, and Jianqiang Wang for their help and support.

Last but not least, I would like to thank my family, especially my beloved parents, Xueqin Li and Han Xing for their endless and unconditional support and love in my whole life.

Dedication

To my beloved parents, Xueqin Li and Han Xing

ABSTRACT OF THE DISSERTATION

Transcriptomic Profiling of *Arabidopsis* Abscisic Acid Sensitivity and Receptor Function

by

Zenan Xing

Doctor of Philosophy, Graduate Program in Plant Biology
University of California, Riverside, March 2023
Dr. Sean Cutler, Chairperson

As a major phytohormone, abscisic acid (ABA) regulates responses to abiotic and biotic stress, transpiration, seed dormancy and germination, root growth, and many other aspects of plant physiology and development. ABA levels in plants vary by two orders of magnitude, and several processes, such as root growth inhibition and root architecture, show dose-dependent responses to ABA. ABA plays a major role in transcriptional response to abiotic stress. More than 10% of *Arabidopsis* genes respond to the relatively high levels of ABA produced by *de novo* biosynthesis triggered by water stress or other factors. Although ABA transcriptional responses have been extensively characterized over the past few decades, very few studies have examined ABA responses using dose-response curves, which are valuable tools that allow one to infer a gene's sensitivity to ABA. In my thesis, I used transcriptomic analyses to systematically characterize ABA dose-dependent responses and develop transcriptional markers for ABA sensitivity. To do this, I analyzed the transcriptional responses of wild-type *Arabidopsis* (Col-0) seedlings treated with ABA concentrations spanning five orders of magnitude (low nanomolar to high micromolar). This analysis identified a set of 5749 ABA-responsive genes that I grouped

into 9 clusters according to their dose-dependent response profiles. I additionally defined ABA-response sensitivity for most ABA-responsive genes by inferring ED_{50}s (effective dose for 50% response) and BMDs (benchmark dose). My clustering analyses binned most genes into simple monotonic up- or down-regulated responses characterized by low, medium, or high-sensitivity sigmoidal-shaped response curves. Unexpectedly, approximately 20% (1097/5749) of ABA-responsive genes show atypical biphasic dose responses; they have bell- or U-shaped dose-response curves that suggest the genes are tuned to specific concentrations for their maximal responses. Analyses of the 9 clusters using gene ontology methods suggest functional enrichments for our different clusters. For example, many genes classified as participating in water response (e.g., aquaporins, mainly *PIP*s) are enriched in the bell-shaped subset, and genes involved in ribosomal RNA biogenesis are U-shaped genes.

My genome-wide insights into ABA sensitivity provide a new set of tools to study ABA signaling, responses, and sensitivity. I have used this to examine the roles of different ABA receptors in mediating dose-dependent responses. ABA signaling is mediated by a core signaling module consisting of three major players, ABA receptors (PYR/PYL/RCARs), clade A PP2Cs (protein phosphatase 2C), and SnRK2s (SNF1-related protein kinase type 2). In *Arabidopsis*, ABA receptors are encoded by 14 genes classified into three subfamilies that differ in their oligomeric states and affinities for ABA. The dimeric receptors subfamily III, which includes the genes PYR1 and PYLs1 - 3, have a lower affinity for ABA than the other two subfamilies, which are monomeric. To connect my sensitivity analyses to receptor function, I characterized three *pyl* mutant strains that remove each receptor subfamily. I carried out an RNA-seq analysis on the dose-dependent transcriptional response of these three mutant strains compared to the wild

type. My analyses show that the genetic removal of subfamily III receptors has the largest effect on ABA-regulated gene expression. The number of DEGs in subfamily III mutants (*subIII*) was the largest in all the clusters identified in Chapter 1, and most of them possessed medium sensitivity to ABA. And the GO enrichment analysis also showed that more unique terms were enriched among DEGs identified in *subIII*, such as cell wall biogenesis, lateral root growth, and stomata closure. Our results also show that genes with lower sensitivity to ABA are preferentially affected in *subIII*, which is in line with their lower affinity for ABA. Thus, the molecular basis for ABA's wide dose-response range is likely due, in part, to differences in receptor affinities for ABA.

Lastly, to create a more comprehensive understanding of the role of ABA signaling in osmotic stress, a classic ABA-mediated abiotic stress response, I used an antagonist of ABA receptor function (antabactin, or ANT) to block ABA signaling during osmotic stress caused by PEG treatment. Prior work has shown that the osmotic stress response can be partitioned into an ABA-dependent and ABA-independent set of transcriptional responses based on characterizing each gene's response to exogenous ABA. Unexpectedly, my analyses show that this distinction is an artifact of how ABA-responsive genes were previously defined because the use of ANT demonstrates that the large set of "ABA-independent" genes requires ABA signaling for normal osmotic stress responses. Instead of classifying the osmotic-stress responders into two distinct groups, I quantitatively defined the ABA dependency of genes under osmotic stress by their response to ANT during osmotic stress using a **π**-value, a product of log-fold change and log-transformed *p*-value. The **π**-value increases as the reduced effect of ANT on osmotic-stress responses became stronger. Using *cis*-element motif analyses, my results show a correlation

between ABA dependency and *cis*-elements; as the ABA dependency increases, the more significant ABA-related motifs are enriched in the promoter regions of those genes.

Collectively, my studies have (i) illuminated the complexities of the ABA signaling network, (ii) defined a robust set of genes that respond to exogenous ABA, (iii) delivered transcriptional markers for characterizing ABA sensitivity, (iv) uncovered a large set of genes with unexpected, atypical dose-response curves, (v) shown that defining ABA transcriptional responses by exogenous ABA is problematic, illustrating the value of pharmacological, and (vi) demonstrated that differences in ABA receptor affinity underpin part of the large range over which ABA exerts its effects.

Table of Contents

List of Figures

Chapter 1

Chapter 2

Chapter 3

Appendices

List of Tables

Chapter 1

Chapter 1 Transcriptomic Analyses of *Arabidopsis* Seedling ABA Sensitivity

Abstract

Abscisic acid (ABA) is an essential phytohormone that participates in broad aspects of the plant's life and mediates both developmental processes and responses to environmental stresses. To characterize ABA dose-dependent responses, we conducted an RNA-seq experiment on the wildtype Col-0 seedlings treated with a serial concentration of ABA. A robust set of ABA-responsive genes were identified. We also modified a previously published method that enabled the estimation of ED_{50} (Effective Dose 50) and BMD (Benchmark Dose) from the DRCs (dose-response curves) to illustrate the sensitivity of the ABA responders and made it possible to get a broad view of the ABA sensitivity genome-wide. The ABA-responsive genes can be classified into 9 clusters by their trends and sensitivity based on their DRCs. Most ABA-responsive genes showed a typical monotonic up or down dose-dependent response, while we also discovered a large number of genes, approximately 20%, exhibited an unexpected biphasic dose-response pattern. Further functional analysis showed they participate in different signaling pathways.

Introduction

As a major phytohormone, ABA (abscisic acid) plays a crucial role in the regulation of many physiological processes of plants, including inhibition of root length growth, seed germination, dormancy, flowering, and plant senescence (Park et al., 2009; Wan et al., 2017; Ye et al., 2017). ABA is also involved in response to a variety of abiotic and biotic

stresses, such as pathogen response, drought, salinity, and extreme temperature, which can impair the productivity of almost all the major crops and constitute the primary cause of crop loss worldwide (Wang et al., 2003; Santiago et al., 2009; de Zelicourt et al., 2016). For instance, ABA can maintain water conservation by reducing water transpiration by mediating stomatal closure during drought (Gonzalez-Guzman et al., 2012; Helander et al., 2016).

Since ABA participates in such broad aspects of plant development and deals with stress responses, ABA levels in plants vary by two orders of magnitude in plants, ranging from low nanomolar to low micromolar (Finkelstein, 2013). Research conducted by De Smet showed a dosage effect of ABA on the development of root architecture and seed dormancy. It turns out that 1 μM of ABA was sufficient to cause a reduction of visible lateral roots, but primary root growth was not affected until 10 μM (De Smet et al., 2003). This result indicates the difference in ABA sensitivity between lateral roots and primary roots, and this implies that there are mechanisms that differentially regulate different facets of ABA signaling in response to varying concentrations. There has been a debate on whether plant development is regulated by changes in the concentration or the sensitivity of phytohormones since a long time ago (Trewavas and Cleland, 1983), while there is still no solid conclusion on that subject.

The diversity of the physiological and environmental responses to ABA also indicated that the ABA signaling might have potential crosstalks with other signaling pathways in the plants. The evidence began to accumulate that some of the ABA-mediated biological processes were also influenced by the antagonistic or synergistic action of other hormones, such as gibberellin (GA), salicylic acid (SA), ethylene (ET), and jasmonic acid

(JA). The antagonistic role of ABA and GA in regulating seed dormancy and germination has been well-studied (Liu and Hou, 2018). And it has been well established that there was a crosstalk between ABA signaling and ET, JA, and SA during immune responses (Adie et al., 2007; García-Andrade et al., 2020). However, the complexity of the ABA signaling network implies there are still many fundamental mechanisms that remain to be investigated.

It has been shown that up to 10% of the genome can be regulated by ABA in various contexts (Finkelstein, 2013). This relays on the core ABA-signaling pathway, which has been studied in the past decades. This core module contains three major players: the ABA receptors, i.e., Pyrabactin Resistance/Pyrabactin resistance-like/Regulatory Component of ABA Receptor (PYR/PYL/RCAR); Protein Phosphatase 2C (PP2C) group A family; and Sucrose non-fermenting 1 (SNF1)-Related Protein Kinases type 2 (SnRK2s) (Fujii et al., 2009; Park et al., 2009). Without ABA, the activity of SnRK2s is repressed by PP2Cs, preventing the SnRK2 protein kinases from phosphorylating their downstream targets, such as the basic leucine zipper (bZIP) transcription factors called ABFs, which bind to ABA-responsive promoter elements (ABRE) (Fujii et al., 2009). In the presence of ABA, PYR/PYL/RCAR receptors undergo a conformational change that allows their binding to the catalytic site of PP2C, which in turn abolishes the activity of PP2Cs via a gate-latch-lock mechanism (Melcher et al., 2009; Cutler et al., 2010). Subsequently, the inhibition of PP2Cs leads to SnRK2 autophosphorylation and activation, which phosphorylate and activate downstream effectors such as ABFs (Boudsocq et al., 2007). These transcription factors can induce the expression of the genes directly involved in stress response, such as *RD29A/B* and *RAB18*, to promote resistance to stresses in the plants (Lång and Palva, 1992; Yamaguchi-Shinozaki and Shinozaki, 1994). All these players in the ABA signaling

are considered ABA-responsive genes, and the up-regulation of these genes is a classic paradigm of ABA-dependent regulation in numerous previous studies (Zhu, 2002; Fujii et al., 2009; Ma et al., 2009; Park et al., 2009; Santiago et al., 2009). While the down-regulated genes in ABA signaling are rarely used as marker genes to imply the involvement of ABA signaling in other biological processes.

To investigate the comprehensive network of ABA signaling pathways, a lot of research has been conducted to identify the ABA-responsive genes on a genome-wide scale. The experiments were usually conducted with other treatments to study the cross-talk between ABA signaling and other pathways. Jing-Ke conducted RNA-seq experiments with ABA and two other ABA catabolites to study the putative hormonal activity of ABA catabolites and identified 4441 ABA-regulated genes (Weng et al., 2016). In another study, transcriptome sequencing was also performed to investigate the drought response regulated by ABA-dependent or independent pathways, and 537 genes were considered significant ABA-responsive genes (Liu et al., 2018). However, only one concentration of ABA was used in the previous studies, which makes it hard to explore the sensitivity of each gene to ABA.

In my study, I conducted an RNA-seq experiment for the wildtype *Arabidopsis* Col-0 treated with different concentrations of ABA ranging from low nanomolar to high micromolar. A set of ABA-responsive genes were defined. Different dose-response trends were observed in our study, and the profiles of the genes' sensitivity to ABA were also provided. This study provides a more comprehensive and systematic view of ABA signaling in *Arabidopsis.*

Methods and Materials

Plant Materials and Treatment

The seeds of *Arabidopsis* thaliana wild-type (Col-0) were sterilized with 70% ethanol and 0.05% Triton X-100 for 7 minutes, followed by 70% ethanol for another 7 minutes, and then washed with 100% ethanol for one time, and another wash with sterile distilled water for three times. The sterilized seeds were sown on the top of a square nylon mesh (1.5 inches * 1.5 inches, 100 μm mesh) on a the ½ Murashige-Skoog (MS) medium (0.25% sucrose and 1% agar, pH 5.7) before kept at 4 ℃ for four days, and then grown vertically as previously described (Bargmann and Birnbaum, 2010) under 16h/8h light/dark at 22 ℃ for 6 days before the treatments.

The nylon meshes carrying the seedlings were treated on 2 layers of filter paper soaked with 6 mL of ½ MS liquid medium (0.25% sucrose, pH 5.7) supplemented with either DMSO control or different concentrations of ABA for 10 hours. The ABA was first dissolved and diluted to 12 different concentrations in DMSO and then diluted to the final concentrations (0 μM, 0.003 μM, 0.01 μM, 0.03 μM, 0.09 μM, 0.27 μM, 0.8 μM, 2 μM, 7 μM, 22 μM, 102 μM, 160 μM, and 200 μM) by ½ MS liquid medium (0.25% sucrose, pH 5.7), and the DMSO control contained the same amount of DMSO (0.1% v/v). Each treatment has three biological replicates. The seedlings were harvested by lightly scraping them off the nylon mesh and collected in the 1.5 mL tubes, and then frozen in liquid nitrogen.

RNA Extraction and Library Preparation

The total RNA was extracted using RNeasy Plant Mini Kit (QIAGEN, Cat No. 74904), and an on-column DNase digestion was performed by the RNase-Free DNase Set (QIAGEN, Cat No. 79254) during the purification. After the extraction, the purity and the quality of RNA were assessed by gel electrophoresis.

Approximately 2.5 μg of the purified RNA of each sample was used as the starting material to isolate intact poly(A)+ RNA by NEBNext Poly(A) mRNA Magnetic Isolation Module (NEB #E7490). The cDNA libraries were then constructed by NEBNext Ultra RNA Library Prep Kit (NEB #E7530) as described in the manufacturer's instructions. During the preparation, the clean-ups were done by the Agencourt AMPure XP PCR purification system (Beckman Coulter, A63881) and the NEBNext Multiplex Oligos (Index Primers Set 1-48; NEB #E7735S, NEB #E7500S, NEB #E7710S, and NEB #E7730S) were used to barcode the libraries. The Bioanalyzer is used to assess the quality and concentration of the libraries.

Illumina Sequencing and Data Preprocessing

The sequencing for the libraries was performed on the HiSeq platform by Novogene Corporation Inc. Four lanes were used, and barcoded libraries were pooled together randomly to be sequenced for each lane.

The analysis of the sequencing results followed the workflow for RNA-Seq described in the SystemPipeR package (H Backman and Girke, 2016). Briefly, the raw reads were mapped against the *Arabidopsis* genome using TopHat2 (Kim et al., 2013), and the reads counting was performed by the summarizeOverlaps function in the GenomicAlignments package (Lawrence et al., 2013). The genes with CPM (count per million) above 10 in at

least 3 samples and have at least 15 reads across all the samples are defined as expressed genes. After this filtering process, 19425 genes are considered in the following analysis. The edgeR package was used for the ANOVA test and pairwise sample comparison (Robinson et al., 2010).

Dose-Response Clustering Analysis of ABA-Responsive Genes

The expression level of each gene is normalized by transcripts per million (TPM) before the clustering analysis. The fuzzy c-means clustering was performed following the workflow described in the Mfuzz package and a shiny app, RNfuzzyApp (Kumar and E Futschik, 2007; Haering and Habermann, 2021). Briefly, the expression values were standardized to have a mean value of zero and a standard deviation of one to ensure the genes have similar changes in expression. Then we determined the number of clusters by the *inertia* method and the *elbow* method introduced in RNfuzzApp (Haering and Habermann, 2021). Both methods indicated the appropriate number of clusters is 9. After fuzzy clustering was performed by the algorithm implemented in the Mfuzz package (fuzzifier m = 1.206336), we also checked the overlap of clusters by *Mfuzz::overlap.plot* function, and the clusters are well-separated, which indicated we had chosen the suitable number of clusters.

Effective Dose Estimation

The procedure of ED_{50} and BMD estimation is summarized in Figure 1.2C. It is developed by modifying two published tools used in EC (effective concentration estimation), BMDx and DRomics (Larras et al., 2018; Serra et al., 2020). To avoid over-fitting, different candidate model lists were provided for dose-response data to select the best-fit model according to their dose-response trend. The log-logistic model and Weibull I and II models

were included in the candidate model list used to describe the monotonic curves (clusters 1-6), while the Brian-Cousens model and Beta model, which are used in describing biphasic trends, are only included in the candidate models used to fit the biphasic dose-response curves (genes in clusters 7-9). The best-fit model for each gene was selected as the one with the lowest AIC (Akaike Information Criterion). These analyses were performed using the *drc* package and *aomisc* package (Ritz et al., 2015; Onofri). After fitting the dose-response data to the best-fit model, the half response and benchmark response were calculated. And the ED_{50} and BMD values were estimated by the *approx()* function in the *stats* package.

Functional Enrichment Analysis

ClusterProfiler was used for functional enrichment analysis (Yu et al., 2012; Wu et al., 2021). GO (Gene Ontology) and pathway enrichment analysis was applied to the ABA-responsive genes in each cluster. The *p*-value was calculated by Fisher's exact test. FDR was used to correct *p*-values. Significant GO terms and pathways were identified with a cutoff for adjusted *p*-value (adj. *p*-value < 0.05). Fold enrichments for all the enriched terms were also calculated to interpret the results better. It is defined as the ratio of the frequency of input genes annotated in a term to the frequency of all genes annotated to that term.

In order to get a more effective interpretation from the analysis, some redundant GO terms (with semantic similarities over 0.7) were removed by applying the *simplify* function in the package. This function can only remove the highly similar GO terms. Some GO terms with a parent-child semantic relationship having exactly the same *p*-values and geneRatio (ratio of input genes that are annotated in a term) were still in the enriched GO term list. For those GO terms, the parent terms were eliminated.

Results

Transcriptional Profile of ABA-Responsive Genes

The wildtype Col-0 was treated with 13 concentrations of ABA across five orders of magnitudes. A statistically robust set of ABA-responsive genes (5749 genes) was identified using the ANOVA-like test (FDR < 0.0001) and pairwise comparison described in the edgeR package, the genes were significantly differentially expressed (|FoldChange| $\geqslant$ 1.5, FDR < 0.0005) at any of the ABA treatments compared with the DMSO control (Mock treatment).

As shown in the MDS (Multi-Dimensional Scaling) plot, the samples tend to cluster together based on different ranges of ABA treatments, which indicates that the transcriptional profile is similar between the treatments within each cluster, and it also shows excellent agreement between the biological replicates (Figure 1.1B).

The bar plot showed that there are more up-regulated genes than down-regulated genes, and the number of ABA-responsive genes increased as the concentration of ABA applied to the seedlings increased (Figure 1.1C), but not in an accumulative way (Figure 1.1D). A significant number of DEGs just respond to ABA within a specific sensitivity window and are not considered as significantly differentially expressed under a higher concentration of ABA, which indicates that it is insufficient to define ABA-responsive genes by using a single concentration.

Different Dose-Response Patterns of ABA-Responsive Genes

The upset plot in Figure 1.1D indicates distinct dose-response patterns among the ABA-responsive genes. Thus, I explored the expression pattern of some well-known ABA-responsive genes. *AtRD29A* (AT5G52310) has been frequently used as an ABA-responsive marker gene in previous studies. And *AtERD4* (AT1G08930) is down-regulated under exogenous ABA treatment (Wang et al., 2011). We can observe a monotonic trend in their dose-response curves (DRCs). Meanwhile, *AtEM1* (AT3G51810), an ABA-responsive gene that was reported to be exogenous ABA-induced, showed an atypical biphasic trend in the DRC, which was not observed in previous studies (Baumbusch et al., 2004; Parcy et al.) (Figure 1.2A).

To define the dose-response relationship of the whole genome on the transcriptional level, fuzzy c-means clustering was performed on all ABA-responsive genes. Fuzzy c-means clustering is a soft clustering method frequently applied in temporal RNA-seq data analysis (Lu et al., 2016; Liu et al., 2022). It provides the membership value indicating the degree of belongingness of the selected gene to a certain cluster.

After the clustering, 96.5% (5549/5749) of the ABA-responsive genes with a membership value higher than 0.5, which indicates most of the ABA-responsive genes belong to a unique cluster since a membership value of 0.5 is used to define the *empty cluster* empirically, i.e., if the membership values of all the genes in a certain cluster are below 0.5, this cluster is defined as an *empty cluster*, which means the genes with the membership value of 0.5 unlikely belong to this cluster (Futschik and Carlisle, 2005).

Using Mfuzz, we identified nine different clusters of ABA-responsive genes. These nine clusters could be classified into three major groups based on their shapes, the monotonic

up-regulated group (clusters 1-3, ABA-induced genes), the monotonic down-regulated group (clusters 4-6, ABA-repressed genes), and the biphasic group (clusters 9-11). Interestingly, a considerable number of genes fall into the biphasic group, which showed an atypical dose-response pattern. Genes in clusters 7 and 8 were induced by ABA and reached the peak response around 10 μM and 100 μM, respectively, and were down-regulated at a higher level of ABA. While ABA gradually repressed the genes in cluster 9 until around 10 μM, followed by a slight upregulation. These two unique dose-response patterns were referred to as *bell-shaped* (or *Bell*) and *U-shaped* (or *U*) in the following analysis.

ABA-Responsive Genes Have Distinct Sensitivity to ABA

There are 3 distinct clusters in each monotonic group and two in the bell-shaped group. Based on the expression patterns, even though these clusters have the same trend, they began to respond to ABA at different concentrations. Take the monotonic up group, for example; the genes in cluster 1 are most sensitive to ABA than those in the other clusters in the monotonic up group, and genes in cluster 3 are least sensitive to ABA in the group. These results indicated that the sensitivity of ABA-responsive genes might differ within each group.

We used two parameters to describe the sensitivity of each gene, the ED_{50} (ED_{50}, Effective Dose 50) and BMD (Benchmark Dose). Both of the parameters are concentrations. They are frequently used in the assessment of the potency of certain chemicals in toxicology studies, and both of them are obtained from the dose-response curves.

The dose corresponding to 50% of the maximum response is the most classic metric to indicate the sensitivity of certain chemicals. However, the previous definition of ED_{50}

makes this metric only valid when the full dose-response curves can be generated from the experiments since the ED_{50} is usually estimated directly from the parameter in the log-logistic model with four parameters, a model widely used in biochemical studies. The accuracy of estimation for this parameter is highly dependent on the accurate estimation of the other parameters, such as c and d, the upper and lower plateaus in a typical sigmodal curve. Thus, since we have a lot of genes without full dose-response curves, such as the genes in clusters 3 and 6, we introduced a new way of defining ED_{50}, which has already been used in the previous ED_{50} estimation for large datasets such as RNA-seq experiments (Serra et al., 2020). Instead of using the estimated upper plateau as the maximum response, we define the maximum response as the highest response obtained from the best model within the dose range tested in the experiment.

The BMD is the dose of the compound associated with a predefined small change in the response from the background response level. The change in response, referred to as BMR (benchmark response), is usually set to 5% or 10% discussed by the community as it is not scientifically reasoned (Jensen et al., 2020). In our study, the BMR is set to 1.349 multiplied by the standard deviation of the response under DMSO controls; this calculated BMR is a 10% increase over the assumed background rate of response and has been frequently used in previous studies (Thomas et al., 2007; Chappell et al., 2021; Peshdary et al., 2021).

Six models were applied to the dose-response data, and the formulas and basic descriptions are listed in Table 1.1. The composition of best-fit models is presented in Figure 1.2D. For monotonic dose-response curves, models used in describing the asymmetrical sigmoidal curves are predominant in fitting dose-response data of clusters

1-2 and 4-5, which seem to have the full dose-response curves. In contrast, symmetrical sigmoidal curves are preferred in describing the curves in clusters 3 and 6, which don't have an upper or lower plateau. The Brian-Cousens is the main model used in fitting the curves in biphasic clusters. The difference in dominated best-fit models indicates the dissimilarity of the dose-response trend of different clusters.

The ED_{50} and BMD values were estimated after fitting the curves to their corresponding best-fit models. The ED_{50}s can be generated from all dose-response curves, and 99.5% (5721 out of 5749) of the curves could give us valid BMD values. The results of some representative genes were listed in Table 2. Increasing ED_{50} and BMD values in the clusters were observed within the monotonic up/down groups. Genes in cluster 7 have higher ED_{50} and BMD values than cluster 8, which also follows a bell-shaped dose-response trend. And the differences are statistically significant. Since low ED_{50} and BMD indicate high sensitivity, this indicates the difference in the sensitivity of genes within these clusters. This is consistent with what has been found in the clustering results (Figure 1.2B). Thus, we can also classify the clusters of ABA-responsive genes into high (clusters 1, 4, 7, 9), medium (clusters 2, 5, 8), and low (clusters 3 and 6) groups according to their sensitivity to ABA (Figure1.2D).

Functional Validation of ABA-Responsive Genes With Different Dose-Response Patterns

To investigate the biological function and molecular mechanism controlling ABA response, we performed GO term enrichment analysis to explore the overrepresented functional categories in the groups of genes with different dose-response patterns. In total, we identified 303, 39, and 96 GO terms belonging to Biological Process, Cellular Component,

and Molecular Function, respectively, and 37 significant pathways in KEGG analysis. Since there are too many GO terms in the Biological Process category, we further classified them into 5 types, Development, Environment Response, Hormone, Cell Biology, and Metabolism. The results are presented in Figure 1.3 and Appendix Figure 1.1.

Most functional categories were only linked to genes with a specific dose-response pattern, and only a few GO terms were enriched in multiple clusters. For example, “response to light intensity” and “response to cold” are not only enriched in the up-regulated clusters (clusters 1, 2, 7) but also enriched in the down-regulated clusters (clusters 5, 6, and 8).

As expected, functional terms associated with some well-known biological processes with cross-talks with ABA signaling were highly enriched in the up-regulated group (clusters 1-3). For instance, GO terms related to seed germination, leaf senescence, stomatal movement, response to the nematode and salt, and pathways related to fatty acid metabolism are enriched in cluster1, the highly sensitive cluster. And “response to water deprive” , “response to far red/blue light” , “response to heat”, and “response to decreased oxygen levels” were highly enriched in the clusters with relatively lower sensitivity to ABA (Clusters 2 and 3).

Down-regulated genes (clusters 4-6) are highly related to GO terms associated with abiotic stresses and immune responses. SA and JA (salicylic acid and jasmonic acid) related terms were also enriched in the down-regulated genes, which are also reported to be involved in defense responses. Besides, these genes are highly sensitive to ABA. In addition, GO terms related to the detoxification biological process were also enriched in

the highly sensitive down-regulated group. Genes involved in alpha-amino acid biosynthesis process and glucose metabolic process are only enriched in the cluster with medium sensitivity to ABA (Cluster 5). GO terms associated with photosynthesis and carbon fixation were enriched in the lower sensitivity cluster, cluster 6.

The unique bell-shaped group (clusters 7 and 8) mainly comprised genes involved in water transport, lipid storage, lateral root formation, and response to sucrose and freezing biological processes. While we also found that the ribosome biogenesis pathway is highly enriched in KEGG pathway analysis for U-shaped cluster. This result was supported by a great number of highly enriched GO terms related to the rRNA-related biological processes (Appendix Figure 1.1, “Cell Biology” category). In addition, the enrichment results in “Cellular Component” category indicated located in preribosome was also a piece of evidence for the results (Appendix Figure 1.1, “Cellular Component” category).

We also generate a plot for enriched GO terms which are related to phytohormones. To our surprise, some broad ABA-stimulus-related annotations, such as “ABA biosynthetic process” and “cellular response to ABA stimulus” are only enriched in the up-regulated groups (Cluster1-2, 8) but not significantly enriched in any of the down-regulated groups. Auxin, jasmonic acid, salicylic acid, and brassinosteroid-related processes are enriched only in the down-regulated groups. Gibberellin and ethylene-involved signaling are enriched in both up, and down-regulated GO terms.

Discussion

In this study, we performed a comprehensive transcriptomic analysis to identify core gene sets responding to a wide range of ABA concentrations. We defined a statistically robust set of ABA-responsive genes with 5749 members. These ABA responders could be further

classified into 9 clusters according to their dose-response trends and sensitivity to ABA. In order to describe the sensitivity of genes to ABA, we introduced two parameters frequently used in toxicology, BMD and ED_{50}. The method to estimate effective dose developed in the study makes it possible to estimate the ED_{50} and BMD values from the dose-response curves of all ABA responders. The results showed that ABA-responsive genes have a wide range of sensitivity to ABA. This is the first time describing the sensitivity of genes to ABA on the transcriptional level.

Genes with similar expression patterns are likely to be involved in similar signaling pathways. Our GO enrichment analysis on different clusters of ABA-responsive genes confirmed that genes with the same dose-response trends and sensitivity tend to participate in the same pathways.

As expected, the most sensitive up-regulated ABA responders were involved in the well-characterized ABA-regulated biological process, such as seed dormancy, leaf senescence, and stomata movement. And this phenomenon could be explained by the rapid up-regulation of some main players of the core members in ABA signaling. As shown in Figure 1.4A, *ABF*s and *MAP3K*s involved in ABA signaling were up-regulated upon application of ABA. MYB96 is also a well-characterized transcription factor induced by ABA (Lee and Seo, 2019). And some ABA-responsive genes frequently used as the marker genes in previous studies are also up-regulated with a clear trend in our study (*MAP3K17* and *MAP3K18*, *RD29B*, and *RAB18*). Another interesting finding is that a lot of fatty acid biosynthesis genes are up-regulated upon ABA application (Figure 1.4B). KCSs (3-ketoacyl-CoA synthase) and KCR1 (b-ketoacyl reductase) and KCR2 are key enzymes for VLCFAs (very long chain fatty acids) biosynthesis (Beaudoin et al., 2009;

Lee et al., 2009). These genes exhibited a similar expression pattern which was activated with a relatively higher concentration of ABA. VLCFAs are essential for cuticular waxes and lipid molecules deposition on plant surfaces which provide protection against pathogen attack and avoid water loss during osmotic stress (Lee et al., 2009; Raffaele et al., 2009). The raised level of these VLCFAs may contribute to the enrichment of GO terms like “cuticle development”, “lipid localization” and “lipid transport” in the upregulated group.

It has been demonstrated that ABA may be involved in pathogen attacks by both sides, i.e. playing the protective role as well as reducing the resistance to pathogens (Cao et al., 2011). And the effect of ABA is mostly related to the crosstalks with other phytohormones, such as SA and JA (Adie et al., 2007). And in our research, most of the genes associated with immune response are down-regulated ABA responders, such as *LIK1*, *VIP1*, *GSTU13*, and *CYP71A12* (Figure 1.4D). CYP71A12 (Cytochrome P450, Family 71, Subfamily A, Polypeptide 12) and GSTU13 (Glutathione S-transferase tau 13) were reported to be positive regulators involved in immune response (Piślewska-Bednarek et al., 2018; Pastorczyk et al., 2020), which suggests ABA might play a negative role in the immune response in the pathways those genes are involved in. LIK1 (Lysm RLK1-Interacting Kinase 1) and VIP1 (VirE2-interacting protein 1) are also positive components in JA-mediated immune responses (Le et al., 2014; Laha et al., 2015). The down-regulation of these genes is consistent with the fact that the key enzymes involved in JA biosynthesis were also reduced upon ABA application (Figure 1.4E).

One unanticipated finding is that we have observed many biphasic dose-response trends in ABA-responsive genes exhibiting either bell-shaped or U-shaped (clusters 7-9, Figure 1.2B). Furthermore, GO term enrichment analysis suggests that they were associated with

distinct biological processes. Many *PIPs* (the plasma membrane intrinsic proteins) presented a bell-shaped behavior upon ABA treatment (Figure 1.4 C). PIPs are one of five groups of aquaporins in plants and can be further divided into two isoforms (PIP3 is also known as PIP2;7) (Alexandersson et al., 2005). PIPs are located in the plasma membrane and mediate the water transport in roots and leaves, and they are also responsible for membrane permeability to CO_2, thus influencing the transpiration efficiency (Groszmann et al., 2017). Thus, the repression of the PIPs under relatively high concentrations of ABA may account for the enrichment of "Photosynthesis" and "Carbon fixation in photosynthetic organisms" among the down-regulated ABA responders, and these terms only enriched among genes response to higher ABA concentrations (Cluster 6, Figure 1.3). The observation of bell-shaped DRC among PIPs also provided evidence for the previous findings that root hydraulic parameters exhibited similar bell-shaped dose-dependent responses to water deficit (Rosales et al., 2019).

And a majority of genes involved in ribosomal RNA (rRNA) biosynthesis exhibited a U-shaped dose-response relationship (Figure 1.4 F). The control of ribosomal RNA biogenesis is essential for regulating protein synthesis (Harscoët et al., 2010). Previous reports showed ABA repressed the transcription of ribosomal RNA by hypoacetylation of the rRNA gene promoter region (Zhang et al., 2012), which is partially in line with what we observed in our study. Most of the members belonging to transducin/WD40 repeat-like superfamily proteins, NUGWD1 (Nuclear Glucose-responsive WD40 protein 1), PCP1 (Plant-specific Component of the Pre-rRNA processing complex1), and SWA1 (SLOW WALKER1) were co-localized and might regulate rRNA synthesis (Ishida et al., 2016). Most of the genes shown in Figure 1.4F were involved in the maturation of SSU-rRNA (Small SubUnit ribosomal RNA).

The biphasic dose response, either bell-shaped or U-shaped might be due to the incorrect folding of specific transcription factors since many GO terms associated with unfolded protein response were only enriched under a relatively higher concentration of ABA. Thus, we hypothesize that those affected proteins might be transcription factors and since they were inactivated because of the conformational change, the expression behavior of the aquaporins and the rRNA biosynthesis-related genes exhibited this biphasic action under high-level ABA treatment. However, this hypothesis needs further validation.

The ABA signaling network is more complex than we expected. A more comprehensive and integrative network analysis should be conducted to get a complete view of the ABA signaling pathway.

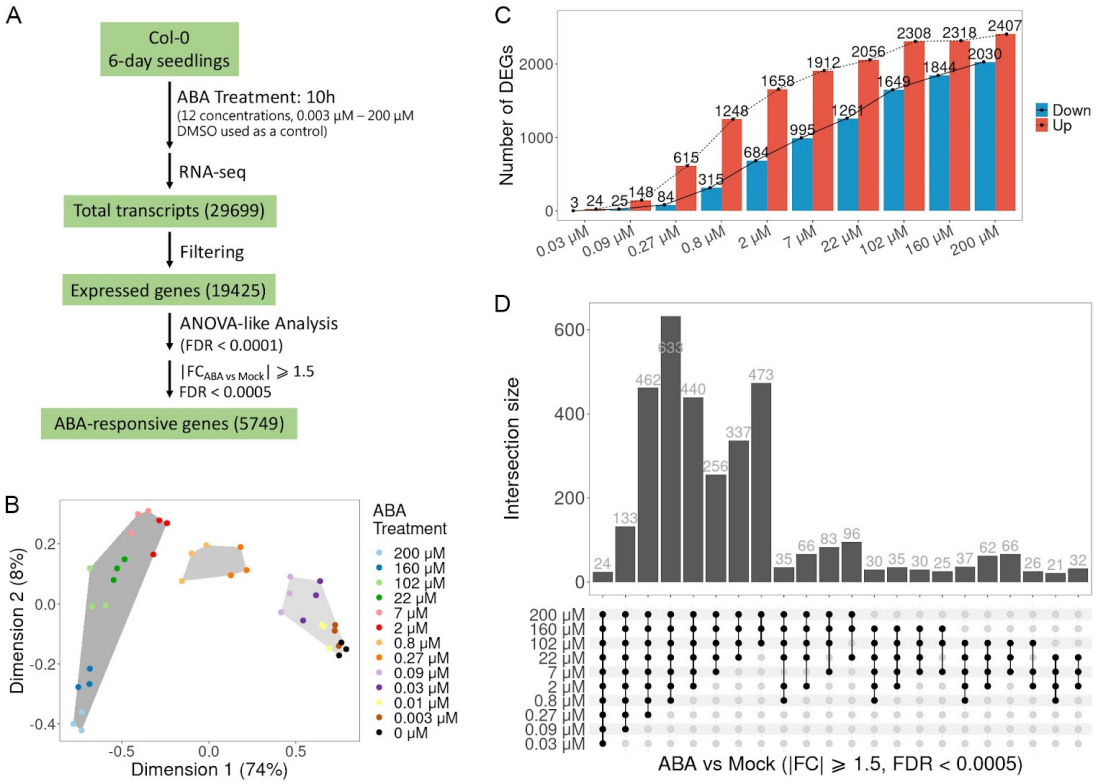

Figure 1.1 Transcriptional profile of ABA-responsive genes over a wide range of concentrations. (A) Diagram of the workflow for preparation of libraries and definition of ABA-responsive genes. The numbers in the parentheses are the number of genes left after each step. **(B)** MDS plot of gene expression in each biological replicate and ABA concentration. Three replicates are shown in the same color for each concentration. K-means clustering was performed to cluster the samples. **(C)** Bar plot of the up-regulated (Up, in red) or down-regulated (Down, in blue) DEGs under ABA treatments. Numbers on top of the bars indicate the number of DEGs identified under each concentration of ABA compared with the Mock (DMSO) treatment. **(D)** The upset plot of identified DEGs shared by different concentrations of ABA treatment. Only the overlaps among 3 or more ABA concentrations and the overlaps with no less than 20 DEGs are shown. The number on top of each bar in the upper plot indicates the number of DEGs in each overlapping combination.

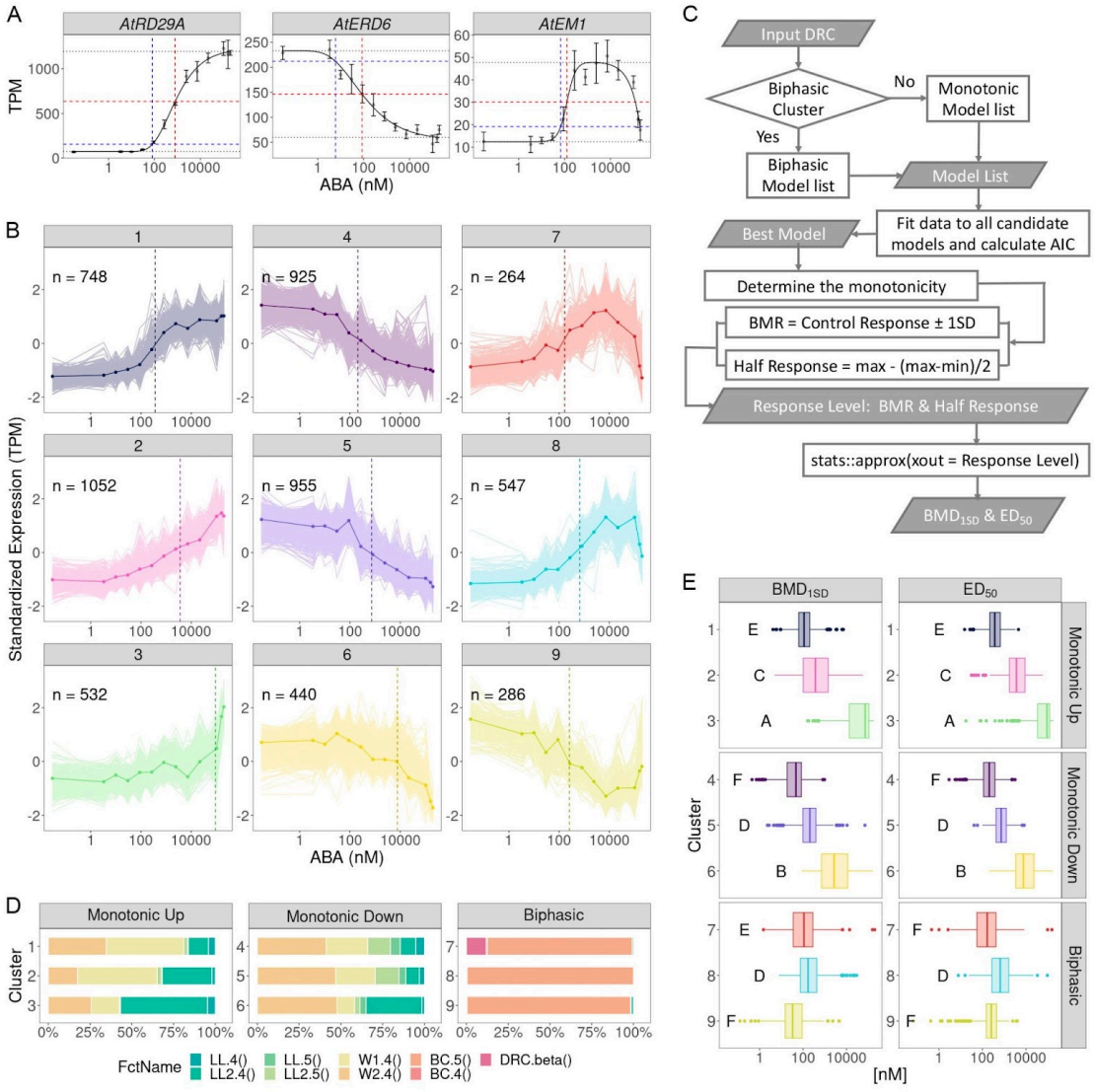
A
AtRD29A
AtERD6
AtEM1
TPM
ABA (nM)
B
n = 748
n = 925
n = 264
n = 1052
n = 955
n = 547
n = 532
n = 440
n = 286
Standardized Expression (TPM)
ABA (nM)
C
Input DRC
Biphasic Cluster
No
Monotonic Model list
Yes
Biphasic Model list
Model List
Best Model
Fit data to all candidate models and calculate AIC
Determine the monotonicity
BMR = Control Response ± 1SD
Half Response = max - (max-min)/2
Response Level: BMR & Half Response
stats::approx(xout = Response Level)
BMD1SD & ED50
D
Monotonic Up
Monotonic Down
Biphasic
Cluster
FctName
LL.4()
LL2.4()
LL.5()
LL2.5()
W1.4()
W2.4()
BC.5()
BC.4()
DRC.beta()
E
BMD1SD
ED50
Monotonic Up
Monotonic Down
Biphasic
Cluster
[nM]

Figure 1.2 Clustering of dose-response patterns and ED estimation of ABA-responsive genes. (A) Representative genes in different groups of well-known ABA-responsive genes. Horizontal dotted grey lines indicate the maximum and minimum response estimated by the best-fit models. The horizontal dashed blue and red lines represent the BMR (benchmark response, 10% above the minimum response) and half of the maximum response, respectively. The doses which give the BMR and half-response, i.e., BMD and ED_{50} are indicated by the vertical lines in the same corresponding color. **(B)** Expression profiles for ABA-responsive genes based on the dose-response patterns. The number in each panel is the total number of ABA-responsive genes belonging to each cluster. Dark points represent the average standardized expression of genes under each concentration of ABA within each cluster and are connected by a solid line in the same color. Vertical dotted lines represent the median value of ED_{50}. **(C)** Diagram of the workflow for ED estimation from the dose-response curve of each gene. **(D)** Composition of best-fitting models for ED estimation of genes in each cluster. The models corresponding to the function names (FctName) are listed in Table1.1. **(E)** Box plot shows distributions of BMD and ED_{50} of each cluster. Uppercase letters indicate the significant difference between different clusters assessed by Games and Howell's test ($p < 0.01$).

Table 1.1 Models used for estimating effective doses

Curve type	Model Name	Function Name	Equation	Description	References
Monotonic Symmetrical Sigmoidal Curve	Log-logistic	LL.4()	$y = c + \frac{d-c}{1+\exp\left(b\left(\log\left(x\right)-e\right)\right)}$	Log-logistic model with 4 parameters	(Ritz, 2010)
		LL2.4()	$y = c + \frac{d-c}{1+\exp\left(b\left(\log\left(x\right)-\log\left(e\right)\right)\right)}$		
Monotonic Asymmetrical Sigmoidal Curve	Log-logistic	LL.5()	$y = c + \frac{d-c}{\left(1+\exp\left(b\left(\log\left(x\right)-e\right)\right)\right)^{f}}$	Log-logistic model with 5 parameters	
		LL2.5()	$y = c + \frac{d-c}{\left(1+\exp\left(b\left(\log\left(x\right)-\log\left(e\right)\right)\right)\right)^{f}}$		
	Weibull I	W1.4()	$y = c + \left(d-c\right)\exp\left(-\exp\left(b\left(\log\left(x\right)-\log\left(e\right)\right)\right)\right)$	Weibull I model with 4 parameters	
	Weibull II	W2.4()	$y = c + \left(d-c\right)\left(1-\exp\left(-\exp\left(b\left(\log\left(x\right)-\log\left(e\right)\right)\right)\right)\right)$	Weibull II model with 4 parameters	
Biphasic Curve	Brian-Cousens	BC.5()	$y = c + \frac{d-c+fx}{1+\exp\left(b\left(\log\left(x\right)-\log\left(e\right)\right)\right)}$	Brian-Cousens model with 5 parameters	(Brain and Cousens, 1989)
		BC.4()	$y = \frac{d+fx}{1+\exp\left(b\left(\log\left(x\right)-\log\left(e\right)\right)\right)}$	Brian-Cousens model with 4 parameters	
	Beta	DRC.beta()	$y = d\left\{\left(\frac{x-X_b}{X_o-X_b}\right)\left(\frac{X_c-x}{X_c-X_o}\right)^{\frac{X_c-X_o}{X_o-X_b}}\right\}^{b}$	Beta model	(Yin et al., 1995; Yin et al., 2003)

Table 1.2 ED estimation of representative genes

Category	AGI	Gene Description	Best Fit Model	ED_{50}		BMD	
				Mean	95% Confidence Interval	Mean	Confidence Interval
Monotonic Up ABA signaling	AT5G59220	*HAI1*	W1.4()	748.70	[563.25 - 1005.56]	169.52	[103.66 - 266.24]
	AT4G34000	*ABF3*	W2.4()	404.14	[301.87 - 535.32]	36.38	[16.55 - 68.9]
	AT3G19290	*ABF4*	W2.4()	891.17	[586.81 - 1316.48]	189.65	[90.37 - 368.08]
	AT5G62470	*MYB96*	W1.4()	455.84	[300.97 - 743.92]	84.84	[40.97 - 150.34]
	AT2G32510	*MAPKKK17*	W2.4()	587.11	[394.86 - 828.85]	149.17	[74.61 - 281.49]
	AT1G05100	*MAPKKK18*	W1.4()	1109.43	[501.69 - 3293.85]	97.71	[25.17 - 228.18]
	AT5G52300	*RD29B*	W2.4()	4274.60	[2751.53 - 6712.86]	198.42	[72.45 - 475.96]
	AT5G66400	*RAB18*	W2.4()	2593.56	[1511.81 - 4177.57]	321.11	[128.65 - 750.16]
Monotonic Up Fatty acid biosynthesis	AT1G04220	*KCS2*	W1.4()	3058.43	[2157.63 - 4424.08]	34.41	[14.2 - 68.41]
	AT1G07720	*KCS3*	W1.4()	1427.47	[1099.95 - 1880.21]	106.93	[63.58 - 173.56]
	AT1G19440	*KCS4*	LL2.4()	10852.87	[5878.61 - 20074.07]	173.33	[39.92 - 496.13]
	AT1G25450	*KCS5*	W1.4()	3539.83	[1999.23 - 6650.83]	152.39	[52.84 - 334.95]
	AT2G16280	*KCS9*	W1.4()	740.84	[308.97 - 2085.34]	50.82	[12.73 - 130.83]
	AT2G26250	*KCS10*	W1.4()	1443.85	[818.71 - 2699.97]	109.30	[42.79 - 228.26]
	AT1G67730	*KCR1*	W1.4()	722.09	[398.85 - 1444.74]	34.95	[12.45 - 73.34]
	AT1G24470	*KCR2*	W1.4()	8141.14	[4235.66 - 17900.62]	926.75	[266.37 - 2006.85]
Monotonic Down Immune response	AT3G14840	*LIK1*	LL2.4()	217.75	[158.59 - 298.95]	29.77	[14.9 - 53.75]
	AT3G01310	*VIP1*	W1.4()	305.61	[209.9 - 440.58]	22.25	[8.22 - 45.85]
	AT1G27130	*GSTU13*	LL2.5()	603.74	[334.15 - 1183.17]	71.06	[35.64 - 117.92]
	AT2G30750	*CYP71A12*	W1.4()	103.12	[67.74 - 150.29]	6.55	[1.8 - 15.76]

Table 1.2 ED estimation of representative genes (Continued)

Category	AGI	Gene Description	Best Fit Model	ED_{50}		BMD	
				Mean	Confidence Interval	Mean	Confidence Interval
Monotonic Down JA biosynthesis	AT1G20510	*OPCL1*	LL2.4()	566.74	[354.93 - 930.03]	17.38	[5.03 - 42.41]
	AT3G25760	*AOC1*	W1.4()	1497.63	[886.07 - 2540.42]	37.74	[9.98 - 105.51]
	AT5G42650	*AOS*	LL2.5()	738.81	[404.46 - 1590.03]	207.74	[127.47 - 335.96]
	AT2G06050	*OPR3*	W1.4()	1435.18	[648.64 - 3307.73]	33.58	[5.21 - 131.02]
Bell shaped Water transport	AT4G35100	*PIP3*	BC.5()	657.81	[454.84 - 918.07]	61.53	[26.61 - 135.7]
	AT3G61430	*PIP1A*	BC.5()	316.46	[236.04 - 422.32]	63.92	[34.47 - 111.39]
	AT2G45960	*PIP1B*	BC.5()	163.88	[1.97 - 1574.28]	72.04	[12.61 - 851.5]
	AT1G01620	*PIP1C*	BC.5()	7.69	[0.59 - 24.4]	2.44	[0.09 - 10.21]
	AT3G53420	*PIP2A*	BC.5()	133.18	[86.9 - 196.55]	21.08	[9.4 - 41.74]
	AT2G37170	*PIP2B*	BC.5()	120.88	[47.15 - 321.55]	110.56	[42.4 - 294.72]
	AT2G39010	*PIP2E*	BC.5()	569.58	[381.08 - 826.18]	87.65	[42.24 - 170.07]
U-shaped rRNA biosynthesis	AT5G11240	*NUGWD1*	BC.5()	645.74	[292.68 - 1352.26]	148.72	[47.54 - 379.49]
	AT1G15440	*PWP2*	BC.5()	128.44	[54.85 - 300.28]	7.47	[0.83 - 24.55]
	AT1G15420	*PCP1*	BC.5()	251.58	[125.74 - 498.24]	22.87	[5.56 - 60.51]
	AT2G47990	*SWA1*	BC.5()	287.09	[95.2 - 762.45]	35.14	[5.31 - 125.94]
	AT3G57940	GNAT acetyltransferase	BC.5()	508.71	[225.79 - 988.61]	70.66	[19.42 - 205.63]
	AT5G22100	RNA cyclase family protein	BC.5()	193.54	[79.32 - 417.26]	12.50	[1.8 - 43.91]
	AT4G04940	Transducin/WD40 repeat-like superfamily protein	BC.5()	184.98	[61.99 - 480.24]	13.54	[1.37 - 52.04]
	AT2G18900		BC.5()	241.04	[96.56 - 584.04]	16.96	[2.22 - 57.42]
	AT1G27470		BC.5()	399.32	[194.56 - 771.39]	66.38	[20.4 - 169.75]
	AT3G21540		BC.5()	310.62	[133.35 - 611.88]	55.46	[15.93 - 155.46]

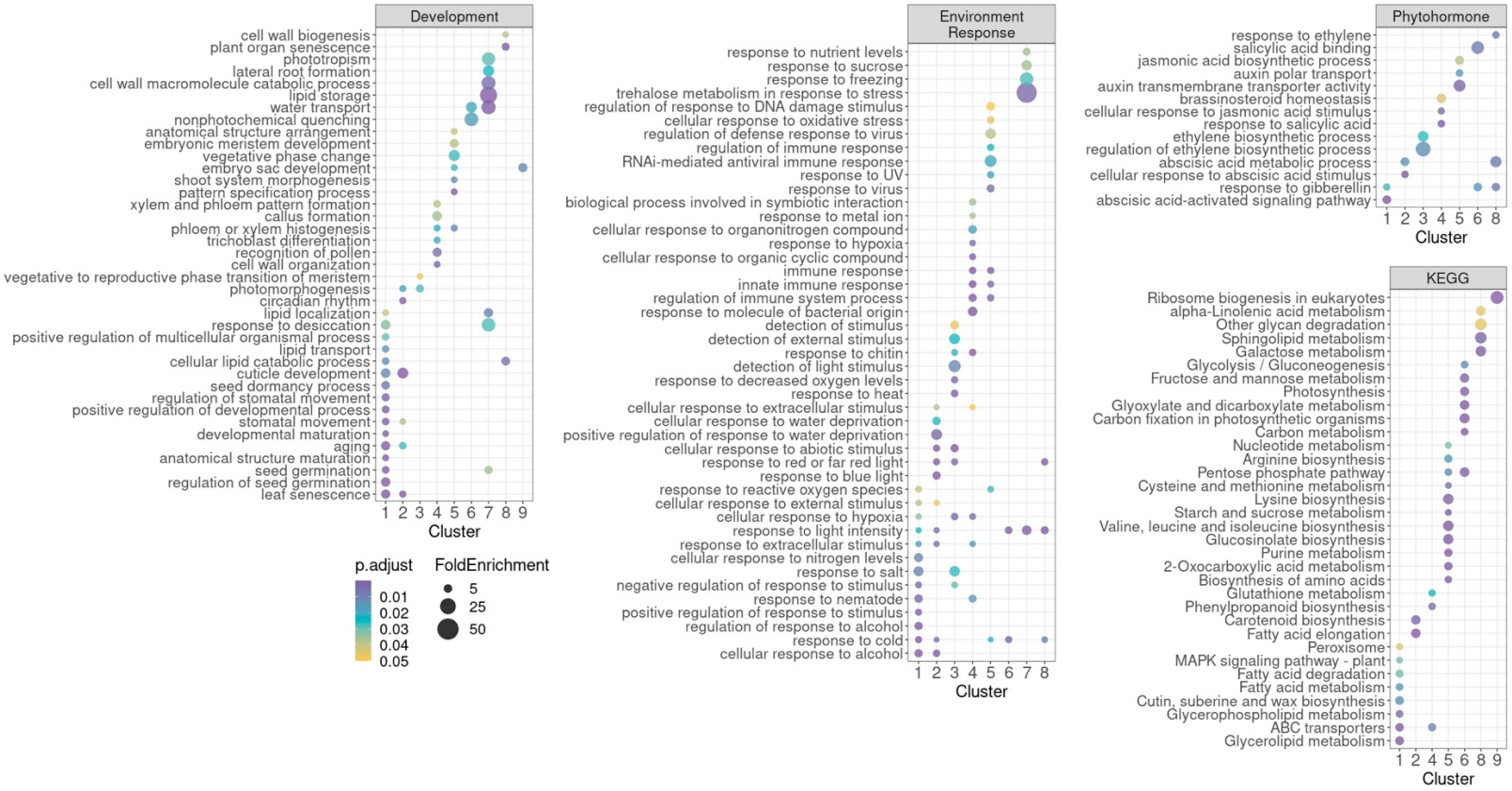

Figure 1.3 Comparison of functional profiles among different clusters of ABA-responsive genes. Top GO (Gene Ontology) and KEGG (Kyoto Encyclopedia of Genes and Genomes) pathways highly enriched in different clusters (adjusted *p*-value < 0.05) were presented. The results were visualized as a dot plot with different facet panels indicating three representative classes in the Biological Process category and KEGG pathway, with the size of the dots indicating the fold enrichment and the color corresponding to the adjusted *p*-value of each enriched GO term. (Note: If a cluster didn't appear in the x-axis, it means no GO terms were significantly enriched in that cluster.)

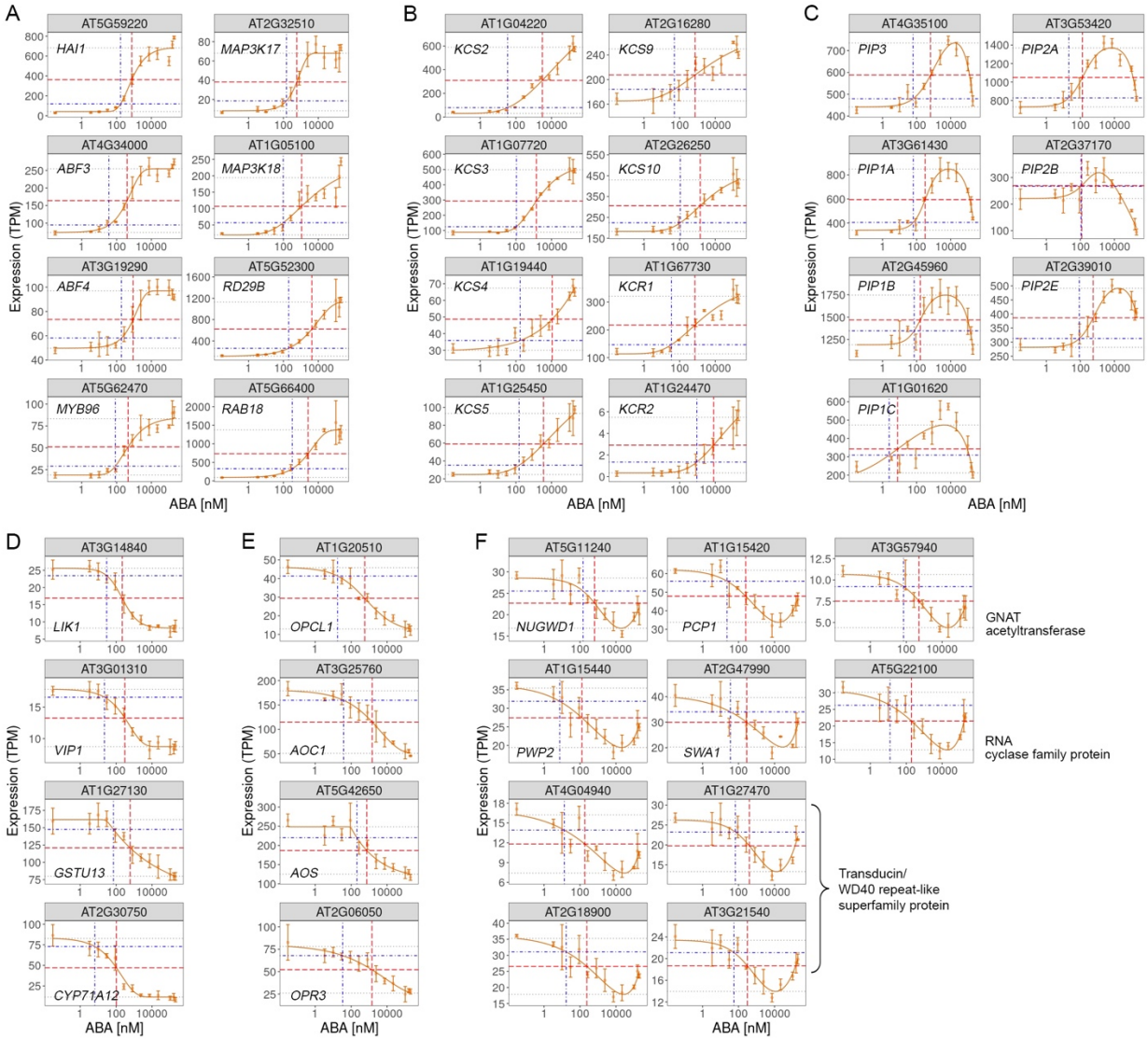
A
AT5G59220
HAI1
AT2G32510
MAP3K17
AT4G34000
ABF3
AT1G05100
MAP3K18
AT3G19290
ABF4
AT5G52300
RD29B
AT5G62470
MYB96
AT5G66400
RAB18
B
AT1G04220
KCS2
AT2G16280
KCS9
AT1G07720
KCS3
AT2G26250
KCS10
AT1G19440
KCS4
AT1G67730
KCR1
AT1G25450
KCS5
AT1G24470
KCR2
C
AT4G35100
PIP3
AT3G53420
PIP2A
AT3G61430
PIP1A
AT2G37170
PIP2B
AT2G45960
PIP1B
AT2G39010
PIP2E
AT1G01620
PIP1C
Expression (TPM)
ABA [nM]
D
AT3G14840
LIK1
AT3G01310
VIP1
AT1G27130
GSTU13
AT2G30750
CYP71A12
E
AT1G20510
OPCL1
AT3G25760
AOC1
AT5G42650
AOS
AT2G06050
OPR3
F
AT5G11240
NUGWD1
AT1G15420
PCP1
AT3G57940
GNAT acetyltransferase
AT1G15440
PWP2
AT2G47990
SWA1
AT5G22100
RNA cyclase family protein
AT4G04940
AT1G27470
AT2G18900
AT3G21540
Transducin/ WD40 repeat-like superfamily protein

Figure 1.4 Dose-response curves of representative ABA-responsive genes. **(A-F)** plots showing the representative genes involved in the following pathways. **(A)** ABA signaling **(B)** Fatty acid biosynthesis **(C)** Aquaporins in water transport **(D)** Immune response **(E)** JA biosynthesis **(F)** rRNA biosynthesis. The gene names were presented in the corner of each facet, The horizontal dashed blue and red lines represent the BMR (benchmark response) and half of the maximum response, respectively. The doses which give the BMR and half-response, i.e., BMD and ED_{50} are indicated by the vertical lines in the same corresponding color.

References

Adie BAT, Pérez-Pérez J, Pérez-Pérez MM, Godoy M, Sánchez-Serrano J-J, Schmelz EA, Solano R (2007) ABA is an essential signal for plant resistance to pathogens affecting JA biosynthesis and the activation of defenses in *Arabidopsis*. Plant Cell **19**: 1665–1681

Alexandersson E, Fraysse L, Sjövall-Larsen S, Gustavsson S, Fellert M, Karlsson M, Johanson U, Kjellbom P (2005) Whole gene family expression and drought stress regulation of aquaporins. Plant Mol Biol **59**: 469–484

Bargmann BOR, Birnbaum KD (2010) Fluorescence activated cell sorting of plant protoplasts. J Vis Exp. doi: 10.3791/1673

Baumbusch LO, Hughes DW, Galau GA, Jakobsen KS (2004) LEC1, FUS3, ABI3 and Em expression reveals no correlation with dormancy in *Arabidopsis*. J Exp Bot **55**: 77–87

Beaudoin F, Wu X, Li F, Haslam RP, Markham JE, Zheng H, Napier JA, Kunst L (2009) Functional characterization of the *Arabidopsis* beta-ketoacyl-coenzyme A reductase candidates of the fatty acid elongase. Plant Physiol **150**: 1174–1191

Boudsocq M, Droillard M-J, Barbier-Brygoo H, Laurière C (2007) Different phosphorylation mechanisms are involved in the activation of sucrose non-fermenting 1 related protein kinases 2 by osmotic stresses and abscisic acid. Plant Mol Biol **63**: 491–503

Brain P, Cousens R (1989) An equation to describe dose responses where there is stimulation of growth at low doses. Weed Res **29**: 93–96

Cao FY, Yoshioka K, Desveaux D (2011) The roles of ABA in plant–pathogen interactions. J Plant Res **124**: 489–499

Chappell GA, Heintz MM, Haws LC (2021) Transcriptomic analyses of livers from mice exposed to 1,4-dioxane for up to 90 days to assess potential mode(s) of action underlying liver tumor development. Curr Res Toxicol **2**: 30–41

Cutler SR, Rodriguez PL, Finkelstein RR, Abrams SR (2010) Abscisic acid: emergence of a core signaling network. Annu Rev Plant Biol **61**: 651–679

De Smet I, Signora L, Beeckman T, Inzé D, Foyer CH, Zhang H (2003) An abscisic acid-sensitive checkpoint in lateral root development of *Arabidopsis*. Plant J **33**: 543–555

Finkelstein R (2013) Abscisic Acid synthesis and response. *Arabidopsis* Book **11**: e0166

Fujii H, Chinnusamy V, Rodrigues A, Rubio S, Antoni R, Park S-Y, Cutler SR, Sheen J, Rodriguez PL, Zhu J-K (2009) In vitro reconstitution of an abscisic acid signalling pathway. Nature **462**: 660–664

Futschik ME, Carlisle B (2005) Noise-robust soft clustering of gene expression time-course data. J Bioinform Comput Biol **3**: 965–988

García-Andrade J, González B, Gonzalez-Guzman M, Rodriguez PL, Vera P (2020) The Role of ABA in Plant Immunity is Mediated through the PYR1 Receptor. Int J Mol Sci. doi: 10.3390/ijms21165852

Gonzalez-Guzman M, Pizzio GA, Antoni R, Vera-Sirera F, Merilo E, Bassel GW, Fernández MA, Holdsworth MJ, Perez-Amador MA, Kollist H, et al (2012) *Arabidopsis* PYR/PYL/RCAR receptors play a major role in quantitative regulation of stomatal aperture and transcriptional response to abscisic acid. Plant Cell **24**: 2483–2496

Groszmann M, Osborn HL, Evans JR (2017) Carbon dioxide and water transport through plant aquaporins. Plant Cell Environ **40**: 938–961

H Backman TW, Girke T (2016) systemPipeR: NGS workflow and report generation environment. BMC Bioinformatics **17**: 388

Haering M, Habermann BH (2021) RNfuzzyApp: an R shiny RNA-seq data analysis app for visualisation, differential expression analysis, time-series clustering and enrichment analysis. F1000Res **10**: 654

Harscoët E, Dubreucq B, Palauqui J-C, Lepiniec L (2010) NOF1 encodes an *Arabidopsis* protein involved in the control of rRNA expression. PLoS One **5**: e12829

Helander JDM, Vaidya AS, Cutler SR (2016) Chemical manipulation of plant water use. Bioorg Med Chem **24**: 493–500

Ishida T, Maekawa S, Yanagisawa S (2016) The Pre-rRNA Processing Complex in *Arabidopsis* Includes Two WD40-Domain-Containing Proteins Encoded by Glucose-Inducible Genes and Plant-Specific Proteins. Mol Plant **9**: 312–315

Jensen SM, Kluxen FM, Streibig JC, Cedergreen N, Ritz C (2020) bmd: an R package for benchmark dose estimation. PeerJ **8**: e10557

Kim D, Pertea G, Trapnell C, Pimentel H, Kelley R, Salzberg SL (2013) TopHat2: accurate alignment of transcriptomes in the presence of insertions, deletions and gene fusions. Genome Biol **14**: R36

Kumar L, E Futschik M (2007) Mfuzz: a software package for soft clustering of microarray data. Bioinformation **2**: 5–7

Laha D, Johnen P, Azevedo C, Dynowski M, Weiß M, Capolicchio S, Mao H, Iven T, Steenbergen M, Freyer M, et al (2015) VIH2 Regulates the Synthesis of Inositol Pyrophosphate InsP8 and Jasmonate-Dependent Defenses in *Arabidopsis*. Plant Cell **27**: 1082–1097

Lång V, Palva ET (1992) The expression of a rab-related gene, rab18, is induced by abscisic acid during the cold acclimation process of *Arabidopsis* thaliana (L.) Heynh. Plant Mol Biol **20**: 951–962

Larras F, Billoir E, Baillard V, Siberchicot A, Scholz S, Wubet T, Tarkka M, Schmitt-Jansen M, Delignette-Muller M-L (2018) DRomics: A Turnkey Tool to Support the Use of the Dose-Response Framework for Omics Data in Ecological Risk Assessment. Environ Sci Technol **52**: 14461–14468

Lawrence M, Huber W, Pagès H, Aboyoun P, Carlson M, Gentleman R, Morgan MT, Carey VJ (2013) Software for computing and annotating genomic ranges. PLoS Comput Biol **9**: e1003118

Le MH, Cao Y, Zhang X-C, Stacey G (2014) LIK1, a CERK1-interacting kinase, regulates plant immune responses in *Arabidopsis*. PLoS One **9**: e102245

Lee HG, Seo PJ (2019) MYB96 recruits the HDA15 protein to suppress negative regulators of ABA signaling in *Arabidopsis*. Nat Commun **10**: 1713

Lee S-B, Jung S-J, Go Y-S, Kim H-U, Kim J-K, Cho H-J, Park OK, Suh M-C (2009) Two *Arabidopsis* 3-ketoacyl CoA synthase genes, KCS20 and KCS2/DAISY, are functionally redundant in cuticular wax and root suberin biosynthesis, but differentially controlled by osmotic stress. Plant J **60**: 462–475

Liu S, Lv Z, Liu Y, Li L, Zhang L (2018) Network analysis of ABA-dependent and ABA-independent drought responsive genes in *Arabidopsis* thaliana. Genet Mol Biol **41**: 624–637

Liu W, Zhang Y, Fang X, Tran S, Zhai N, Yang Z, Guo F, Chen L, Yu J, Ison MS, et al (2022) Transcriptional landscapes of de novo root regeneration from detached *Arabidopsis* leaves revealed by time-lapse and single-cell RNA sequencing analyses. Plant Commun 100306

Liu X, Hou X (2018) Antagonistic Regulation of ABA and GA in Metabolism and Signaling Pathways. Front Plant Sci **9**: 251

Lu L, McCurdy S, Huang S, Zhu X, Peplowska K, Tiirikainen M, Boisvert WA, Garmire LX (2016) Time Series miRNA-mRNA integrated analysis reveals critical miRNAs and targets in macrophage polarization. Sci Rep **6**: 37446

Ma Y, Szostkiewicz I, Korte A, Moes D, Yang Y, Christmann A, Grill E (2009) Regulators of PP2C phosphatase activity function as abscisic acid sensors. Science **324**: 1064–1068

Melcher K, Ng L-M, Zhou XE, Soon F-F, Xu Y, Suino-Powell KM, Park S-Y, Weiner JJ, Fujii H, Chinnusamy V, et al (2009) A gate-latch-lock mechanism for hormone signalling by abscisic acid receptors. Nature **462**: 602–608

Onofri A aomisc: Utilities for stat courses. Github

Parcy, Valon, Raynal, Gaubier-Comella, Delseny, ai' Regulation of Gene Expression Programs during *Arabidopsis* Seed Development: Roles of the AB13 Locus and of Endogenous Abscisic Acid. Plant Cell

Park S-Y, Fung P, Nishimura N, Jensen DR, Fujii H, Zhao Y, Lumba S, Santiago J, Rodrigues A, Chow T-FF, et al (2009) Abscisic acid inhibits type 2C protein phosphatases via the PYR/PYL family of START proteins. Science **324**: 1068–1071

Pastorczyk M, Kosaka A, Piślewska-Bednarek M, López G, Frerigmann H, Kułak K, Glawischnig E, Molina A, Takano Y, Bednarek P (2020) The role of CYP71A12 monooxygenase in pathogen-triggered tryptophan metabolism and *Arabidopsis* immunity. New Phytol **225**: 400–412

Peshdary V, Hobbs CA, Maynor T, Shepard K, Gagné R, Williams A, Kuo B, Chepelev N, Recio L, Yauk C, et al (2021) Transcriptomic pathway and benchmark dose analysis of Bisphenol A, Bisphenol S, Bisphenol F, and 3,3',5,5'-Tetrabromobisphenol A in H9 human embryonic stem cells. Toxicol In Vitro **72**: 105097

Piślewska-Bednarek M, Nakano RT, Hiruma K, Pastorczyk M, Sanchez-Vallet A, Singkaravanit-Ogawa S, Ciesiołka D, Takano Y, Molina A, Schulze-Lefert P, et al (2018) Glutathione Transferase U13 Functions in Pathogen-Triggered Glucosinolate Metabolism. Plant Physiol **176**: 538–551

Raffaele S, Leger A, Roby D (2009) Very long chain fatty acid and lipid signaling in the response of plants to pathogens. Plant Signal Behav **4**: 94–99

Ritz C (2010) Toward a unified approach to dose-response modeling in ecotoxicology. Environ Toxicol Chem **29**: 220–229

Ritz C, Baty F, Streibig JC, Gerhard D (2015) Dose-Response Analysis Using R. PLoS One **10**: e0146021

Robinson MD, McCarthy DJ, Smyth GK (2010) edgeR: a Bioconductor package for differential expression analysis of digital gene expression data. Bioinformatics **26**: 139–140

Rosales MA, Maurel C, Nacry P (2019) Abscisic Acid Coordinates Dose-Dependent Developmental and Hydraulic Responses of Roots to Water Deficit. Plant Physiol **180**: 2198–2211

Santiago J, Rodrigues A, Saez A, Rubio S, Antoni R, Dupeux F, Park S-Y, Márquez JA, Cutler SR, Rodriguez PL (2009) Modulation of drought resistance by the abscisic acid receptor PYL5 through inhibition of clade A PP2Cs: Regulation of HAB1 by ABA-binding proteins. Plant J **60**: 575–588

Serra A, Saarimäki LA, Fratello M, Marwah VS, Greco D (2020) BMDx: a graphical Shiny application to perform Benchmark Dose analysis for transcriptomics data. Bioinformatics **36**: 2932–2933

Thomas RS, Allen BC, Nong A, Yang L, Bermudez E, Clewell HJ 3rd, Andersen ME (2007) A method to integrate benchmark dose estimates with genomic data to assess the functional effects of chemical exposure. Toxicol Sci **98**: 240–248

Trewavas AJ, Cleland RE (1983) Is plant development regulated by changes in the concentration of growth substances or by changes in the sensitivity to growth substances? Trends in Biochemical Sciences **8**: 354–357

Wan C, Wang M, Yang D, Han X, Che C, Ding S, Xiao Y, Qin Z (2017) Synthesis and Biological Activity of 2′,3′-iso-Aryl-abscisic Acid Analogs. Molecules; Basel **22**: 2229

Wang R-S, Pandey S, Li S, Gookin TE, Zhao Z, Albert R, Assmann SM (2011) Common and unique elements of the ABA-regulated transcriptome of *Arabidopsis* guard cells. BMC Genomics **12**: 216

Wang W, Vinocur B, Altman A (2003) Plant responses to drought, salinity and extreme temperatures: towards genetic engineering for stress tolerance. Planta **218**: 1–14

Weng J-K, Ye M, Li B, Noel JP (2016) Co-evolution of Hormone Metabolism and Signaling Networks Expands Plant Adaptive Plasticity. Cell **166**: 881–893

Wu T, Hu E, Xu S, Chen M, Guo P, Dai Z, Feng T, Zhou L, Tang W, Zhan L, et al (2021) clusterProfiler 4.0: A universal enrichment tool for interpreting omics data. Innovation (Camb) **2**: 100141

Yamaguchi-Shinozaki K, Shinozaki K (1994) A novel cis-acting element in an *Arabidopsis* gene is involved in responsiveness to drought, low-temperature, or high-salt stress. Plant Cell **6**: 251–264

Ye Y, Zhou L, Liu X, Liu H, Li D, Cao M, Chen H, Xu L, Zhu J-K, Zhao Y (2017) A Novel Chemical Inhibitor of ABA Signaling Targets All ABA Receptors. Plant Physiol **173**: 2356–2369

Yin X, Goudriaan J, Lantinga EA, Vos J, Spiertz HJ (2003) A Flexible Sigmoid Function of Determinate Growth. Ann Bot **91**: 361–371

Yin X, Kropff MJ, McLaren G, Visperas RM (1995) A nonlinear model for crop development as a function of temperature. Agric For Meteorol **77**: 1–16

Yu G, Wang L-G, Han Y, He Q-Y (2012) clusterProfiler: an R package for comparing biological themes among gene clusters. OMICS **16**: 284–287

de Zelicourt A, Colcombet J, Hirt H (2016) The Role of MAPK Modules and ABA during Abiotic Stress Signaling. Trends Plant Sci **21**: 677–685

Zhang L, Hu Y, Yan S, Li H, He S, Huang M, Li L (2012) ABA-mediated inhibition of seed germination is associated with ribosomal DNA chromatin condensation, decreased transcription, and ribosomal RNA gene hypoacetylation. Plant Mol Biol **79**: 285–293

Zhu J-K (2002) Salt and drought stress signal transduction in plants. Annu Rev Plant Biol **53**: 247–273

Chapter 2 Genetic and Transcriptomic Analyses of *Arabidopsis* ABA Receptor Subfamily Function

Abstract

Abscisic acid (ABA) can only properly function in stress responses and plant development with the perception by the ABA receptors. ABA receptors are PYR/PYL/RCAR family, which contains 14 members and can be classified into three subfamilies, I, II, and III, according to their oligomeric states and affinity to ABA. Subfamilly III receptors, the dimeric receptors, have a lower affinity for ABA than the other two subfamilies, which are monomeric. To explore the biological roles of each subfamily, we generated three *pyl* mutants with mutations in the receptors of different subfamilies. All mutants showed reduced sensitivity to ABA or ABA agonists, which indicated the importance of all the ABA receptor subfamilies. Then we carried out an RNA-seq analysis on these three mutants; compared with the wildtype, the removal of subfamily III receptors has the largest effect on ABA-regulated gene expression. GO enrichment analysis also showed that more unique terms were enriched among DEGs identified in subfamily III mutant. Our results also demonstrated that subfamily III receptors tend to regulate genes with lower sensitivity to ABA, in line with the fact that these receptors showed a lower affinity for ABA in the plants.

Introduction

ABA is involved in different facets of plant development and participates in both abiotic and biotic stress responses. The proper action of ABA signaling is highly dependent on the core ABA signaling pathway, as described in the previous chapter. As a major player

in the core ABA signaling pathway, ABA receptors are encoded by multigenic families, whose members are largely functionally redundant. *Arabidopsis* encodes 14 ABA receptors, the PYR/PYL/RCAR receptors, that can be divided into three subfamilies (Figure 2.1) (Park et al., 2009). This is by far the largest receptor family of phytohormones.

Massive research has been conducted to study the difference between these receptors. The PYR/PYL/RCAR receptors exhibited a diversity in biochemical properties. Subfamily III receptors (PYR1, PYL1-3) encode dimeric receptors, while the other subfamilies are monomeric. Subfamily III showed lower sensitivity and affinity to ABA than the other two subfamilies (Nishimura et al., 2009; Hao et al., 2011; Okamoto et al., 2013). This property was assessed by a very fundamental experiment in biochemistry, PP2C assay. This assay is used to illustrate the receptor-mediated inhibitory effect of ABA on PP2C by using a serial of ABA doses. The IC_{50} (dose of ABA gives 50% inhibition of PP2Cs) of each receptor in this assay indicated the sensitivity of the receptor to ABA; the lower the value, the higher the sensitivity. The IC_{50} of each receptor is presented in Figure 2.1. This difference in affinity may be due to the thermodynamic penalty imposed by dimer dissociation since the receptors should function as the inhibitor of PP2C in the monomeric state (Dupeux et al., 2011; Helander et al., 2016).

The distinct biological properties of PYR/PYL/RCAR receptors suggested that they might be involved in different ABA signaling. ABA selective agonists and antagonists, which are only active on a specific subset of ABA receptors, are an effective tool to study the distinct role of ABA receptors. Previous studies showed that pyrabactin is a selective ABA agonist which can specifically promote the interaction of PP2C with a subset of ABA receptors (especially potent with PYR1) (Park et al., 2009; Helander et al., 2016). And since

pyrabactin can inhibit seed germination to a great extent, it can be illustrated that PYR1 plays a key role in ABA-dependent seed germination inhibition (Park et al., 2009). Quinabactin (QB) is also an effective agonist of ABA, and it mostly strongly activates the dimeric subfamily III receptors and weakly actives PYL5. Application of QB induced guard cell closure and reduced transpiration, which suggested that the dimeric receptors are vital under water deficit situations (Okamoto et al., 2013). Hexabactin (HB) is a selective ABA agonist which preferentially activates the monomeric receptors. It was not sufficient to induce a strong ABA-like response as QB in ABA-mediated amino acid accumulation, which demonstrated that the monotonic receptors were less likely to participate in this biological process (Helander, 2017). Since the agonists or antagonists which are only effective on a certain subfamily of ABA receptors are not available, it is hard to use this chemical tool to investigate the functions of different receptor subfamilies.

Mutants of different receptors have been used to investigate the function of different ABA receptors. Most of the single mutants of PYR/PYL/RCAR receptors have a weak or no phenotype in the control of stomatal conductance and transcriptional responses (Park et al., 2009; Gonzalez-Guzman et al., 2012). However, the single mutants of receptors with high affinity to ABA behaved differently under stress. For instance, Zhao et al. discovered that the *pyl9* single mutant showed reduced leaf senescence compared with the wild type (Zhao et al., 2016). *Pyl4* and *pyl5* single mutants were hypersensitive to JA and exhibited a significant decrease in shoot biomass (Lackman et al., 2011). In addition, some transgenic plants with the expression of a single receptor driven by promotors from other genes were used to explore the receptor functions. In Zhao's study, *pRD29A::PYL9* were used and showed enhanced ABA-indued leaf senescence, and this evidence supports that PYL9 promotes ABA-mediated drought resistance and leaf senescence. Another

example using transgenic plants was conducted by Quan; in their study, *pGC1::AtPYL5* transgenic *Arabidopsis* exhibited a reduced transpiration rate and decreased water loss after drought treatment, which suggested that PYL5 is involved in drought tolerance (Quan et al., 2018). Most of the studies would rather use double mutant or even high-order receptor mutants to dissect the function of ABA receptors. *pyl8/pyl9* double mutant showed a longer ABA-induced quiescence on lateral root growth and reduced sensitivity to ABA on primary root growth and lateral root elongation, which suggests that these two receptors play an important role in regulating lateral root growth (Xing et al., 2016). Higher-order mutants *pyl1/2/3/4/5/6/12* and *pyl7/8/9/10/11/13* were generated and used to study their roles in rice growth and productivity (Miao et al., 2018). Zhao et al. generated the *pyl* quattuordecuple mutant removing all 14 ABA receptors. The mutant was severely impaired and couldn't be used for experiments. By using the *pyl* duodecuple mutant *pyr1pyl1/2/3/4/5/7/8/9/10/11/12*, they found the mutant was extremely insensitive to ABA effects on seed germination and other aspects of ABA signaling (Zhao et al., 2018). However, none of the studies generated the receptor subfamilies mutants to explore the specific functions of distinct receptor subfamilies.

In this study, we generated three ABA receptor subfamily mutants, which are denoted as *subI*, *subII*, and *subIII*, using a combination of genetic crossing and CRISPR/Cas9 technology. The characterization of these mutants provides essential insights into the diversity of functions of ABA receptor subfamilies.

Methods and Materials

Construction of Different Subfamilies of ABA Receptor Mutants

The *pyr1/pyl1/pyl2/pyl3* quadruple mutant (*subIII*, *0/1/2/3*), *pyl4/pyl5/pyl6/pyl11/pyl12/pyl13* sextuple mutant (*subII, 4/5/6/11/12/13*), and the *pyl7/pyl8/pyl9/pyl10* quadruple mutant (*subI, 7/8/9/10*), three ABA receptor subfamily mutants, were generated by a combination of genetic crossing and CRISPR/Cas9 technology. The physical map is provided in Appendix Figure 2.1A.

To generate *subI* and *subII*, *pyl4*, *pyl5*, *pyl8*, and *pyl9* single mutants were firstly isolated from T-DNA knockout lines obtained from the *Arabidopsis* Biological Resource Center (www.arabiopsis.org) (Sail_517_C08, SM_3_3493, SALK_1269_A02, and SALK_083621C, respectively). The homozygous mutants were selected followed the T-DNA genotyping pipeline described previously (O'Malley et al., 2015).

For constructing the *subI* mutant, the *pyl8/pyl9* double mutant was first obtained by crossing *pyl8* and *pyl9* single mutants. Then the mutation of *pyl7* and *pyl 10* was introduced to the homozygous double mutant separately by CRISPR/Cas9, and two triple mutants, *pyl7/pyl8/pyl9* and *pyl8/pyl9/pyl10*, were generated from this procedure. Finally, the quadruple mutant *subI* was obtained from the cross of those homozygous triple mutants.

To generate the *subII* mutant, we first crossed the *pyl4* and *pyl5* single mutants to get the homozygous *pyl4/pyl5* double mutant. Then *pyl6*, *pyl11*, and *pyl12* were introduced to the double mutant by CRISPR/Cas9. Among the T2 generation, we isolated a heterozygous quintuple mutant *pyl4/pyl5/pyl6/pyl11/pyl12* ("*4/5/6/11/12*"), then this mutant was crossed

to the *pyl4/pyl5* double mutant to get the homozygous quintuple mutant "*4/5/6/11/12*". Finally, the *pyl13* was introduced to the quintuple mutant to obtain the *subII*.

For *subIII* mutant, *pyr1/pyl1* double mutant was isolated in the process of construction of quadruple mutant (*pyr1/pyl1/pyl2/pyl4*) strain (Park et al., 2009). *Pyl2* and *pyl3* mutations were introduced by CRISPR/Cas9 technology to the double mutant to get the *subIII* mutant. This mutant is referred to as *subIII* #1 and used in the RNA-seq experiment. However, this mutant has the Ler background since *pyl2* is a T-DNA insertion line which is in the Ler background. So we generated a new *subIII* mutant which has mutations in four subfamily III receptors by CRISPR/Cas9. The new mutant strain is referred to as *subIII* new (The physical maps were shown in Appendix Figure 2.1B). Besides, we also used another *subIII* mutant generated independently by our collaborator, Dr. Masanori Okamoto, referred to as *subIII* M1.

Generation of Corresponding Partial Complementation Lines for *subII* and *subII*

Genomic DNA of AtPYL4 (AT2G38310), AtPYL5 (AT5G05440), AtPYL7 (AT4G01026), and AtPYL8 (AT5G53160) including promoter region and coding sequences were PCR amplified. The terminators including stop codon were amplified separately to introduce tag sequences (3x Flag-6x His) at the 3' end of coding sequences. The following sequences are 5' of promoter (F) and 3' end of terminator ® that used to amplify genes for partial complementation strains.

AtPYL4gF: GTGAAGCTCAATACACAATA

AtPYL4gR: AAGTTTGAGGACCTAGTTAAATCA

AtPYL5gF: CGTTATTCTTACAGGGCATGA

AtPYL5gR: GACAGTGGAACAGTTATTGGCT

AtPYL7gF: GTGTGTAACGAGCCAACTCTAG

AtPYL7gR: CAGGTTATGTGCCAGACACAAG

AtPYL8gF: CTATCCAATAATTGAGTCAGCTCTC

AtPYL8gR: CAGCTTACAAGGTCCTCTGATG

The amplified sequences including the tagged fragment were assembled. AtPYL4-AtPYL5-Flag-His and AtPYL7-AtPYL8-Flag-His were assembled by Golden Gate Assembly (GGA) method or HiFi assembly method. The assembled sequences were cloned into pCambia 3300 vector to make the following two constructs (Appendix Figure 2.2, image generated by Snapgene^{TM} software).

pCambia-proAtPYL4::AtPYL4-Flag-His-proAtPYL5::AtPYL5-Flag-His-CaMV35S::mCherry

pCambia-proAtPYL7::AtPYL7-Flag-His-proAtPYL8::AtPYL8-Flag-His-CaMV35S::mCherry

Both constructs have mCherry as a selection marker. These constructs were transferred to *Agrobacterium tumefaciens* C58 by electroporation and used to transform the *subII* and *subI* mutants following the floral dip method (Clough and Bent, 1998), respectively to make the corresponding partial complementation lines 4+5/*subII* and 7+8/*subI*. By screening the T3 progeny, two independent lines were tested homozygous for each partial complementation line. All the T3 seeds exhibited red fluorescence, and these partial complementation lines were referred to as 4+5/*subII* #3-4, 4+5/*subII* #7-12, 7+8/*subI* #9-12, and 7+8/*subI* #14-11, respectively. Then these T3 seeds were used for the seedling establishment assays.

Seedling Establishment Assays

Greening experiments for the Col-0 and the mutants were performed in 24-well polystyrene petri plates as previously described (Vaidya et al., 2021). The seeds were gas sterilized and plated onto ½ Murashige-Skoog (MS) medium (0.25% sucrose and 0.7% agar, pH 5.7) supplemented with ABA or ABA agonists. The same amount of DMSO (0.5% v/v) was supplemented to the ½ MS on the same plate as the mock treatment.

The *subI* mutants and the corresponding partial complementation lines (7+8/*subI* #9-12 and 7+8/*subII* #14-11) were treated with 6.8 µM QB (Quinabactin); *subII* mutants and the corresponding partially complementation lines (4+5/*subII* #3-4 and 4+5/*subII* #7-12) were treated with 1.2 µM ABA, and the *subIII* mutants (*subIII* #1, *subIII* M1, *subIII* new) were treated with 16.2 µM HB (Hexabactin). Col-0 was included in all the experiments. Three biological replicates were included in the experiment.

After 4 days of stratification (4 ℃), the plates were transferred to a growth chamber under 16-hour day/8-hour night illumination and photographed on both day 0 and day 6. Seed counts (day 0) and green pixel counts (day 6) were quantified using ImageJ (v2.9.0) through modification of the Hue, Saturation, and Brightness thresholding parameters selected to include only the seeds (day 0) or green cotyledons (day 6). The % greening was used to describe the average seedling establishment for each genotype under different treatments. This parameter was calculated in the following steps. Firstly, the greening area per seed in each well was calculated by dividing the greening area (green pixel counts on day 6) by the number of seeds (seed counts on day 0) in each well. The greening per seed in each well was normalized to the average value of the greening per seed of Col-0 under mock treatment.

ABA Treatment for Three Subfamily Mutants and Col-0

The seeds of *Arabidopsis* thaliana wild-type (Col-0) and three subfamily mutants (*subI*, *subII*, and *subIII* #1) were sterilized with 70% ethanol and 0.05% Triton X-100 for 7 minutes, followed by 70% ethanol for another 7 minutes, and then washed with 100% ethanol for one time, and another wash with sterile distilled water for three times. The sterilized seeds were sown on the top of a square nylon mesh (1.5 inches * 1.5 inches, 100 μm mesh) on a the ½ Murashige-Skoog (MS) medium (0.25% sucrose and 1% agar, pH 5.7) before kept at 4 ℃ for four days, and then grown vertically as previously described (Bargmann and Birnbaum, 2010) under 16h/8h light/dark at 22 ℃ for 6 days before the treatments.

The nylon meshes carrying the seedlings were treated on 2 layers of filter paper soaked with 6 mL of ½ MS liquid medium (0.25% sucrose, pH 5.7) supplemented with either DMSO control or different concentrations of ABA for 10 hours. The ABA was first dissolved and diluted to 12 different concentrations in DMSO and then diluted to the final concentrations (0 μM, 0.003 μM, 0.01 μM, 0.03 μM, 0.09 μM, 0.27 μM, 0.8 μM, 2 μM, 7 μM, 22 μM, 102 μM, 160 μM, and 200 μM) by ½ MS liquid medium (0.25% sucrose, pH 5.7), and the DMSO control contained the same amount of DMSO (0.1% v/v). Each treatment has three biological replicates. The seedlings were harvested by lightly scraping them off the nylon mesh and collected in the 1.5 mL tubes, and then frozen in liquid nitrogen.

RNA Extraction and Library Preparation

The total RNA was extracted using RNeasy Plant Mini Kit (QIAGEN, Cat No. 74904), and an on-column DNase digestion was performed by the RNase-Free DNase Set (QIAGEN, Cat No. 79254) during the purification. After the extraction, the purity and the quality of RNA were assessed by gel electrophoresis.

Approximately 2.5 μg of the purified RNA of each sample was used as the starting material to isolate intact poly(A)+ RNA by NEBNext Poly(A) mRNA Magnetic Isolation Module (NEB #E7490). The cDNA libraries were then constructed by NEBNext Ultra RNA Library Prep Kit (NEB #E7530) as described in the manufacturer's instructions. During the preparation, the clean-ups were done by the Agencourt AMPure XP PCR purification system (Beckman Coulter, A63881), and the NEBNext Multiplex Oligos (Index Primers Set 1-48; NEB #E7735S, NEB #E7500S, NEB #E7710S, and NEB #E7730S) were used to barcode the libraries. The Bioanalyzer is used to assess the quality and concentration of the libraries.

Illumina Sequencing and Data Preprocessing

The sequencing for the libraries was performed on the HiSeq platform by Novogene Corporation Inc. Four lanes were used, and barcoded libraries were pooled together randomly to be sequenced for each lane.

The analysis of the sequencing results followed the workflow for RNA-Seq described in the SystemPipeR package (H Backman and Girke, 2016). Briefly, the raw reads were mapped against the *Arabidopsis* genome using TopHat2 (Kim et al., 2013). The reads counting was performed by the summarizeOverlaps function in the GenomicAlignments package (Lawrence et al., 2013). The genes with CPM (count per million) above 10 in at

least 3 samples and have at least 15 reads across all the samples are defined as expressed genes. After this filtering process, 20181 genes are considered in the following analysis. The edgeR package was used for the ANOVA test and pairwise sample comparison (Robinson et al., 2010).

Functional Enrichment Analysis

ClusterProfiler was used for functional enrichment analysis (Yu et al., 2012; Wu et al., 2021). GO (Gene Ontology) and pathway enrichment analysis was applied to the DEGs identified in each mutant. The *p*-value was calculated by Fisher's exact test. FDR was used to correct *p*-values. Significant GO terms and pathways were identified with a cutoff for adjusted *p*-value (adj. *p*-value < 0.05). Fold enrichments for all the enriched terms were also calculated to interpret the results better. It is defined as the ratio of the frequency of input genes annotated in a term to the frequency of all genes annotated to that term.

In order to get a more effective interpretation from the analysis, some redundant GO terms (with semantic similarities over 0.7) were removed by applying the *simplify* function in the package. This function can only remove the highly similar GO terms. Some GO terms with a parent-child semantic relationship having exactly the same *p*-values and geneRatio (ratio of input genes that are annotated in a term) were still in the enriched GO term list. For those GO terms, the parent terms were eliminated.

Results

Removal of ABA Receptor Subfamilies Leads to Reduced Sensitivity to ABA

Since the homologous ABA receptor genes in the same subfamily may have functional redundancy, we generated mutants of three receptor subfamilies separately, i.e., *subI* (*pyl7/pyl8/pyl9/pyl10* quadruple mutant), *subII* (*pyl4/pyl5/pyl6/pyl11/pyl12/pyl13* sextuple

mutant), and *subIII* #1 (*pyr1/pyl1/pyl2/pyl3* quadruple mutant). Seedling establishment experiments was performed to investigate whether the removal of the receptors could affect their sensitivity to ABA or ABA agonists.

As shown in Figure 2.2A, the germination of Col-0 was inhibited to a great extent by ABA or ABA agonists, and all the receptor subfamily mutants had lower sensitivity to ABA or ABA agonists compared to the wild type. The partial complementation lines for subI and subII could fully restore the phenotype of wild type under ABA agonists treatment. We don't have partial complementation lines for *subIII* #1 for now since the background issue described in the materials and methods. However, a new *subIII* mutant (*subIII* new) and another *subIII* mutant generated by another lab independently (*subIII* M1) were also tested for seedling establishment. All the *subIII* mutants showed reduced sensitivity to Quinabactin, a selective ABA agonist. The difference observed in the experiments were significant statistically (Figure 2.2B).

The Effect of Different ABA Receptor Subfamilies Mutations on ABA-Regulated Gene Expression

In Chapter 1, we identified a robust set of ABA-responsive genes. Since ABA receptors play a vital role in ABA signaling and different ABA receptor subfamilies have a distinct affinity to ABA and tend to be involved in different signaling pathways, we further investigated whether removing the different subfamily receptors could affect the behavior of the ABA-responsive genes.

The three subfamily receptor mutants, *subI*, *subII*, and *subIII #1* were treated with 13 concentrations of ABA as previously described in Chapter 1. According to the MDS plot (Figure 2.3 B), the transcriptional profile of *subIII* samples was well-separated from the

wild type, while the other two receptor subfamily mutants tended to cluster together with Col-0. In addition, the plot also showed great agreement between the three biological replicates. The maximum ABA response of all ABA-responsive genes was compared between the wild type and each mutant (Figure 2.3C). If the maximum expression of the gene under ABA treatment in the mutant is the same as that in the wild type, then the point would fall onto the diagonal line. The scatter plot showed that the linear regression lines of points in all three mutants were all tilted and away from the diagonal line. As shown in the MDS plot, we observed the largest effect of the mutation in subfamily III receptors on all the ABA-responsive genes.

The differentially expressed genes (DEGs) in each mutant were identified first by a two-way ANOVA-like test (FDR < 5E-6) to select the genes significantly differentially expressed in the mutant compared with Col-0 at any concentration of ABA, and then a pairwise comparison (|FoldChange| $\geqslant$ 1.5, FDR < 0.001) described in the edgeR package. In total, 325, 651, and 3488 DEGs were identified in *subI*, *subII*, and *subIII*, respectively, with *subIII* having the largest number of DEGs compared with the wild type (Figure 2.4A). In addition, there were more DEGs (2881) identified only in the *subIII* mutant than that in the other two receptor subfamily mutants, which is another evidence that the removal of subfamily III receptors has the largest effect on ABA-regulated gene expression. Besides, most of the DEGs in *subI* (263/325, 80.9%) and *subII* (491/651, 75.4%) are also identified in *subIII*.

The comparison of the maximum ABA response of genes between mutant and wild type was also conducted among the DEGs identified in each mutant (Figure 2.4B). The results showed that the removal of subfamily III reduced the expression of the ABA-responsive

DEGs to a significant extent compared to that in the wild type. Interestingly, the ABA-responsive DEGs identified in *subI* and *subII* presented an increased expression compared to the wild type.

ABA Receptor Subfamilies Regulate Genes With Different Sensitivity to ABA

In the previous Chapter, we established that we can use ED_{50} and BMD values to illustrate the sensitivity of genes to ABA. Since it is hard to generate a clear dose-response curve for most of the DEGs identified in the mutants, we investigated whether there are any differences in the sensitivity of those DEGs to ABA in the wild type. We estimated the ED_{50} and BMD values of the DEGs identified in each mutant from the wild-type dose-response curves, and as shown in the violin plot, the genes differentially expressed in the *subIII* had significantly higher ED_{50} and BMD compared with the other two mutants. This is supported by the stacked bar plot (Figure 2.4B), most of the DEGs in *subIII* fall into the clusters with medium sensitivity to ABA, while in the other mutants, the largest number of DEGs were in high-sensitivity clusters. Besides, the up-regulated genes were dominant in DEGs identified in *subIII*, and there were more down-regulated DEGs than the biphasic and up-regulated DEGs in the other two mutants, and the down-regulated genes tend to be more sensitive to ABA than the genes with an up-regulated trend (Figure 1.2E).

These observations implied that subfamily III receptors tend to regulate genes that are less sensitive to ABA, which is in correlation with the fact that subfamily III receptors have a lower affinity for ABA than the receptors in the other subfamilies.

Functional Analysis of Differentially Expressed Genes in Mutants

To gain an overview of the functions of the DEGs identified in each mutant, we carried out GO enrichment analysis between the DEGs in the three mutants. In total, we identified 192, 10, and 70 GO terms belonging to Biological Process, Cellular Component, and Molecular Function, respectively, and 24 significant pathways in KEGG analysis. The GO terms enriched in the Biological Process category were further classified into 5 types as described in Chapter 1. The results are presented in Figure 2.5 and Appendix Figure 2.3. There are a lot of overlapped enriched GO terms in *subIII* and the other two mutants since there are a lot of overlapped genes identified in the *subIII* mutant with the other two mutants.

As expected, ABA-response-related GO terms were enriched in all mutants to a similar extent. GO terms associated with aging, leaf senescence, seed germination, maturation, dormancy, and response to ethylene were enriched in all mutants with *subIII* having the highest enrichment. Interestingly, some GO terms were enriched in all the mutants, but *subI* has the highest enrichment, such as “response to nematode”, “response to cold”, “response to desiccation”, “response to red or far red light” and “sucrose transport”.

Some interesting GO terms were only enriched in *subII* and *subIII*. Most of them have a higher fold enrichment in *subIII* than *subII*, such as GO terms related to water transport, response to salt and salinity, immune response associated GO terms, response to GA and SA, and detoxification. While GO terms associated with the auxin signaling were enriched in *subII* with a higher fold enrichment than in *subIII*.

A lot of unique GO terms are enriched only in *subIII*, such as cell wall biogenesis, lateral root and tropism, stomata closure-related, response to light intensity, response to blue

light, flavonoids biosynthesis, and fatty acid biosynthesis process. Interestingly, GO terms associated with JA signaling and hyperosmotic stress response were only enriched in *subII*.

Discussion

In this research, we conducted RNA-seq experiments on the three *pyl* mutants removing the ABA receptor subfamilies and exploring whether the removal of the receptor subfamilies altered the genome profiling of ABA-responsive genes.

The results showed that the removal of subfamily III receptors has the largest effect on ABA-regulated gene expression, and there was a large overlap in identified DEGs and enriched GO terms between *subIII* and the other two mutants. This suggests that even with a relatively low affinity to ABA, the dimeric receptors play a relatively more vital role in ABA response and may be involved in almost all the aspects of ABA signaling than the monomeric receptors. Our results also demonstrated that the subfamily III receptors tend to regulate genes with lower sensitivity to ABA than the other two receptor subfamilies, which is in line with the biochemical difference between the receptor subfamilies.

Our results suggested that the other two subfamilies may play a relatively less important role in ABA signaling. However, the experiments were conducted using seedlings, thus the other two subfamily receptors might be vital at a later stage of plant development. Besides, only one-time point was used in the research. Previous studies have shown that the expression levels of genes under phytohormone treatments changed over time, including ABA (Nemhauser et al., 2006). Since subfamily I and subfamily II receptors have a higher affinity to ABA, they might account for the rapid responses under ABA treatment.

ABA-signaling-related GO terms were enriched in all subfamily mutants, while according to the dose-responsive curves, subfamily III may play a major role in regulating the expression of those important players on the transcriptional level since the expression of these genes was greatly reduced in *subIII* mutants (Figure 2.6A). To our surprise, some of those genes were slightly up-regulated in the *subII* mutant, as we have observed in Figure 2.4B. A similar trend was observed in the responses of all the representative genes we selected in Chapter 1 (Figure 2.6). However, the insensitivity of the *subI* and *subII* to ABA or ABA agonists suggested that those two subfamily receptors are also important for ABA signaling. We hypothesized that maybe the regulation of those receptors was mainly on the post-transcriptional level in the ABA signaling, but this needs to be validated in the future.

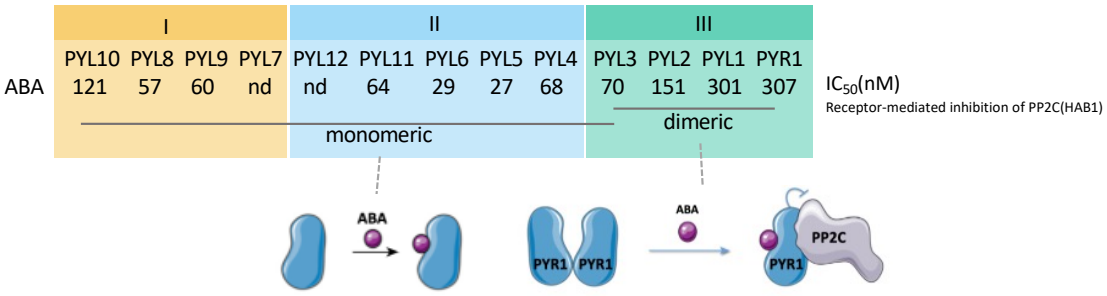

Figure 2.1 Affinity of *Arabidopsis* ABA receptor subfamilies. Adapted from Okamoto and Rodriguez's paper (Okamoto et al., 2013; Rodriguez and Lozano-Juste, 2015), the numbers underneath each receptor presented the IC_{50} of each receptor in receptor-mediated inhibition of PP2C assay.

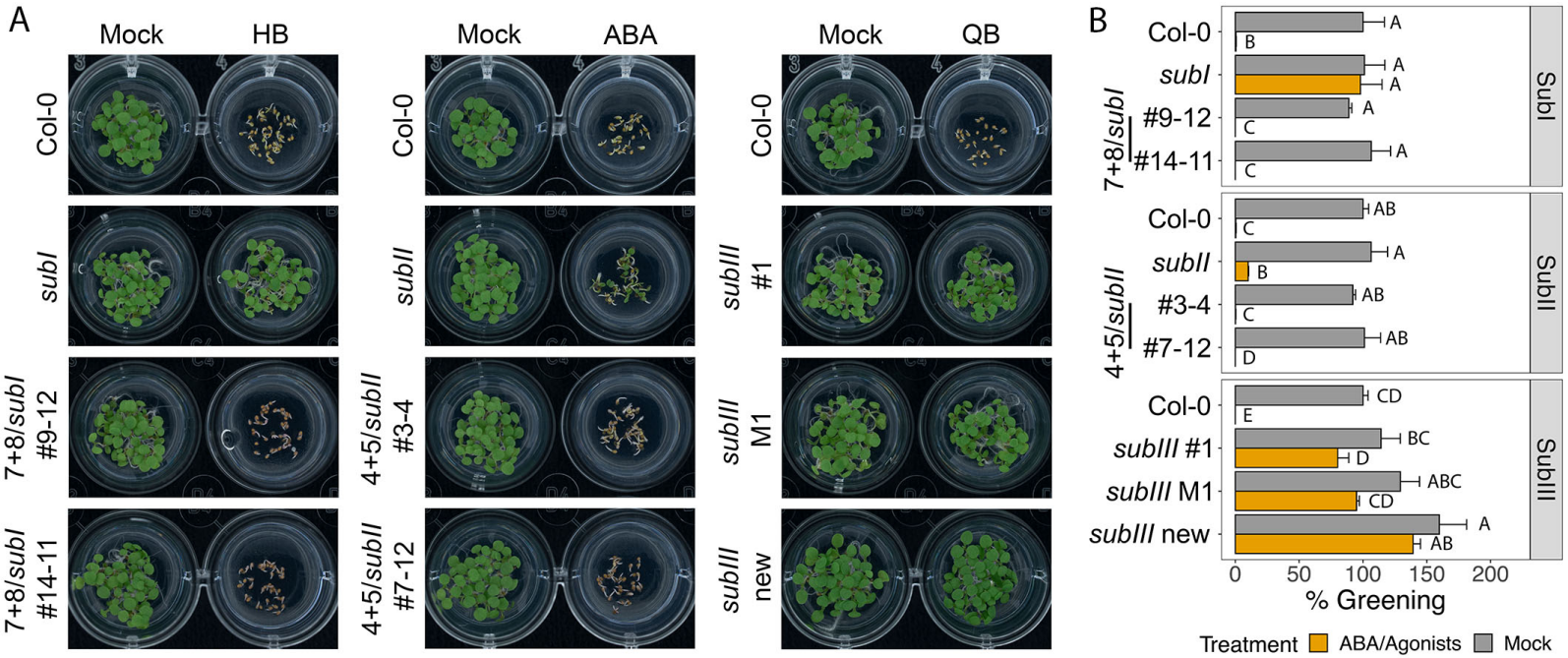

Figure 2.2 Receptor subfamily mutants are less sensitive to ABA/ABA agonists. (A) Phenotypes of mutants under ABA/ABA agonist treatment. Col-0, *subI* and its partial complementation lines were treated with either DMSO(Mock) or Hexabactin (HB); Col-0, *subII* and its partial complementation lines were treated with either DMSO(Mock) or ABA; Col-0 and three *subIII* mutants were treated with either DMSO (Mock) or Quinabactin (QB). HB and QB are selective ABA agonists. The photos were taken at Day 6 after stratification. **(B)** Seedling establishment of mutants under ABA/ABA agonist treatment. The seedling establishment was measured by quantifying the green cotyledon area normalized to seed number 6 days after stratification. % Greening was calculated by normalizing the greening area per seed of different genotypes under different treatments by that of Col-0 under mock treatment. Upper case letters indicate the significant difference between different genotypes under each treatment assessed by Tukey's test ($p < 0.01$).

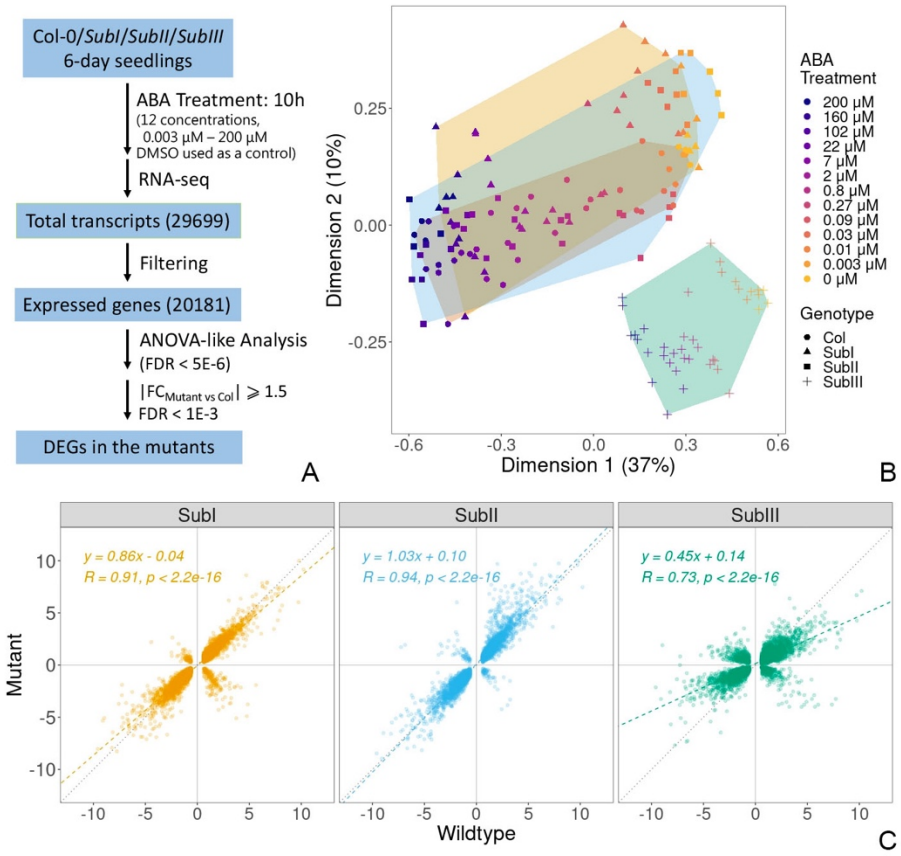

Figure 2.3 Transcriptional profiles of ABA-responsive genes in the mutants. (A) Workflow of libraries preparation and the procedure for selection of DEGs in the mutants. The numbers in the parentheses are the number of genes left after each step. **(B)** MDS plot of gene expression in each mutant under each ABA treatment. The genotypes were indicated by the point shape, and the same genotype were enclosed in the same color of ellipse (red: Col-0, yellow: SubI, blue: SubII, Green: SubIII). "SubI", "SubII", and "SubIII" are short for subfamily I, subfamily II, and subfamily III, respectively, the same in the following plots. All three biological replicates were presented in the plot. **(C)** Comparison of maximum ABA response of all ABA-responsive genes in the mutant and wildtype. The axes plot maximum $\log_2$-transformed expression under ABA treatment compared to Mock treatment in either mutant (y axis) or wildtype (x axis). The dotted grey line is the diagonal line of the coordinates with the equation, y = x. The dashed lines in different color were the linear regression line fitted to the data. The equations of the line, Pearson correlation coefficient, and the *p*-value of F test were shown within the plot. The intercepts and the slopes estimated in the linear models were significant assessed by *t-test* (*p*-value < 0.001).

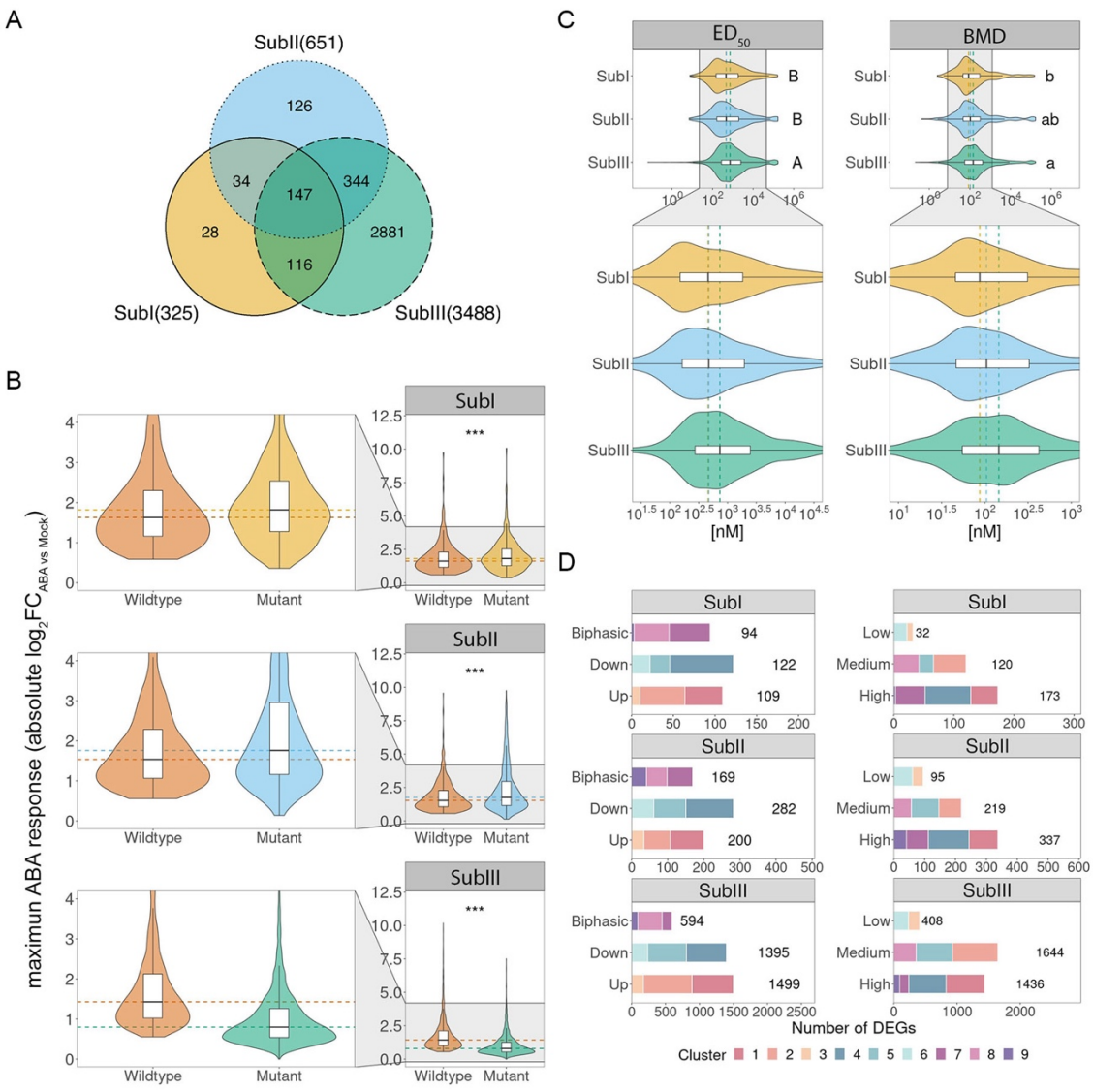
A
SubII(651)
126
34
147
344
28
116
2881
SubI(325)
SubIII(3488)
B
maximun ABA response (absolute log2FC ABA vs Mock)
SubI
SubII
SubIII
***
Wildtype
Mutant
C
ED50
BMD
SubI
SubII
SubIII
B
B
A
b
ab
a
[nM]
D
Biphasic
Down
Up
Low
Medium
High
94
122
109
32
120
173
169
282
200
95
219
337
594
1395
1499
408
1644
1436
Number of DEGs
Cluster 1 2 3 4 5 6 7 8 9

Figure 2.4 Comparisons of ABA-responsive DEGs identified in the mutants (A) Venn diagram illustrating the overlap of ABA-responsive DEGs identified in each mutant. The number in the parentheses after the subfamily names are the total number of ABA-responsive DEGs identified in the mutants. **(B)** Comparison of maximum ABA response of corresponding DEGs in each mutant and the wild type. The maximum ABA response was indicated by the absolute value of maximum log_2-transformed expression under ABA treatment compared to Mock treatment in either mutant or wildtype. *** indicated the significant difference between wildtype and the mutant assessed by permutation paired *t-test* ($p < 0.001$). Zoom-in plot for the y-axis are shown on the left side of each panel. **(C)** Violin plot showing distributions of BMD and ED_{50} estimated from the wild type DRCs of ABA-responsive DEGs identified in each mutant. The dashed lines in corresponding color are the median values of ED estimation in each mutant. The uppercase letters indicate the significant difference between different clusters assessed by Games and Howell's test ($p < 0.01$). Zoom-in plot for the x-axis are shown on the bottom of each panel. **(D)** Composition of cluster identities of the ABA-responsive DEGs in the mutants. The clusters were classified into three groups, the biphasic, down, and up, according to the dose-response trend of the DEGs on the left panel, while on the right panel, the clusters were classified into high, medium, low based on their sensitivity to ABA. The number on the side of each stacked bar represents the number of DEGs in each group.

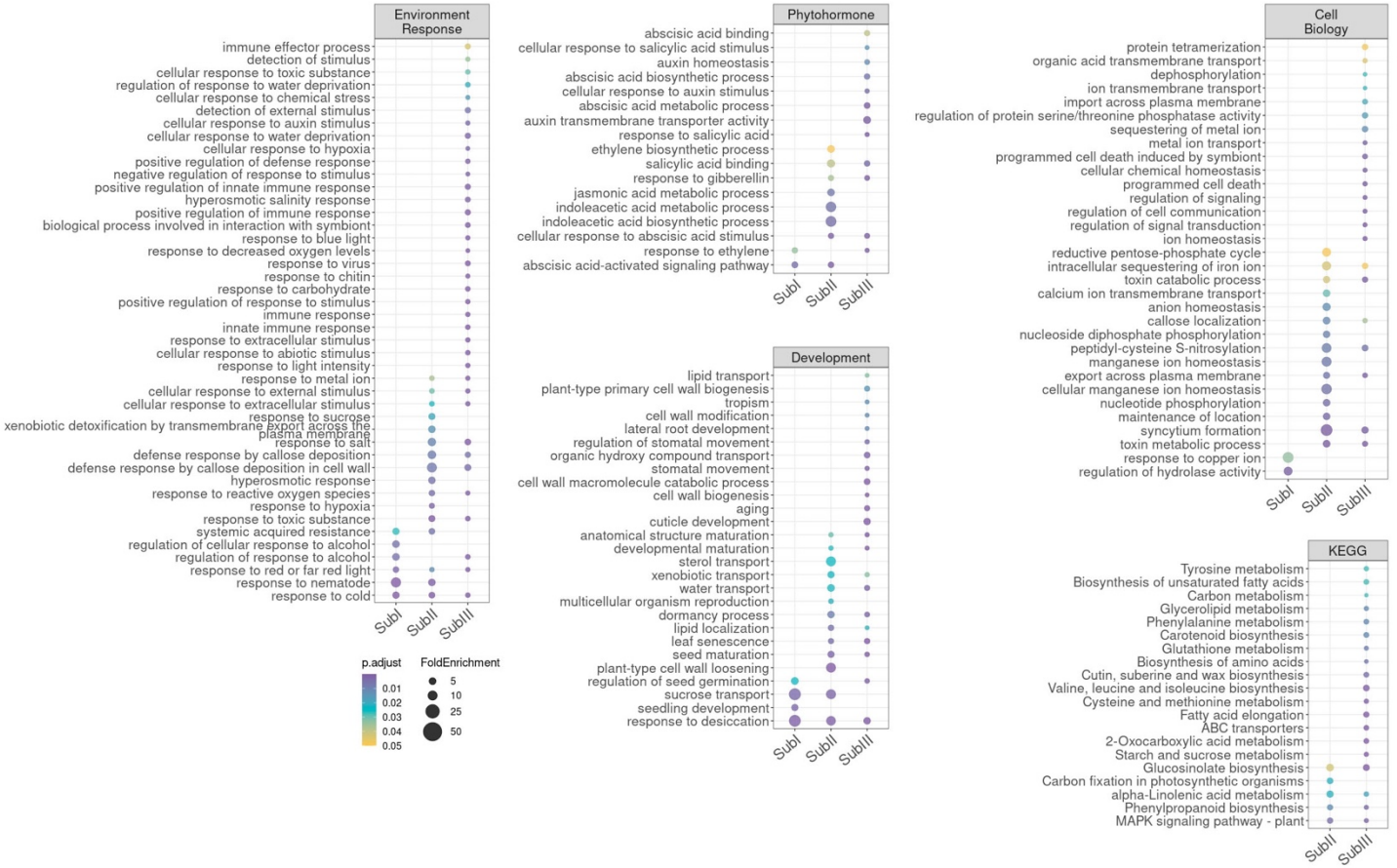

Figure 2.5 Comparison of functional profiles among DEGs in different mutants. Top GO (Gene Ontology) highly enriched among DEGs in different ABA receptor mutants (adjusted *p*-value < 0.05) were presented. The results were visualized as a dot plot with different facet panels indicating Metabolism classe in the Biological Process category and all the enriched GO terms in Molecular Function and Cellular Component categories, with the size of the dots indicating the fold enrichment and the color corresponding to the adjusted *p*-value of each enriched GO term.

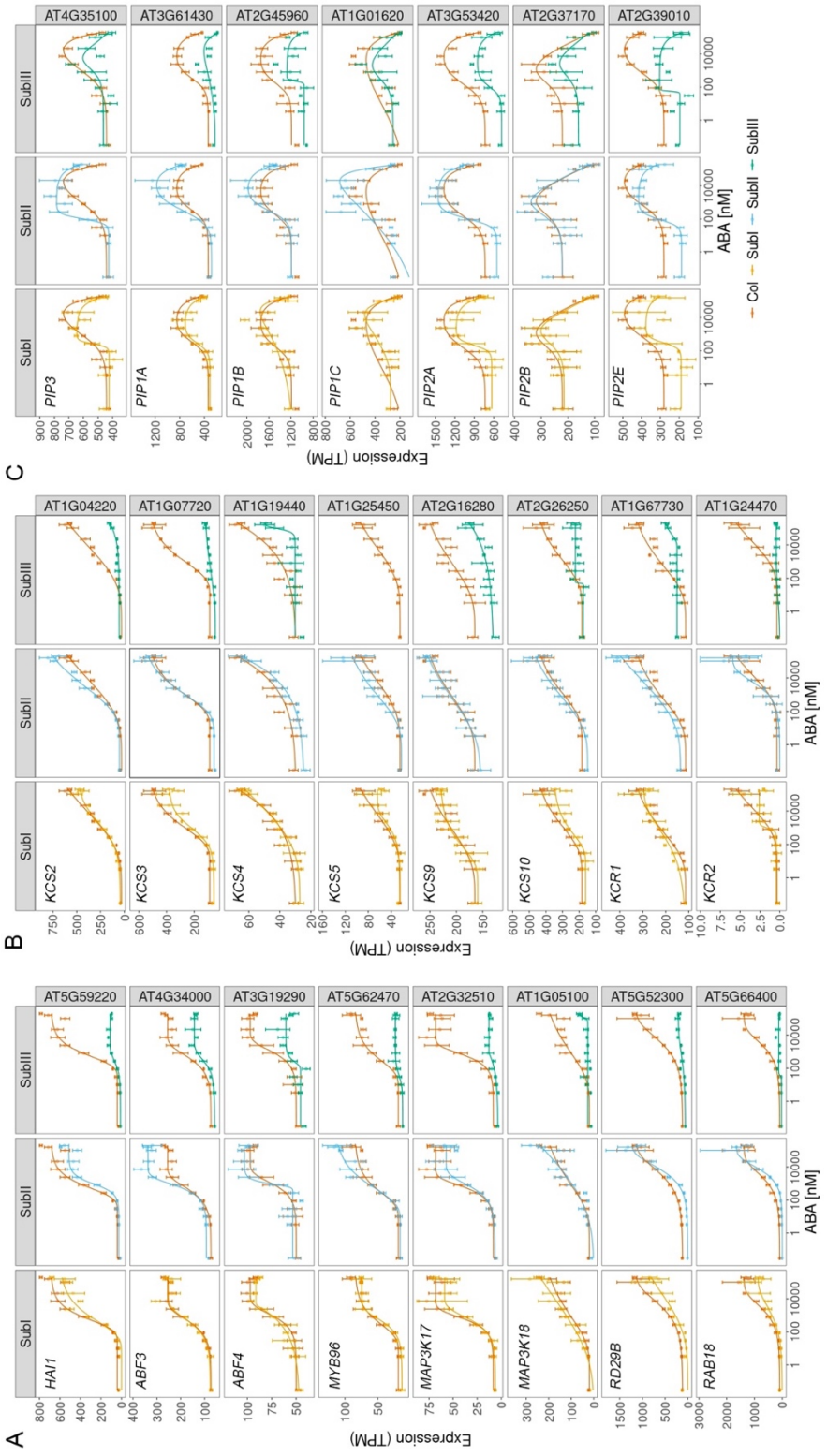
A
B
C
Expression (TPM)
ABA [nM]
Col
Subl
SublI
SublII
AT5G59220
AT4G34000
AT3G19290
AT5G62470
AT2G32510
AT1G05100
AT5G52300
AT5G66400
HAI1
ABF3
ABF4
MYB96
MAP3K17
MAP3K18
RD29B
RAB18
AT1G04220
AT1G07720
AT1G19440
AT1G25450
AT2G16280
AT2G26250
AT1G67730
AT1G24470
KCS2
KCS3
KCS4
KCS5
KCS9
KCS10
KCR1
KCR2
AT4G35100
AT3G61430
AT2G45960
AT1G01620
AT3G53420
AT2G37170
AT2G39010
PIP3
PIP1A
PIP1B
PIP1C
PIP2A
PIP2B
PIP2E

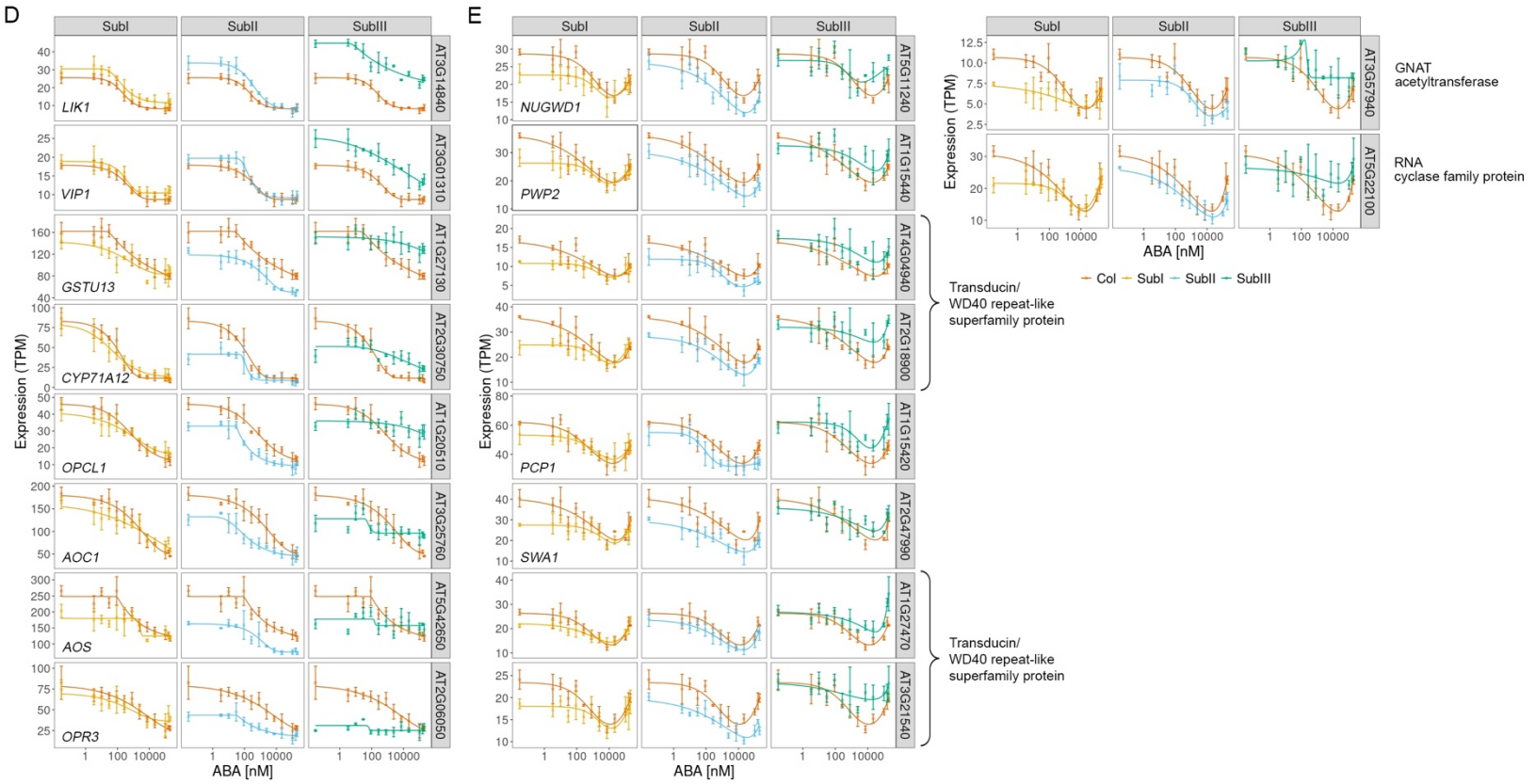

Figure 2.6 Dose-response curves of representative ABA-responsive genes. (A-E) plots showing the representative genes involved in the following pathways. The gene names were presented in the corner of each facet. **(A)** ABA signaling **(B)** Fatty acid biosynthesis **(C)** Aquaporins in water transport **(D)** Immune response & JA biosynthesis **(E)** rRNA biosynthesis

References

Bargmann BOR, Birnbaum KD (2010) Fluorescence activated cell sorting of plant protoplasts. J Vis Exp. doi: 10.3791/1673

Clough SJ, Bent AF (1998) Floral dip: a simplified method forAgrobacterium-mediated transformation of*Arabidopsis* thaliana. Plant J **16**: 735–743

Dupeux F, Santiago J, Betz K, Twycross J, Park S-Y, Rodriguez L, Gonzalez-Guzman M, Jensen MR, Krasnogor N, Blackledge M, et al (2011) A thermodynamic switch modulates abscisic acid receptor sensitivity. EMBO J **30**: 4171–4184

Gonzalez-Guzman M, Pizzio GA, Antoni R, Vera-Sirera F, Merilo E, Bassel GW, Fernández MA, Holdsworth MJ, Perez-Amador MA, Kollist H, et al (2012) *Arabidopsis* PYR/PYL/RCAR receptors play a major role in quantitative regulation of stomatal aperture and transcriptional response to abscisic acid. Plant Cell **24**: 2483–2496

H Backman TW, Girke T (2016) systemPipeR: NGS workflow and report generation environment. BMC Bioinformatics **17**: 388

Hao Q, Yin P, Li W, Wang L, Yan C, Lin Z, Wu JZ, Wang J, Yan SF, Yan N (2011) The molecular basis of ABA-independent inhibition of PP2Cs by a subclass of PYL proteins. Mol Cell **42**: 662–672

Helander JD (2017) Synthetic Agonists of Abscisic Acid Receptors and Their Metabolomic Effects on Plants. Doctor of Philosophy. UC Riverside

Helander JDM, Vaidya AS, Cutler SR (2016) Chemical manipulation of plant water use. Bioorg Med Chem **24**: 493–500

Kim D, Pertea G, Trapnell C, Pimentel H, Kelley R, Salzberg SL (2013) TopHat2: accurate alignment of transcriptomes in the presence of insertions, deletions and gene fusions. Genome Biol **14**: R36

Lackman P, González-Guzmán M, Tilleman S, Carqueijeiro I, Pérez AC, Moses T, Seo M, Kanno Y, Häkkinen ST, Van Montagu MCE, et al (2011) Jasmonate signaling involves the abscisic acid receptor PYL4 to regulate metabolic reprogramming in *Arabidopsis* and tobacco. Proc Natl Acad Sci U S A **108**: 5891–5896

Lawrence M, Huber W, Pagès H, Aboyoun P, Carlson M, Gentleman R, Morgan MT, Carey VJ (2013) Software for computing and annotating genomic ranges. PLoS Comput Biol **9**: e1003118

Miao C, Xiao L, Hua K, Zou C, Zhao Y, Bressan RA, Zhu J-K (2018) Mutations in a subfamily of abscisic acid receptor genes promote rice growth and productivity. Proc Natl Acad Sci U S A **115**: 6058–6063

Nemhauser JL, Hong F, Chory J (2006) Different plant hormones regulate similar processes through largely nonoverlapping transcriptional responses. Cell **126**: 467–475

Nishimura N, Hitomi K, Arvai AS, Rambo RP, Hitomi C, Cutler SR, Schroeder JI, Getzoff ED (2009) Structural mechanism of abscisic acid binding and signaling by dimeric PYR1. Science **326**: 1373–1379

Okamoto M, Peterson FC, Defries A, Park S-Y, Endo A, Nambara E, Volkman BF, Cutler SR (2013) Activation of dimeric ABA receptors elicits guard cell closure, ABA-regulated gene expression, and drought tolerance. Proc Natl Acad Sci U S A **110**: 12132–12137

O'Malley RC, Barragan CC, Ecker JR (2015) A user's guide to the *Arabidopsis* T-DNA insertion mutant collections. Methods Mol Biol **1284**: 323–342

Park S-Y, Fung P, Nishimura N, Jensen DR, Fujii H, Zhao Y, Lumba S, Santiago J, Rodrigues A, Chow T-FF, et al (2009) Abscisic acid inhibits type 2C protein phosphatases via the PYR/PYL family of START proteins. Science **324**: 1068–1071

Quan W, Hu Y, Mu Z, Shi H, Chan Z (2018) Overexpression of AtPYL5 under the control of guard cell specific promoter improves drought stress tolerance in *Arabidopsis*. Plant Physiol Biochem **129**: 150–157

Robinson MD, McCarthy DJ, Smyth GK (2010) edgeR: a Bioconductor package for differential expression analysis of digital gene expression data. Bioinformatics **26**: 139–140

Rodriguez PL, Lozano-Juste J (2015) Unnatural agrochemical ligands for engineered abscisic acid receptors. Trends Plant Sci **20**: 330–332

Vaidya AS, Peterson FC, Eckhardt J, Xing Z, Park S-Y, Dejonghe W, Takeuchi J, Pri-Tal O, Faria J, Elzinga D, et al (2021) Click-to-lead design of a picomolar ABA receptor antagonist with potent activity in vivo. Proc Natl Acad Sci U S A. doi: 10.1073/pnas.2108281118

Wu T, Hu E, Xu S, Chen M, Guo P, Dai Z, Feng T, Zhou L, Tang W, Zhan L, et al (2021) clusterProfiler 4.0: A universal enrichment tool for interpreting omics data. Innovation (Camb) **2**: 100141

Xing L, Zhao Y, Gao J, Xiang C, Zhu J-K (2016) The ABA receptor PYL9 together with PYL8 plays an important role in regulating lateral root growth. Sci Rep **6**: 27177

Yu G, Wang L-G, Han Y, He Q-Y (2012) clusterProfiler: an R package for comparing biological themes among gene clusters. OMICS **16**: 284–287

Zhao Y, Chan Z, Gao J, Xing L, Cao M, Yu C, Hu Y, You J, Shi H, Zhu Y, et al (2016) ABA receptor PYL9 promotes drought resistance and leaf senescence. Proc Natl Acad Sci U S A **113**: 1949–1954

Zhao Y, Zhang Z, Gao J, Wang P, Hu T, Wang Z, Hou Y-J, Wan Y, Liu W, Xie S, et al (2018) *Arabidopsis* Duodecuple Mutant of PYL ABA Receptors Reveals PYL Repression of ABA-Independent SnRK2 Activity. Cell Rep **23**: 3340-3351.e5

Chapter 3 Chemical Dissection of the Role of ABA Signaling in Osmotic Stress Gene Expression

Abstract

Osmotic stress impairs the production of almost all major crops. Endogenous ABA accumulated under osmotic stress, and a majority of genes were regulated by abscisic acid (ABA) to facilitate stress resistance. The osmotic-stress responders were usually classified into ABA-independent and ABA-dependent according to whether they are responsive to exogenous ABA. To investigate the ABA dependency of stress-responsive genes, we used Antabactin (ANT), a pan-antagonist for all ABA receptors, to block ABA signaling during osmotic stress caused by PEG treatment. The results showed that the "ABA-independent" genes defined by the previous approach were also affected by ANT, which suggested that they might also be ABA-dependent to some extent. Here, instead of classifying the osmotic-stress responders into two distinct groups, we define the ABA-dependency of genes under osmotic stress by the reduced effect of ANT on their osmotic response. We utilized a **π**-value to describe the extent of ABA-dependency of certain genes. **π**-value is the product of log-fold change and log-transformed *p*-value. Motif analysis shows that as the ABA dependency of the genes increases, i.e. the **π**-value increases, the more significant ABA-related motifs are enriched in the promoter region of those genes.

Introduction

Abiotic stresses, such as osmotic stress and drought, impair the productivity of almost all the major crops and constitute the primary cause of crop loss worldwide. As sessile organisms, plants must develop different strategies for adaptation to these environmental challenges.

It has been reported that osmotic stress increases the endogenous ABA level due to *de novo* biosynthesis (Guerrero and Mullet, 1986), which indicates the role of ABA in response to this environmental stimulus. Most research has been done to investigate the regulation of ABA in response to osmotic stress in plants (Ozfidan et al., 2013; Ji and Li, 2014). It has been reported that under osmotic stress, ABA interacts with LRD2 (lateral root development 2) and alters the depth of the root system, and inhibits the elongation of the primary root (Deak and Malamy, 2005). ABA could also reduce ROS (Reactive oxygen species) accumulation by inducing two Heat Shock Transcription Factors (HSFA6a AND HSFA6b) in response to osmotic stress (Wenjing et al., 2020).

Because of the essential role of ABA under osmotic stress, the expression of stress-responsive genes is usually classified into ABA-dependent and ABA-independent groups. Conventionally, most research defined the ABA-dependent pathway as the genes that respond to both osmotic stress and exogenous ABA application, while those significantly induced by osmotic stress but not responding to ABA are involved in the ABA-independent pathway (Yoshida et al., 2014). Liu et al. have identified 211 ABA-dependent differentially expressed genes (DEGs) and 1118 ABA-independent DEGs under osmotic stress by transcriptome sequencing and network analysis, and they also found there was an interplay between these two pathways (Liu et al., 2018). Roychoudhury et al. reviewed the

interaction or the convergence between these two pathways. They stated that crosstalk might be mediated by some transcription factors involved in both pathways (Roychoudhury et al., 2013).

The crosstalk between the ABA-dependent and ABA-independent pathways discovered in the previous study suggested that there might be a possibility that all the osmotic stress-responsive genes could be regulated by ABA to some extent.

It has been stated that ABA agonists were frequently used to investigate the role of ABA in certain signaling pathways in Chapter 2, while some antagonists of ABA were also developed in previous studies, such as DFPM ([5-(3,4-dichlor-ophenyl) furan -2-yl]-piperidine-1-ylmethanethione) (Kim et al., 2011), AS6 (Takeuchi et al., 2014), RK460 (Ito et al., 2015), PBI686 (Rajagopalan et al., 2016) and AA1 (ABA ANTAGONIST 1) (Ye et al., 2017). While none of them have been used to explore the influence of ABA in certain pathways.

In our study, a newly developed ABA antagonist, Antabactin (ANT, antagonist of ABA action), has been co-applied with PEG treatment to investigate the effect of ABA in osmotic stress. ANT has an inhibitory effect on all the ABA receptors in the PP2C assay. It makes it possible that we can use this pan-antagonist to inhibit endogenous ABA and get a better and more convincing picture of ABA-mediated signaling under osmotic stress.

Materials and Methods

Plant Materials and Treatment

The seeds of *Arabidopsis* thaliana wild-type (Col-0) were sterilized by 70% ethanol and 0.05% Triton X-100 for 7 minutes, followed by 70% ethanol for another 7 minutes, and then washed with 100% ethanol for one time, and another wash with sterile distilled water for three times. The sterilized seeds were sown on the top of a square nylon mesh (1.5 inches * 1.5 inches, 100 μm mesh) on a the ½ Murashige-Skoog (MS) medium (0.25% sucrose and 1% agar, pH 5.7) before kept at 4 ℃ for four days, and then grown vertically as previously described (Bargmann and Birnbaum, 2010) under 16h/8h light/dark at 22 ℃ for 8 days before the treatments.

The nylon meshes, along with the seedlings, were pretreated on 2 layers of filter paper soaked with 6 mL of ½ MS liquid medium (0.25% sucrose, pH 5.7) supplemented with either DMSO control or 25 μM ANT for 4 hours. The ANT was first dissolved in DMSO and then diluted to 25 μM by ½ MS liquid medium (0.25% sucrose, pH 5.7), and the DMSO control contained the same amount of DMSO (1% v/v). After the pretreatment, the nylon meshes together with the seedlings were transferred to another 2 layers of filter paper soaked with ½ MS liquid medium (0.25% sucrose, pH 5.7) containing either DMSO or 25 μM ANT in the presence or absence of 20% PEG for another 6 hours. Each treatment has three biological replicates. The seedlings were harvested by lightly scraping them off the nylon mesh and collected in the 1.5 mL tubes, and then frozen in liquid nitrogen.

RNA Extraction and Library Preparation

The total RNA was extracted using RNeasy Plant Mini Kit (QIAGEN, Cat No. 74904), and an on-column DNase digestion was performed by the RNase-Free DNase Set (QIAGEN, Cat No. 79254) during the purification. After the extraction, the purity and the quality of RNA were assessed by gel electrophoresis.

Approximately 2.5 μg of the purified RNA of each sample was used as the starting material to isolate intact poly(A)+ RNA by NEBNext Poly(A) mRNA Magnetic Isolation Module (NEB #E7490). The cDNA libraries were then constructed by NEBNext Ultra RNA Library Prep Kit (NEB #E7530) as described in the manufacturer's instructions. During the preparation, the clean-ups were done by the Agencourt AMPure XP PCR purification system (Beckman Coulter, A63881) and the NEBNext Multiplex Oligos (Index Primers Set 1-4; NEB #E7735, NEB #E7500, NEB #E7710, and NEB #E7730) were used to barcode the libraries. The quality and concentration of the libraries were assessed by the Bioanalyzer.

Illumina Sequencing and Data Preprocessing

The sequencing for the libraries was performed on the HiSeq platform by Novogene Corporation Inc. Four lanes were used, and barcoded libraries were pooled together randomly to be sequenced for each lane.

The analysis of the sequencing results followed the workflow for RNA-Seq described in the SystemPipeR package (H Backman and Girke, 2016). Briefly, the raw reads were mapped against the *Arabidopsis* genome using TopHat2 (Kim et al., 2013), and the reads counting was performed by the summarizeOverlaps function in the GenomicAlignments package (Lawrence et al., 2013). The genes with CPM (count per million) above 10 in at

least 3 samples and have at least 15 reads across all the samples are defined as expressed genes. After this filtering process, 19425 genes are considered in the following analysis. The edgeR package was used for the ANOVA test and pairwise sample comparison (Robinson et al., 2010).

Motif Enrichment Analysis

To determine whether known transcription factors (TFs) were enriched in the promoter region of each group of osmotic stress-responsive genes, we conducted an overrepresentation test by SEA algorithm in the MEME Suite (https://meme-suite.org/meme/tools/sea).

Briefly, the promoter sequences defined as the 1000 bp upstream of the transcription start site were retrieved from TAIR (version10). The sequences were then shuffled by using *shuffle_sequences()* function in *universalmotif* package to get the control sequences. Then the original promoter sequences and the control sequences were used as the input sequences in the SEA. This algorithm is used to search for known motifs from certain database in the provided sequences (Bailey and Grant, 2021). The *Arabidopsis* TF database, referred to as *Arabidopsis*DAPv1 in MEME, was used in the analysis (O'Malley et al., 2016). The motifs with E-value < 10 (default) were reported in the results. The enrichment ratio and the q-value, estimated from *p*-value using Benjamini & Hochberg correction, were provided by the program. The motifs with q-value < 0.01 were considered enriched motifs and used in the following analysis.

Results

ANT Alters the Transcriptional Profile of Osmotic-Stress-Responsive Genes

RNA-seq was conducted on wildtype Col-0 treated with or without ANT under osmotic conditions caused by 20% PEG treatment (Figure 3.1A). The MDS plot (Figure 3.2B) showed that the transcriptional profile of the ANT+PEG treatment was well-separated from the samples with PEG treatment only, and both of the treatments were separated from the Mock treatments, which indicated that ANT, the antagonist of ABA, could alter the expression level of osmostress-responsive genes genomewide. In addition, the samples with ANT treatment alone were clustered with the ones under Mock treatment, which indicated that the ANT may not have any effect on the development of plants under common conditions. The plot also showed great agreement among the three biological replicates.

Previous Classification of Genes Under Osmotic Stress Might be Biased

In this study, we identified a group of osmotic-stress-responsive genes with 5306 members by applying 20%PEG. As shown in Chapter 1, a set of ABA-responsive genes using the exogenous ABA application was also defined. Thus, we could classify the osmotic-stress responders into ABA-dependent and ABA-independent pathways as described in numerous previous studies, i.e., only the genes response to both exogenous ABA and osmotic stress are ABA-dependent. In our study, we identified a larger portion of ABA-dependent DEGs than the ABA-independent DEGs (Figure 3.2A), which is inconsistent with previous studies. This should be due to the fact that we used a serial concentration of ABA to identify the ABA-responsive genes, while the other studies usually used one concentration of ABA.

Though we identified more ABA-dependent participators in response to osmotic stress, the results with ANT treatments still suggested that the previous classification might be biased. As shown in Figure 3.2B, the expression level of both ABA-dependent and ABA-independent DEGs with or without ANT treatment under osmotic stress were compared. As expected, ANT treatment significantly repressed the transcriptional level of the ABA-responsive genes (ABA-dependent) since ANT could block the ABA signaling in the plants. However, the expression of osmotic stress responders classified into ABA-independent pathways was also reduced significantly.

We conducted a motif enrichment analysis to see whether the binding sites (motifs) of some well-known transcription factors (TFs) were enriched in the promoter region of both sets of genes. The TFs investigated in this study are bZIPs, DREBs, CBFs, MYBs, NACs, ERFs, and WRKYs. All of them are reported to be involved in osmostress responses in multiple reviews (Roychoudhury et al., 2013; Nakashima et al., 2014; Hrmova and Hussain, 2021). Appendix Figure 3.1 showed the results of motif enrichment for all TFs, and it turned out that except for some WRKY transcription factors, the binding sites of all the TFs were enriched in the promoter of both ABA-dependent and “ABA-independent” DEGs, though the significance of enrichment was relatively smaller in “ABA-independent” group. A group of bZIPs TFs that are well-characterized in previous studies and hypersensitive to ABA showed a great enrichment in the promoter region of both groups (Figure 3.2E), which provides strong evidence that DEGs defined as “ABA-independent” by the previous method was also ABA-responsive. Thus the previous classification might be biased, and almost all the osmotic stress-responsive genes are related to ABA signaling to some extent. The heatmap provides one possible explanation for this phenomenon (Figure 3.2C). Since the previous method only selected the significant ABA-

responsive genes with a certain cutoff for the foldchange in the expression, some ABA-responsive genes with relatively lower induction or reduction would be eliminated from the list.

Define ABA-Dependency of Osmotic-Stress Responders by ANT

We have established that almost all the osmotic-stress responders are ABA-dependent to some extent, thus, we can explore the ABA-dependency by the effect of ANT on the expression of osmotic responses. Since ANT blocks the ABA signaling, we expected that the application of ANT would reduce the effect of osmotic stress, in other words, ANT would cause a reduction in the expression change resulting from osmotic stress, which is referred to as “ANT reduced”. The results showed that most of the osmotic-stress responders are “ANT reduced”, while there is still a small number of genes whose osmotic responses were enhanced upon ANT application (Figure 3.3A). The characterization of this so-called “ANT enhanced” genes should be investigated in the future.

In order to describe the ABA-dependency of the gene, we used a gene significant score, π-value (Xiao et al., 2014). This score combines the *p*-value and fold change in the pairwise comparison results in a typical RNA-seq data analysis. It is the product of log-fold change and log-transformed *p*-value, so the larger the absolute π-value, the more significant gene expression change is. It has been frequently used as a useful approach to rank the genes in various analyses, such as GSEA (gene set enrichment analysis), and has been proven to show better protection against false discoveries (Strobel et al., 2020; Van der Veen et al., 2020; Wang et al., 2020; Deshmukh et al., 2021; Meiler et al., 2021; Molinar-Inglis et al., 2022).

We ranked the DEGs either up-regulated or down-regulated under osmotic stress based on the π-value (ANTPEGvsPEG), then classified the DEGs evenly into 5 clusters. As shown in Figure 3.3B, the significance of the ANT effect on osmotic responses of genes increased from cluster 1 to cluster 5. Then we performed a similar motif enrichment analysis on the genes in each cluster. The results showed that the significance and fold enrichment of certain motifs were increasing as the effect of ANT increased, especially some bZIP binding motifs and CBFs binding motifs, and the trend is only clear among the osmotic stress-induced genes (Appendix Figure 3.2). Figure 3.3C illustrates the increasing trend of the enrichment of well-known ABA-induced TF binding sites.

Discussion

In our study, we have demonstrated that almost all the osmotic-stress-responsive genes are ABA-dependent to some extent. This is consistent with the findings that there are crosstalks between ABA-dependent and “ABA-independent” pathways in the previous studies. However, to our surprise, the osmotic response of some genes was enhanced under ANT treatment, this suggested that ANT may be involved in pathways other than the ABA signaling. Further investigation of those genes should be done in the future.

We also introduced a new strategy to define the ABA-dependency of the genes by a chemical tool, ABA antagonist, ANT. The results of motif enrichment analysis of some highly ABA-induced TFs supported our strategy. However, the repressed genes under osmotic stress didn’t show a similar trend as in the up-regulated genes. We hypothesized that regulating these genes by ABA might be the combination of different motifs rather than the existence and number of one certain motif.

The significance of enrichment in the analysis could provide evidence of whether certain TFs are involved in the ABA-dependent signaling pathway. The enrichment of motifs for most of the bZIPs showed a clear increasing trend as the effect of ANT increased, which means these TFs are largely related to ABA signaling (Appendix Figure 3.2A). However, the binding sites of the WRKY TFs were less likely to be enriched in the osmotic stress up-regulators. Even in the down-regulated group, they tend to be enriched in the cluster showing the least ANT effect (cluster 1), which might indicate that WRKYs are mostly involved in the ABA-independent pathway (Appendix Figure 3.2G). Collectively, this study brought novel insight into the understanding of the ABA involvement in osmotic stress responses.

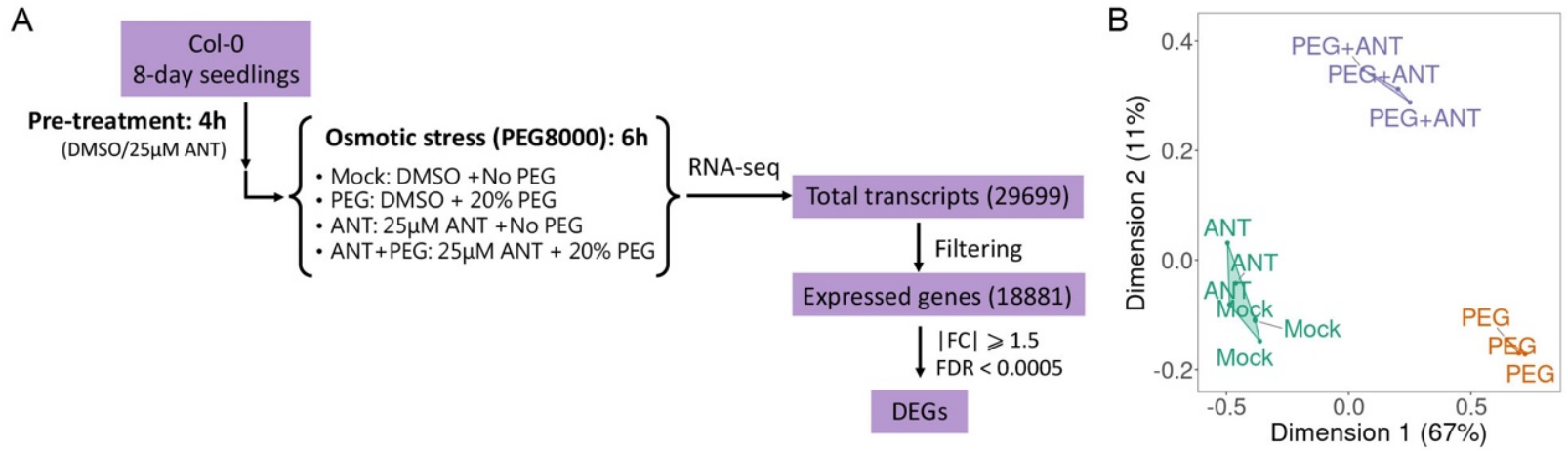

Figure 3.1 Transcriptional profile of ANT-responsive genes under osmotic stress. (A) Diagram of the workflow for preparation of libraries and definition of ABA-responsive genes. The numbers in the parentheses are the number of genes left after each step. **(B)** MDS plot of gene expression in each biological replicate and 4 different treatments. Three replicates are shown in the plot. k-means clustering was performed to cluster the samples.

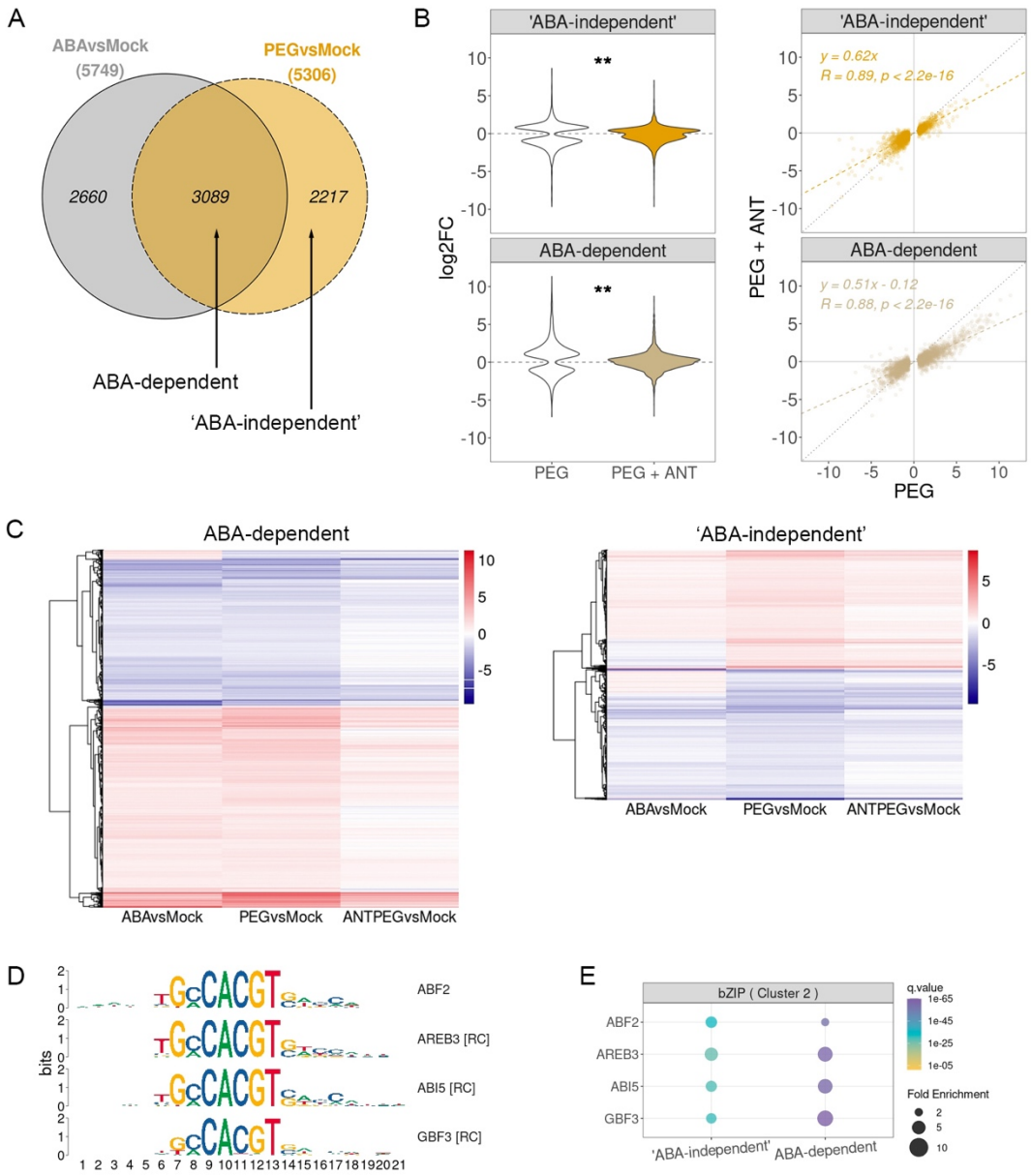
A
ABAvsMock
(5749)
PEGvsMock
(5306)
2660
3089
2217
ABA-dependent
'ABA-independent'
B
'ABA-independent'
ABA-dependent
log2FC
**
PEG
PEG + ANT
y = 0.62x
R = 0.89, p < 2.2e-16
y = 0.51x - 0.12
R = 0.88, p < 2.2e-16
PEG + ANT
PEG
C
ABA-dependent
'ABA-independent'
ABAvsMock
PEGvsMock
ANTPEGvsMock
D
bits
ABF2
AREB3 [RC]
ABI5 [RC]
GBF3 [RC]
E
bZIP (Cluster 2)
ABF2
AREB3
ABI5
GBF3
'ABA-independent'
ABA-dependent
q.value
Fold Enrichment

Figure 3.2 The effect of ANT on "ABA-independent" and ABA-dependent osmotic-stress responsive genes defined by previous method. (A) Venn diagram illustrating the previous way to identify DEGs involved in ABA-dependent or ABA-independent pathway under osmotic stress. The number in the parentheses are the total number of ABA-responsive genes and osmotic-stress responsive genes identified. **(B)** Comparison of the gene expression profiles of "ABA-independent" genes and ABA-dependent genes with or without ANT treatment under osmotic stress. The y-axis in the violin plot and both axes in the scatter plot represent the log2-transformed expression with or without 25 μM ANT under 20% PEG treatment (referred to as "ANT+PEG" and "PEG" respectively in the plot) compared with Mock treatment. ** indicated the significant difference assessed by Wilcoxon paired ($p < 0.01$). In the scatter plot, the dotted grey lines are the diagonal line of the coordinates with the equation, y=x. The dashed lines in different color were the linear regression line fitted to the data. The equations of the line, Pearson correlation coefficient, and the *p*-value of F test were shown within the plot. The intercepts and the slopes estimated in the linear models were significant assessed by *t-test* (*p*-value < 0.001). **(C)** Heatmap showing the expression profile of osmotic-stress responders involved in "ABA-independent" and ABA-dependent pathways. The genes were clustered by hierarchical clustering method. **(D)** Sequence logo depiction of the binding sites for cluster 2 TFs from bZIP TF family. The x axis represents the conserved sequences of the motif. The y axis is a scale of the relative entropy, which reflects the conservation rate of each nucleic acid. The name of the TFs was presented on the right side of the sequence logo. **(E)** Motif enrichment analysis of the TF-specific binding sites shown in C. The size of dot indicated the Enrichment Ratio (Fold enrichment), and the color of dot corresponding to the adjusted *p*-value (q-value) for each motif.

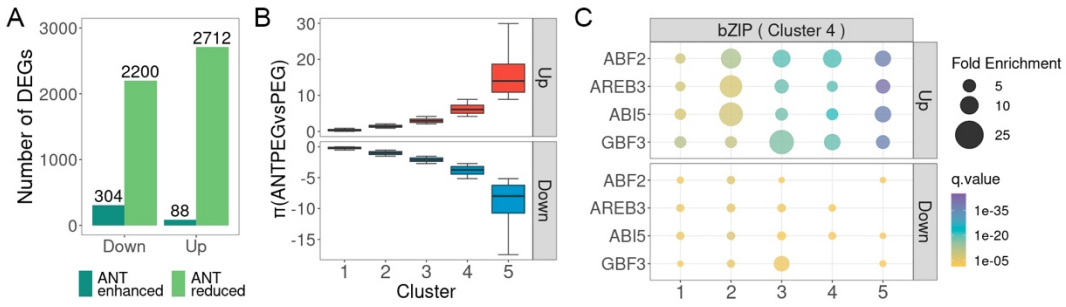

Figure 3.3 The effect of ANT on osmotic-stress responsive genes. (A) Bar plot of ANT-reduced or ANT-enhanced genes among osmotic-stress responders. The up-regulated and down-regulated genes under osmotic stress were presented separately. Numbers on top of the bars indicate the number of DEGs identified in each group. **(B)** The effect of ANT on the clusters of osmotic-stress responders. Box plot showing the *pi*-value of the comparison ANTPEG vs PEG. **(C)** Motif enrichment analysis of the TF-specific binding sites shown in Figure 3.2C. The size of dot indicated the Enrichment Ratio (Fold enrichment), and the color of dot corresponding to the adjusted *p*-value (q-value) for each motif.

References

Bailey TL, Grant CE (2021) SEA: Simple Enrichment Analysis of motifs. bioRxiv 2021.08.23.457422

Bargmann BOR, Birnbaum KD (2010) Fluorescence activated cell sorting of plant protoplasts. J Vis Exp. doi: 10.3791/1673

Deak KI, Malamy J (2005) Osmotic regulation of root system architecture. Plant J **43**: 17–28

Deshmukh AS, Steenberg DE, Hostrup M, Birk JB, Larsen JK, Santos A, Kjøbsted R, Hingst JR, Schéele CC, Murgia M, et al (2021) Deep muscle-proteomic analysis of freeze-dried human muscle biopsies reveals fiber type-specific adaptations to exercise training. Nat Commun **12**: 304

Guerrero F, Mullet JE (1986) Increased Abscisic Acid Biosynthesis during Plant Dehydration Requires Transcription. Plant Physiol **80**: 588–591

H Backman TW, Girke T (2016) systemPipeR: NGS workflow and report generation environment. BMC Bioinformatics **17**: 388

Hrmova M, Hussain SS (2021) Plant Transcription Factors Involved in Drought and Associated Stresses. Int J Mol Sci. doi: 10.3390/ijms22115662

Ito T, Kondoh Y, Yoshida K, Umezawa T, Shimizu T, Shinozaki K, Osada H (2015) Novel Abscisic Acid Antagonists Identified with Chemical Array Screening. Chembiochem **16**: 2471–2478

Ji H, Li X (2014) ABA mediates PEG-mediated premature differentiation of root apical meristem in plants. Plant Signal Behav **9**: e977720

Kim D, Pertea G, Trapnell C, Pimentel H, Kelley R, Salzberg SL (2013) TopHat2: accurate alignment of transcriptomes in the presence of insertions, deletions and gene fusions. Genome Biol **14**: R36

Kim T-H, Hauser F, Ha T, Xue S, Böhmer M, Nishimura N, Munemasa S, Hubbard K, Peine N, Lee B-H, et al (2011) Chemical genetics reveals negative regulation of abscisic acid signaling by a plant immune response pathway. Curr Biol **21**: 990–997

Lawrence M, Huber W, Pagès H, Aboyoun P, Carlson M, Gentleman R, Morgan MT, Carey VJ (2013) Software for computing and annotating genomic ranges. PLoS Comput Biol **9**: e1003118

Liu S, Lv Z, Liu Y, Li L, Zhang L (2018) Network analysis of ABA-dependent and ABA-independent drought responsive genes in *Arabidopsis* thaliana. Genet Mol Biol **41**: 624–637

Meiler A, Marchiano F, Haering M, Weitkunat M, Schnorrer F, Habermann BH (2021) AnnoMiner is a new web-tool to integrate epigenetics, transcription factor occupancy and transcriptomics data to predict transcriptional regulators. Sci Rep **11**: 15463

Molinar-Inglis O, Wozniak JM, Grimsey NJ, Orduña-Castillo LB, Cheng N, Lin Y, Gonzalez Ramirez ML, Birch CA, Lapek JD, Gonzalez DJ, et al (2022) Phosphoproteomic analysis of thrombin- and p38 MAPK-regulated signaling networks in endothelial cells. J Biol Chem **298**: 101801

Nakashima K, Yamaguchi-Shinozaki K, Shinozaki K (2014) The transcriptional regulatory network in the drought response and its crosstalk in abiotic stress responses including drought, cold, and heat. Front Plant Sci **5**: 170

O'Malley RC, Huang S-SC, Song L, Lewsey MG, Bartlett A, Nery JR, Galli M, Gallavotti A, Ecker JR (2016) Cistrome and Epicistrome Features Shape the Regulatory DNA Landscape. Cell **165**: 1280–1292

Ozfidan C, Turkan I, Sekmen AH, Seckin B (2013) Time course analysis of ABA and non-ionic osmotic stress-induced changes in water status, chlorophyll fluorescence and osmotic adjustment in *Arabidopsis* …. and Experimental Botany

Rajagopalan N, Nelson KM, Douglas AF, Jheengut V, Alarcon IQ, McKenna SA, Surpin M, Loewen MC, Abrams SR (2016) Abscisic Acid Analogues That Act as Universal or Selective Antagonists of Phytohormone Receptors. Biochemistry **55**: 5155–5164

Robinson MD, McCarthy DJ, Smyth GK (2010) edgeR: a Bioconductor package for differential expression analysis of digital gene expression data. Bioinformatics **26**: 139–140

Roychoudhury A, Paul S, Basu S (2013) Cross-talk between abscisic acid-dependent and abscisic acid-independent pathways during abiotic stress. Plant Cell Rep **32**: 985–1006

Strobel B, Spöring M, Klein H, Blazevic D, Rust W, Sayols S, Hartig JS, Kreuz S (2020) High-throughput identification of synthetic riboswitches by barcode-free amplicon-sequencing in human cells. Nat Commun **11**: 714

Takeuchi J, Okamoto M, Akiyama T, Muto T, Yajima S, Sue M, Seo M, Kanno Y, Kamo T, Endo A, et al (2014) Designed abscisic acid analogs as antagonists of PYL-PP2C receptor interactions. Nat Chem Biol **10**: 477

Van der Veen DR, Laing EE, Bae S-E, Johnston JD, Dijk D-J, Archer SN (2020) A Topological Cluster of Differentially Regulated Genes in Mice Lacking PER3. Front Mol Neurosci **13**: 15

Wang Y, Eng DG, Kaverina NV, Loretz CJ, Koirala A, Akilesh S, Pippin JW, Shankland SJ (2020) Global transcriptomic changes occur in aged mouse podocytes. Kidney Int **98**: 1160–1173

Wenjing W, Chen Q, Singh PK, Huang Y, Pei D (2020) CRISPR/Cas9 edited HSFA6a and HSFA6b of *Arabidopsis* thaliana offers ABA and osmotic stress insensitivity by modulation of ROS homeostasis. Plant Signal Behav **15**: 1816321

Xiao Y, Hsiao T-H, Suresh U, Chen H-lH, Wu X, Wolf SE, Chen Y (2014) A novel significance score for gene selection and ranking. Bioinformatics **30**: 801–807

Ye Y, Zhou L, Liu X, Liu H, Li D, Cao M, Chen H, Xu L, Zhu J-K, Zhao Y (2017) A Novel Chemical Inhibitor of ABA Signaling Targets All ABA Receptors. Plant Physiol **173**: 2356–2369

Yoshida T, Mogami J, Yamaguchi-Shinozaki K (2014) ABA-dependent and ABA-independent signaling in response to osmotic stress in plants. Curr Opin Plant Biol **21**: 133–139

Appendices

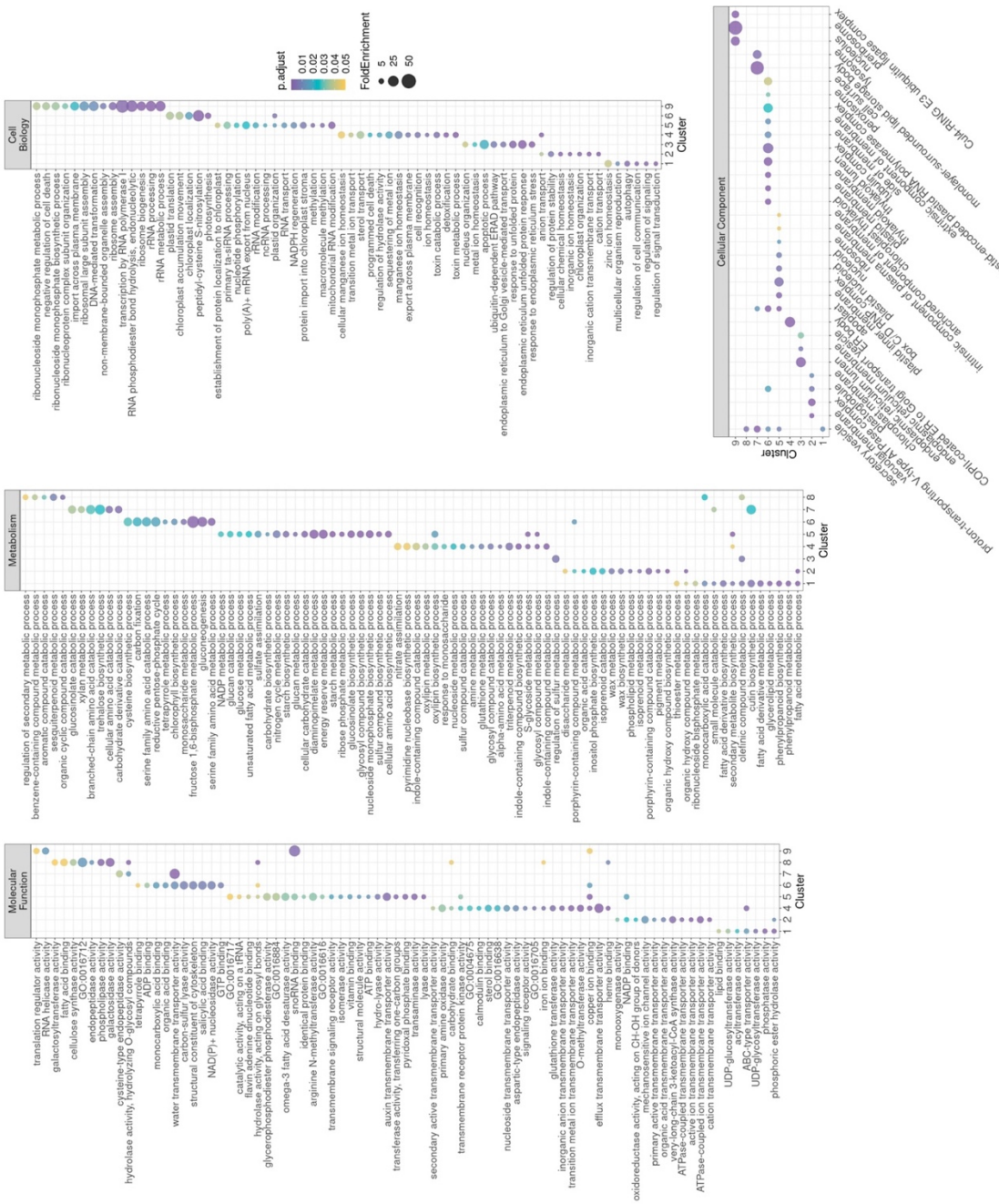
Molecular Function
Metabolism
Cell Biology
Cellular Component
Cluster
p.adjust
FoldEnrichment

Appendix Figure 1.1 Comparison of functional profiles among different clusters of ABA-responsive genes. Top GO (Gene Ontology) highly enriched in different clusters (adjusted *p*-value < 0.05) were presented. The results were visualized as a dot plot with different facet panels indicating two representative classes in the Biological Process category and all the enriched GO terms in Molecular Function and Cellular Component categories, with the size of the dots indicating the fold enrichment and the color corresponding to the adjusted *p*-value of each enriched GO term. (Note: If a cluster didn't appear in the x-axis, it means no GO terms were significantly enriched in that cluster.) Some GO terms only showed as GO term IDs since there are not enough space for display. The detailed descriptions for the GO terms are listed as follows.
GO:0016705, "oxidoreductase activity, acting on paired donors, with incorporation or reduction of molecular oxygen".
GO:0016638, "oxidoreductase activity, acting on the CH-NH2 group of donors".
GO:0004675, "transmembrane receptor protein serine/threonine kinase activity".
GO:0016616, "oxidoreductase activity, acting on the CH-OH group of donors, NAD or NADP as acceptor".
GO:0016717, "oxidoreductase activity, acting on paired donors, with oxidation of a pair of donors resulting in the reduction of molecular oxygen to two molecules of water".
GO:0016712, "oxidoreductase activity, acting on paired donors, with incorporation or reduction of molecular oxygen, reduced flavin or flavoprotein as one donor, and incorporation of one atom of oxygen".

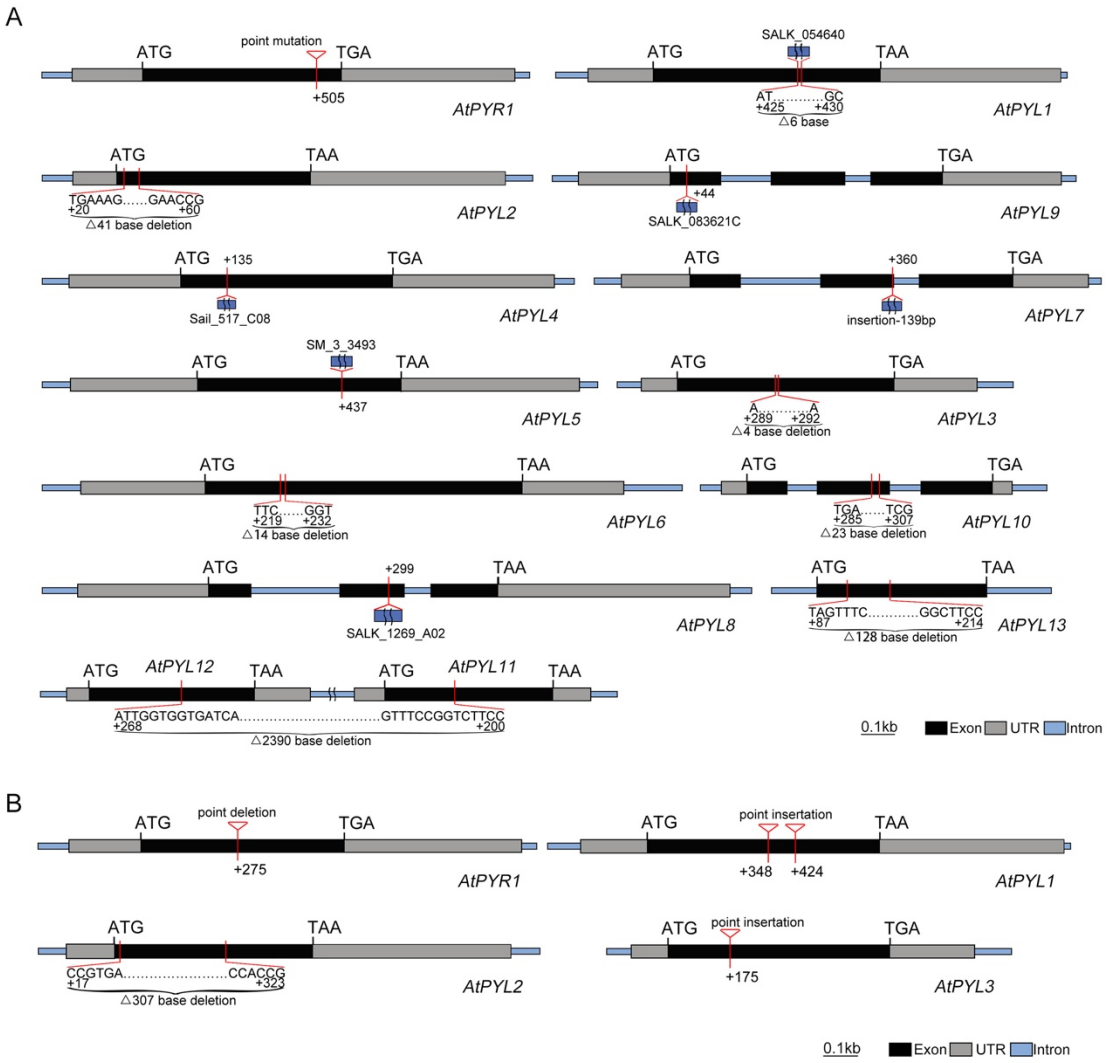

Appendix Figure 2.1 Physical maps of ABA receptor mutants (A) Physical maps of *subI*, *subII*, and *subIII* **(B)** Physical maps of *subIII* new

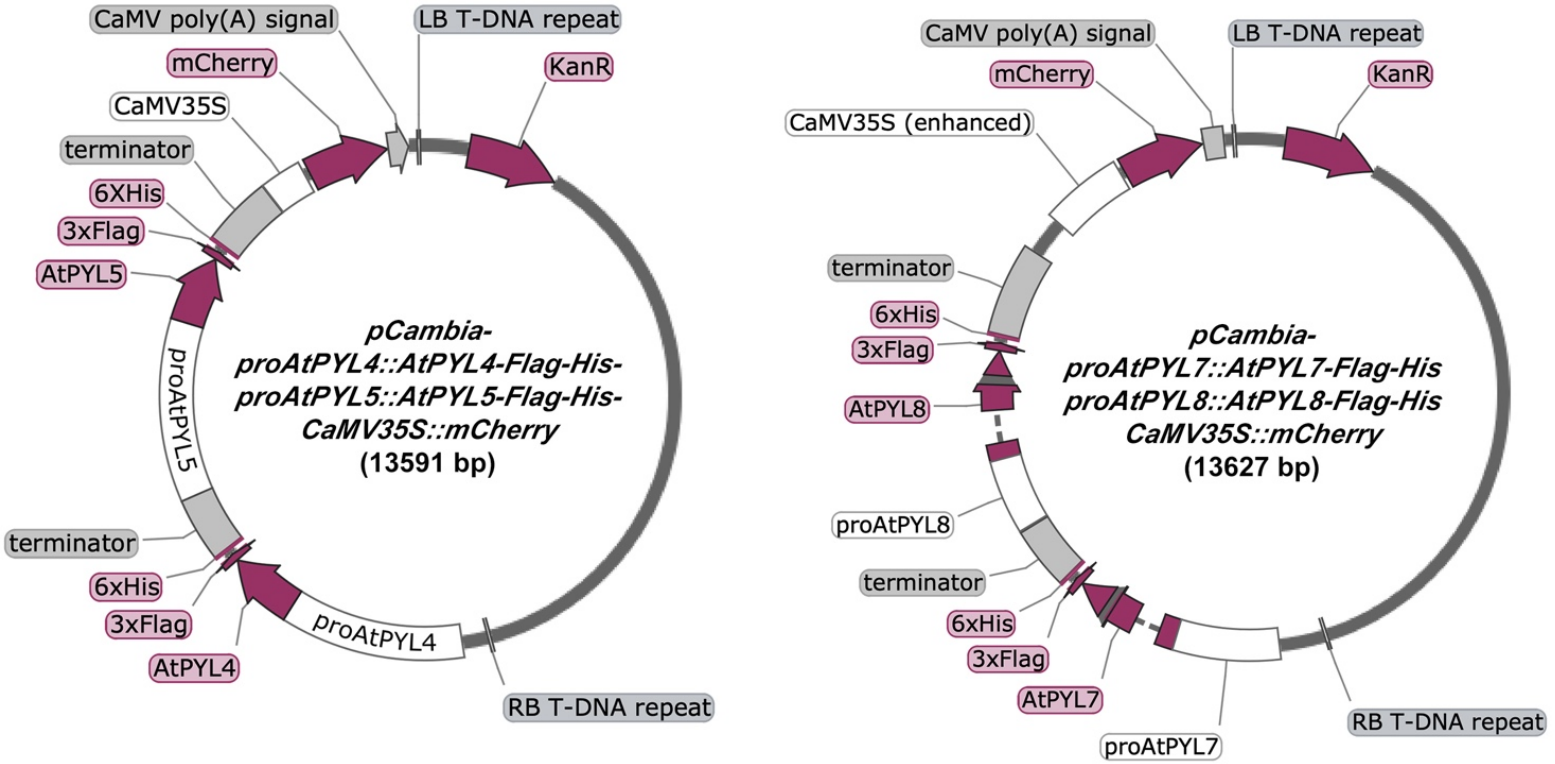

Appendix Figure 2.2 Schematic illustration of constructs used for the generation of complementation lines

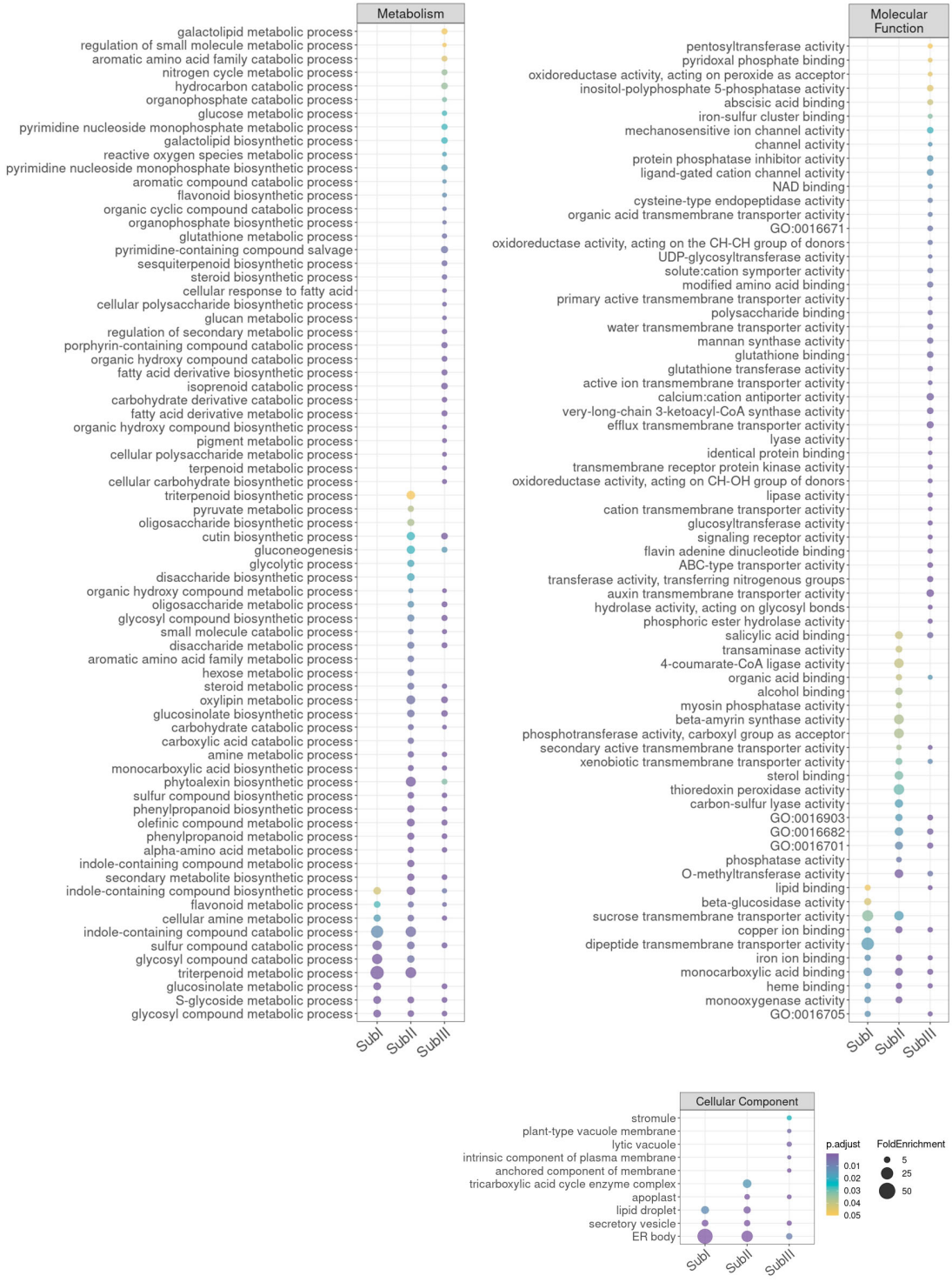
Metabolism
galactolipid metabolic process
regulation of small molecule metabolic process
aromatic amino acid family catabolic process
nitrogen cycle metabolic process
hydrocarbon catabolic process
organophosphate catabolic process
glucose metabolic process
pyrimidine nucleoside monophosphate metabolic process
galactolipid biosynthetic process
reactive oxygen species metabolic process
pyrimidine nucleoside monophosphate biosynthetic process
aromatic compound catabolic process
flavonoid biosynthetic process
organic cyclic compound catabolic process
organophosphate biosynthetic process
glutathione metabolic process
pyrimidine-containing compound salvage
sesquiterpenoid biosynthetic process
steroid biosynthetic process
cellular response to fatty acid
cellular polysaccharide biosynthetic process
glucan metabolic process
regulation of secondary metabolic process
porphyrin-containing compound catabolic process
organic hydroxy compound catabolic process
fatty acid derivative biosynthetic process
isoprenoid catabolic process
carbohydrate derivative catabolic process
fatty acid derivative metabolic process
organic hydroxy compound biosynthetic process
pigment metabolic process
cellular polysaccharide metabolic process
terpenoid metabolic process
cellular carbohydrate biosynthetic process
triterpenoid biosynthetic process
pyruvate metabolic process
oligosaccharide biosynthetic process
cutin biosynthetic process
gluconeogenesis
glycolytic process
disaccharide biosynthetic process
organic hydroxy compound metabolic process
oligosaccharide metabolic process
glycosyl compound biosynthetic process
small molecule catabolic process
disaccharide metabolic process
aromatic amino acid family metabolic process
hexose metabolic process
steroid metabolic process
oxylipin metabolic process
glucosinolate biosynthetic process
carbohydrate catabolic process
carboxylic acid catabolic process
amine metabolic process
monocarboxylic acid biosynthetic process
phytoalexin biosynthetic process
sulfur compound biosynthetic process
phenylpropanoid biosynthetic process
olefinic compound metabolic process
phenylpropanoid metabolic process
alpha-amino acid metabolic process
indole-containing compound metabolic process
secondary metabolite biosynthetic process
indole-containing compound biosynthetic process
flavonoid metabolic process
cellular amine metabolic process
indole-containing compound catabolic process
sulfur compound catabolic process
glycosyl compound catabolic process
triterpenoid metabolic process
glucosinolate metabolic process
S-glycoside metabolic process
glycosyl compound metabolic process
SubI
SubII
SubIII
Molecular Function
pentosyltransferase activity
pyridoxal phosphate binding
oxidoreductase activity, acting on peroxide as acceptor
inositol-polyphosphate 5-phosphatase activity
abscisic acid binding
iron-sulfur cluster binding
mechanosensitive ion channel activity
channel activity
protein phosphatase inhibitor activity
ligand-gated cation channel activity
NAD binding
cysteine-type endopeptidase activity
organic acid transmembrane transporter activity
GO:0016671
oxidoreductase activity, acting on the CH-CH group of donors
UDP-glycosyltransferase activity
solute:cation symporter activity
modified amino acid binding
primary active transmembrane transporter activity
polysaccharide binding
water transmembrane transporter activity
mannan synthase activity
glutathione binding
glutathione transferase activity
active ion transmembrane transporter activity
calcium:cation antiporter activity
very-long-chain 3-ketoacyl-CoA synthase activity
efflux transmembrane transporter activity
lyase activity
identical protein binding
transmembrane receptor protein kinase activity
oxidoreductase activity, acting on CH-OH group of donors
lipase activity
cation transmembrane transporter activity
glucosyltransferase activity
signaling receptor activity
flavin adenine dinucleotide binding
ABC-type transporter activity
transferase activity, transferring nitrogenous groups
auxin transmembrane transporter activity
hydrolase activity, acting on glycosyl bonds
phosphoric ester hydrolase activity
salicylic acid binding
transaminase activity
4-coumarate-CoA ligase activity
organic acid binding
alcohol binding
myosin phosphatase activity
beta-amyrin synthase activity
phosphotransferase activity, carboxyl group as acceptor
secondary active transmembrane transporter activity
xenobiotic transmembrane transporter activity
sterol binding
thioredoxin peroxidase activity
carbon-sulfur lyase activity
GO:0016903
GO:0016682
GO:0016701
phosphatase activity
O-methyltransferase activity
lipid binding
beta-glucosidase activity
sucrose transmembrane transporter activity
copper ion binding
dipeptide transmembrane transporter activity
iron ion binding
monocarboxylic acid binding
heme binding
monooxygenase activity
GO:0016705
SubI
SubII
SubIII
Cellular Component
stromule
plant-type vacuole membrane
lytic vacuole
intrinsic component of plasma membrane
anchored component of membrane
tricarboxylic acid cycle enzyme complex
apoplast
lipid droplet
secretory vesicle
ER body
SubI
SubII
SubIII
p.adjust
0.01
0.02
0.03
0.04
0.05
FoldEnrichment
5
25
50

Appendix Figure 2.3 Comparison of functional profiles among DEGs in different mutants. Top GO (Gene Ontology) highly enriched among DEGs in different ABA receptor mutants (adjusted *p*-value < 0.05) were presented. The results were visualized as a dot plot with different facet panels indicating Metabolism classe in the Biological Process category and all the enriched GO terms in Molecular Function and Cellular Component categories, with the size of the dots indicating the fold enrichment and the color corresponding to the adjusted *p*-value of each enriched GO term. Some GO terms only showed as GO term IDs since there are not enough space for display. The detailed descriptions for the GO terms are listed as follows.
GO:0016903, “oxidoreductase activity, acting on the aldehyde or oxo group of donors”.
GO:0016671, “oxidoreductase activity, acting on a sulfur group of donors, disulfide as acceptor”.
GO:0016701, “oxidoreductase activity, acting on single donors with incorporation of molecular oxygen”.
GO:0016682, “oxidoreductase activity, acting on diphenols and related substances as donors, oxygen as acceptor”.
GO:0016705, “oxidoreductase activity, acting on paired donors, with incorporation or reduction of molecular oxygen”.

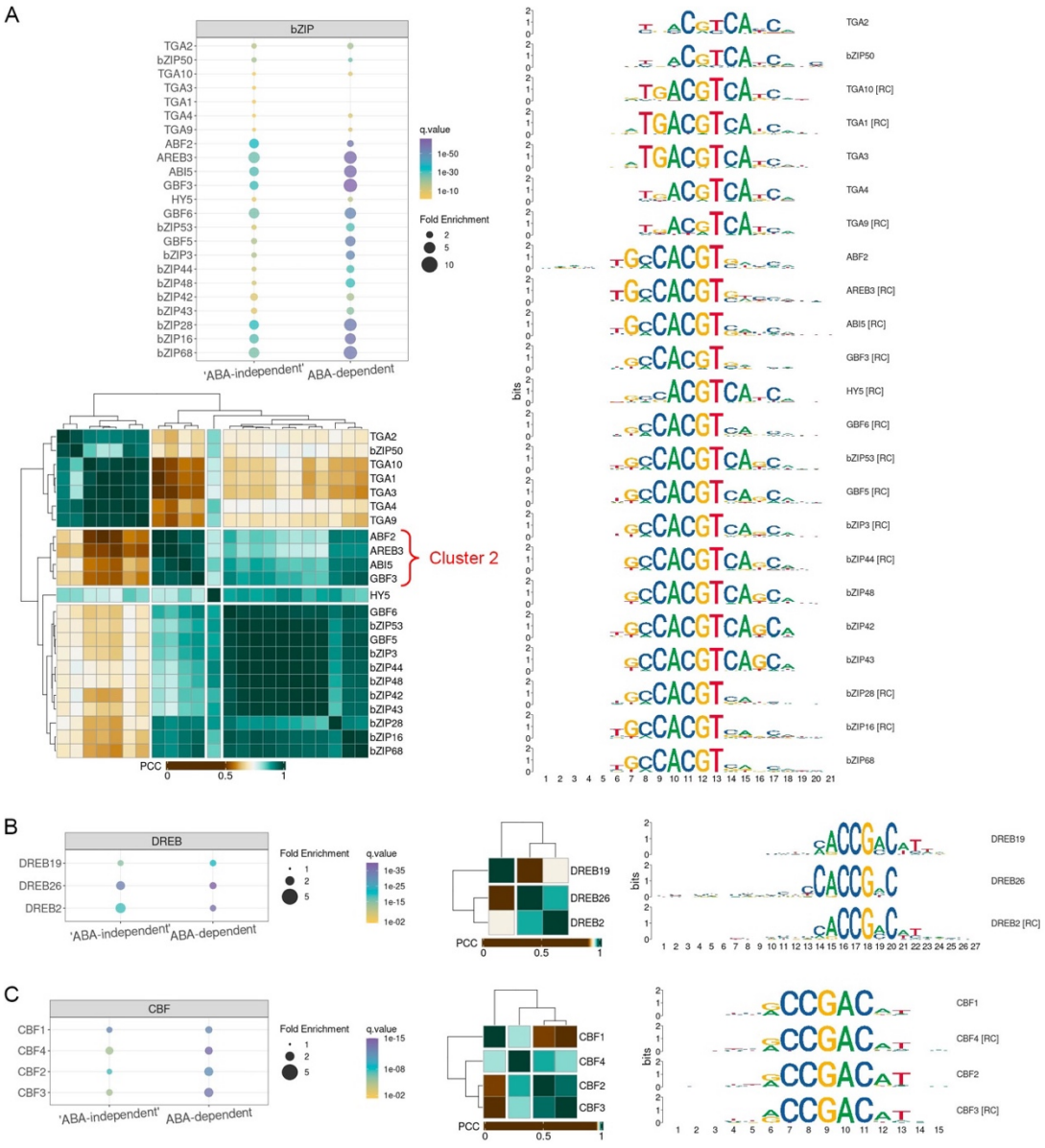
A
bZIP
TGA2
bZIP50
TGA10
TGA3
TGA1
TGA4
TGA9
ABF2
AREB3
ABI5
GBF3
HY5
GBF6
bZIP53
GBF5
bZIP3
bZIP44
bZIP48
bZIP42
bZIP43
bZIP28
bZIP16
bZIP68
'ABA-independent'
ABA-dependent
q.value
1e-50
1e-30
1e-10
Fold Enrichment
2
5
10
Cluster 2
PCC
0
0.5
1
bits
TGA10 [RC]
TGA1 [RC]
TGA3
TGA4
TGA9 [RC]
AREB3 [RC]
ABI5 [RC]
GBF3 [RC]
HY5 [RC]
GBF6 [RC]
bZIP53 [RC]
GBF5 [RC]
bZIP3 [RC]
bZIP44 [RC]
bZIP48
bZIP42
bZIP43
bZIP28 [RC]
bZIP16 [RC]
bZIP68
B
DREB
DREB19
DREB26
DREB2
DREB2 [RC]
C
CBF
CBF1
CBF4
CBF2
CBF3
CBF4 [RC]
CBF3 [RC]

D

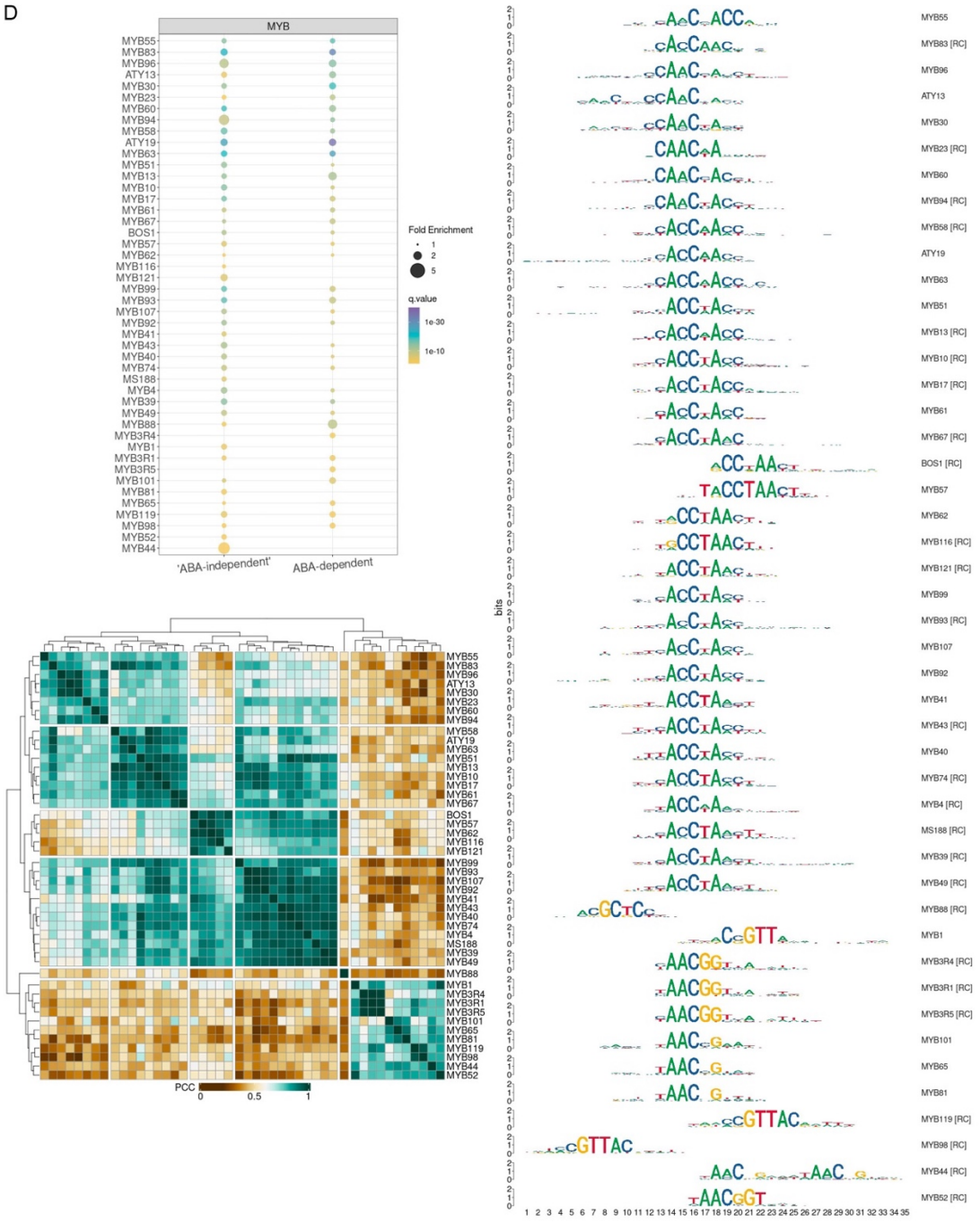
MYB
MYB55
MYB83
MYB96
ATY13
MYB30
MYB23
MYB60
MYB94
MYB58
ATY19
MYB63
MYB51
MYB13
MYB10
MYB17
MYB61
MYB67
BOS1
MYB57
MYB62
MYB116
MYB121
MYB99
MYB93
MYB107
MYB92
MYB41
MYB43
MYB40
MYB74
MS188
MYB4
MYB39
MYB49
MYB88
MYB3R4
MYB1
MYB3R1
MYB3R5
MYB101
MYB81
MYB65
MYB119
MYB98
MYB44
MYB52
'ABA-independent'
ABA-dependent
Fold Enrichment
1
2
5
q.value
1e-30
1e-10
PCC
0
0.5
1
bits
MYB55
MYB83 [RC]
MYB96
ATY13
MYB30
MYB23 [RC]
MYB60
MYB94 [RC]
MYB58 [RC]
ATY19
MYB63
MYB51
MYB13 [RC]
MYB10 [RC]
MYB17 [RC]
MYB61
MYB67 [RC]
BOS1 [RC]
MYB57
MYB62
MYB116 [RC]
MYB121 [RC]
MYB99
MYB93 [RC]
MYB107
MYB92
MYB41
MYB43 [RC]
MYB40
MYB74 [RC]
MYB4 [RC]
MS188 [RC]
MYB39 [RC]
MYB49 [RC]
MYB88 [RC]
MYB1
MYB3R4 [RC]
MYB3R1 [RC]
MYB3R5 [RC]
MYB101
MYB65
MYB81
MYB119 [RC]
MYB98 [RC]
MYB44 [RC]
MYB52 [RC]
1 2 3 4 5 6 7 8 9 10 11 12 13 14 15 16 17 18 19 20 21 22 23 24 25 26 27 28 29 30 31 32 33 34 35

E

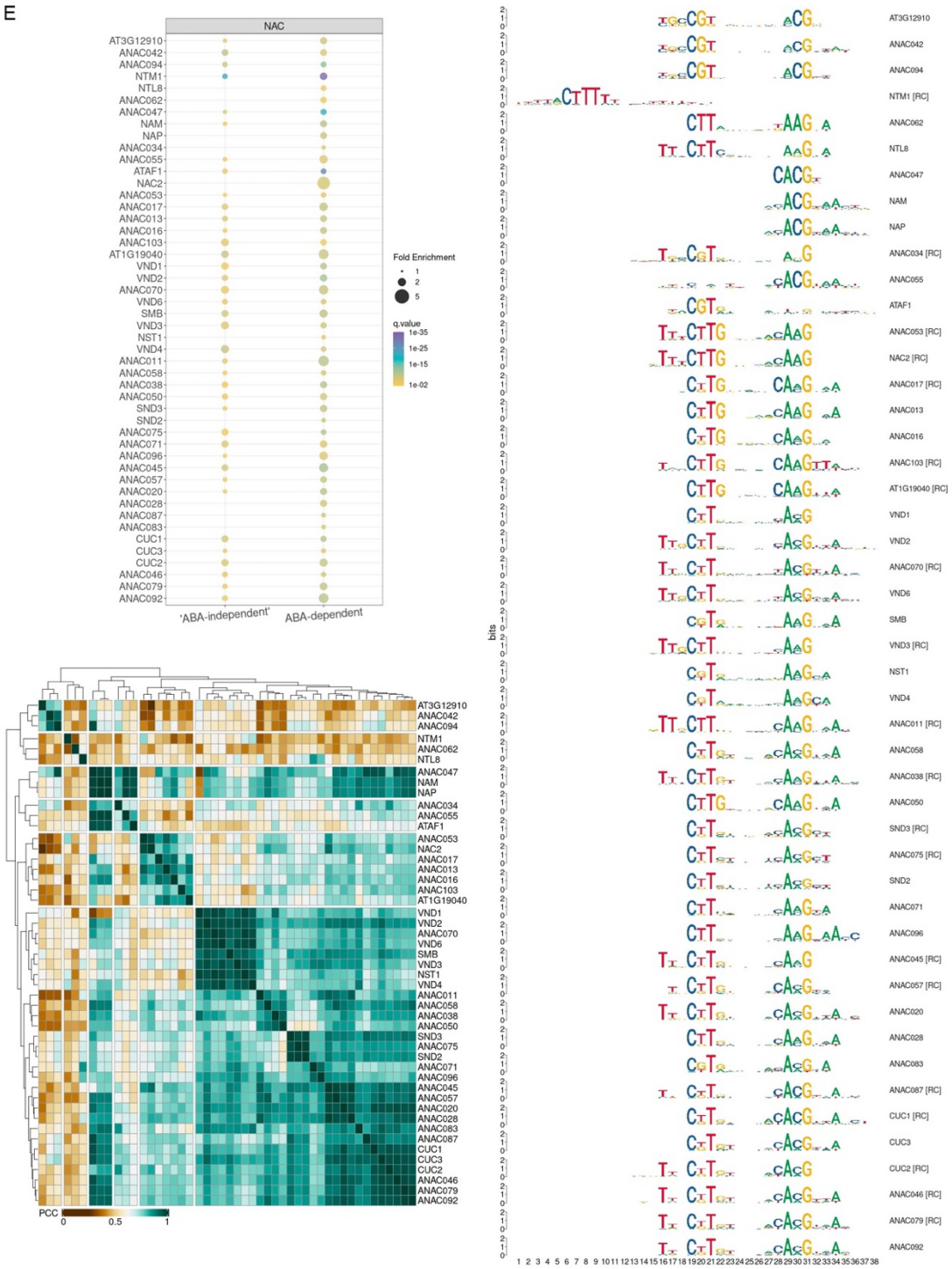
NAC
AT3G12910
ANAC042
ANAC094
NTM1
NTL8
ANAC062
ANAC047
NAM
NAP
ANAC034
ANAC055
ATAF1
NAC2
ANAC053
ANAC017
ANAC013
ANAC016
ANAC103
AT1G19040
VND1
VND2
ANAC070
VND6
SMB
VND3
NST1
VND4
ANAC011
ANAC058
ANAC038
ANAC050
SND3
SND2
ANAC075
ANAC071
ANAC096
ANAC045
ANAC057
ANAC020
ANAC028
ANAC083
ANAC087
CUC1
CUC3
CUC2
ANAC046
ANAC079
ANAC092
'ABA-independent'
ABA-dependent
Fold Enrichment
1
2
5
q.value
1e-35
1e-25
1e-15
1e-02
PCC
0
0.5
1
bits
AT3G12910
ANAC042
ANAC094
NTM1 [RC]
ANAC062
NTL8
ANAC047
NAM
NAP
ANAC034 [RC]
ANAC055
ATAF1
ANAC053 [RC]
NAC2 [RC]
ANAC017 [RC]
ANAC013
ANAC016
ANAC103 [RC]
AT1G19040 [RC]
VND1
VND2
ANAC070 [RC]
VND6
SMB
VND3 [RC]
NST1
VND4
ANAC011 [RC]
ANAC058
ANAC038 [RC]
ANAC050
SND3 [RC]
ANAC075 [RC]
SND2
ANAC071
ANAC096
ANAC045 [RC]
ANAC057 [RC]
ANAC020
ANAC028
ANAC083
ANAC087 [RC]
CUC1 [RC]
CUC3
CUC2 [RC]
ANAC046 [RC]
ANAC079 [RC]
ANAC092
1 2 3 4 5 6 7 8 9 10 11 12 13 14 15 16 17 18 19 20 21 22 23 24 25 26 27 28 29 30 31 32 33 34 35 36 37 38

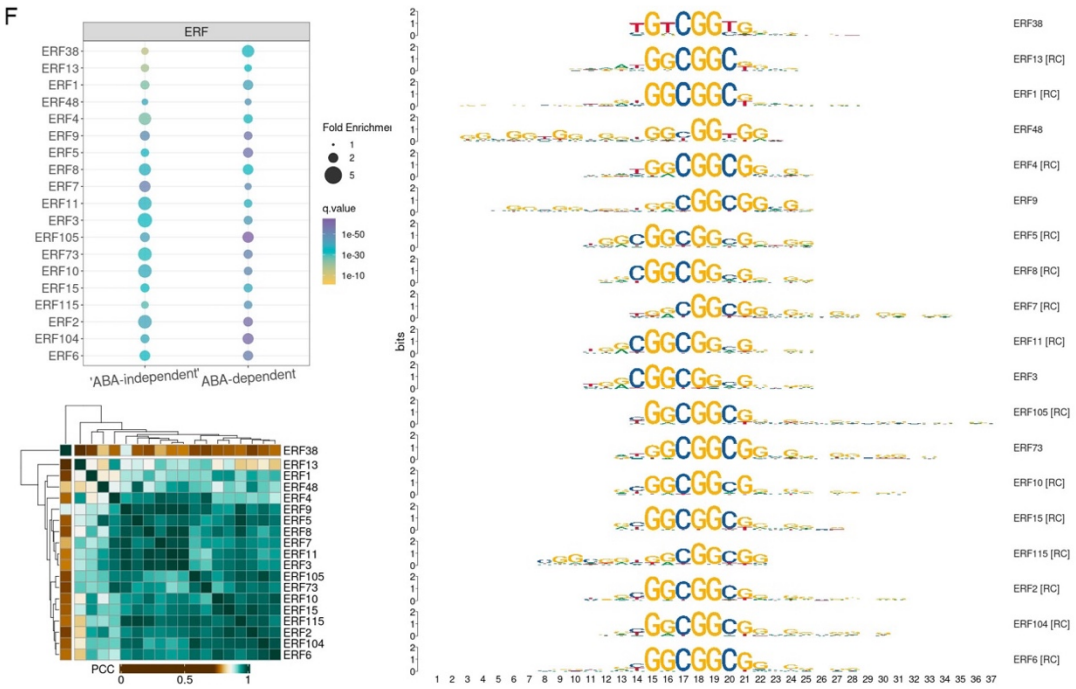
F
ERF
ERF38
ERF13
ERF1
ERF48
ERF4
ERF9
ERF5
ERF8
ERF7
ERF11
ERF3
ERF105
ERF73
ERF10
ERF15
ERF115
ERF2
ERF104
ERF6
'ABA-independent'
ABA-dependent
Fold Enrichmer
1
2
5
q.value
1e-50
1e-30
1e-10
PCC
0
0.5
1
bits
ERF38
ERF13 [RC]
ERF1 [RC]
ERF48
ERF4 [RC]
ERF9
ERF5 [RC]
ERF8 [RC]
ERF7 [RC]
ERF11 [RC]
ERF3
ERF105 [RC]
ERF73
ERF10 [RC]
ERF15 [RC]
ERF115 [RC]
ERF2 [RC]
ERF104 [RC]
ERF6 [RC]

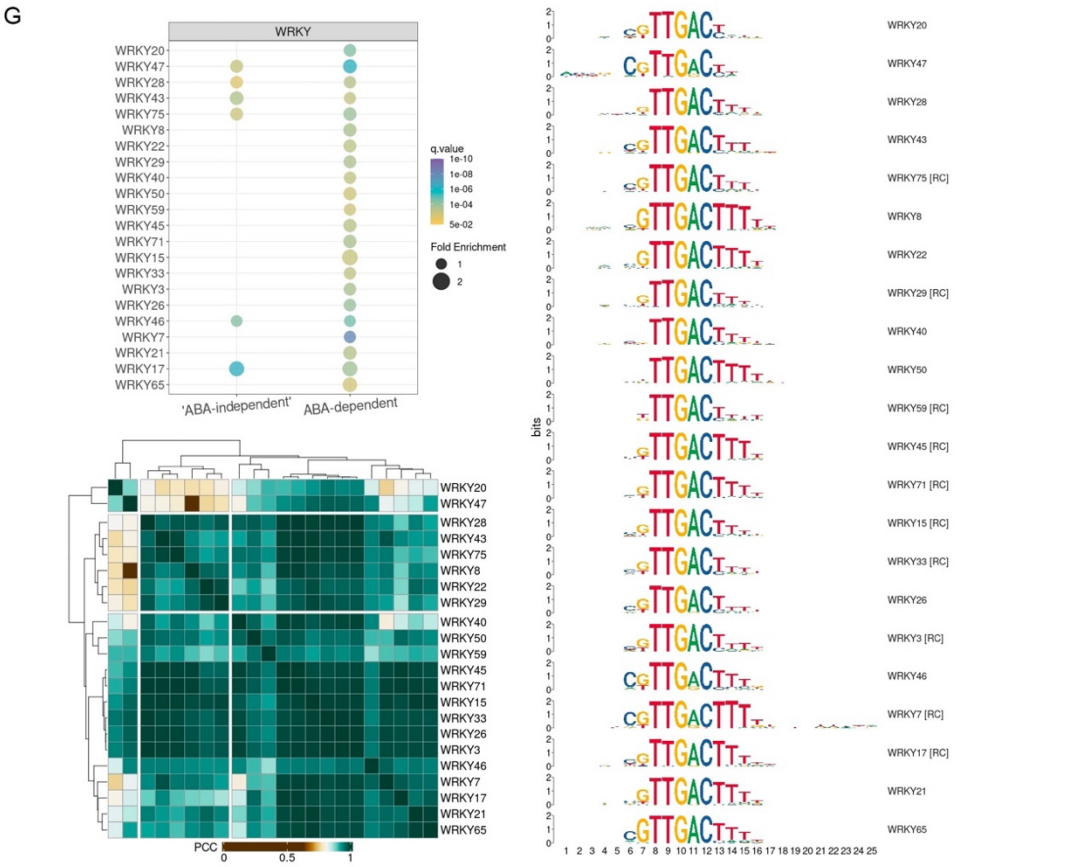
G
WRKY
WRKY20
WRKY47
WRKY28
WRKY43
WRKY75
WRKY8
WRKY22
WRKY29
WRKY40
WRKY50
WRKY59
WRKY45
WRKY71
WRKY15
WRKY33
WRKY3
WRKY26
WRKY46
WRKY7
WRKY21
WRKY17
WRKY65
'ABA-independent'
ABA-dependent
q.value
1e-10
1e-08
1e-06
1e-04
5e-02
Fold Enrichment
1
2
PCC
0
0.5
1
bits
WRKY20
WRKY47
WRKY28
WRKY43
WRKY75 [RC]
WRKY8
WRKY22
WRKY29 [RC]
WRKY40
WRKY50
WRKY59 [RC]
WRKY45 [RC]
WRKY71 [RC]
WRKY15 [RC]
WRKY33 [RC]
WRKY26
WRKY3 [RC]
WRKY46
WRKY7 [RC]
WRKY17 [RC]
WRKY21
WRKY65

Appendix Figure 3.1 Known motif enrichment analysis of 'ABA-independent' and ABA-dependent genes defined by previous method. (A-G) Motif enrichment results of different transcription factor families involved in osmotic stress. Each panel contains three plots. A dot plot indicated the enrichment of motif for specific TF listed on the left side. A heatmap presented the PCC (Pearson Correlation Coefficient) matrix showing the similarity between the enriched motifs. A sequence logo plot depicted the binding sites of the TFs listed on the right. The TFs in all three plots were arranged in the same order based on their similarity shown in the heatmap. **(A)** bZIP **(B)** DREB **(C)** CBF **(D)** MYB **(E)** NAC **(F)** ERF **(G)** WRKY

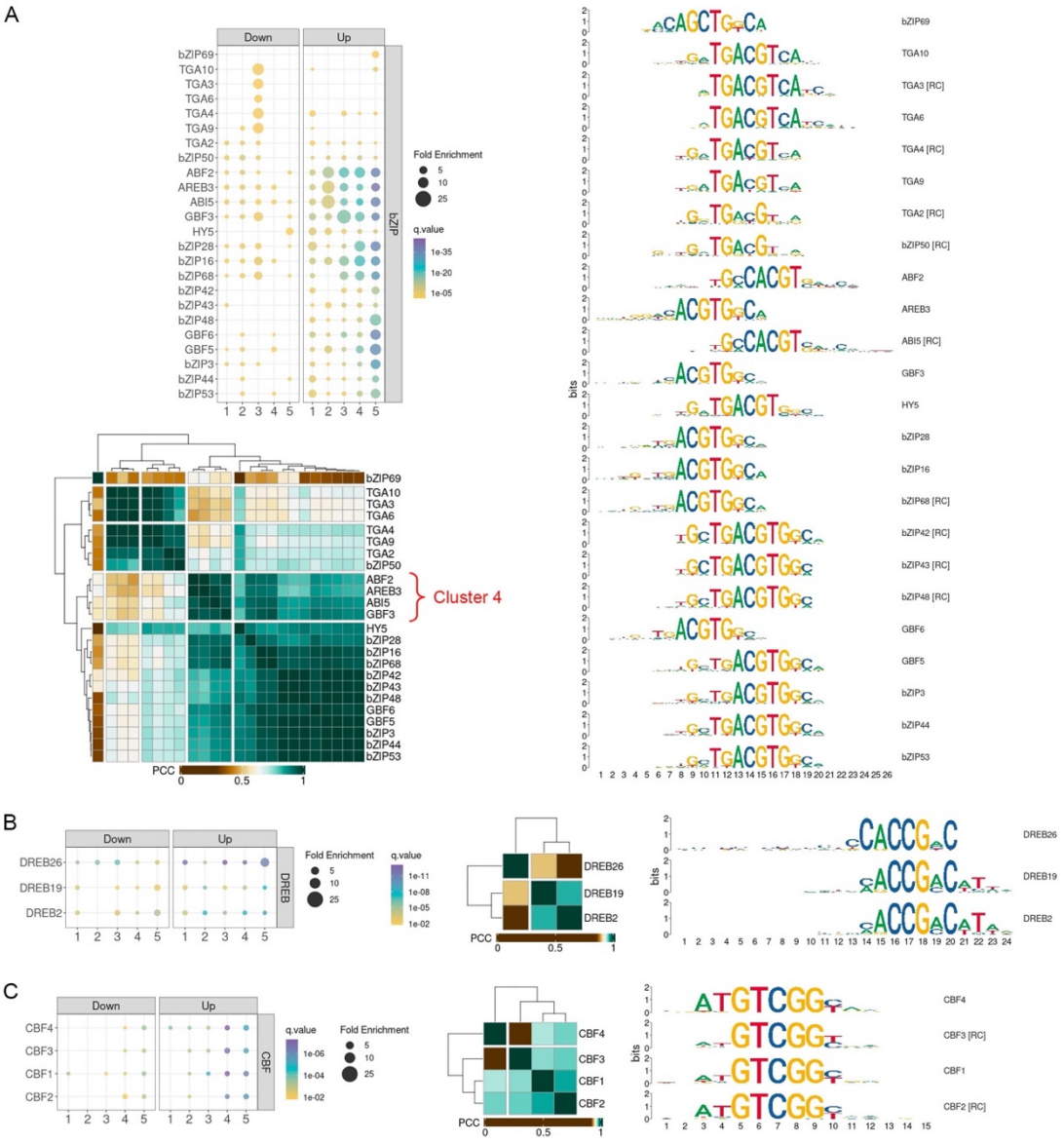
A
Down
Up
bZIP69
TGA10
TGA3
TGA6
TGA4
TGA9
TGA2
bZIP50
ABF2
AREB3
ABI5
GBF3
HY5
bZIP28
bZIP16
bZIP68
bZIP42
bZIP43
bZIP48
GBF6
GBF5
bZIP3
bZIP44
bZIP53
bZIP
Fold Enrichment
5
10
25
q.value
1e-35
1e-20
1e-05
Cluster 4
PCC
0
0.5
1
bits
TGA3 [RC]
TGA6
TGA4 [RC]
TGA9
TGA2 [RC]
bZIP50 [RC]
ABF2
AREB3
ABI5 [RC]
GBF3
HY5
bZIP28
bZIP16
bZIP68 [RC]
bZIP42 [RC]
bZIP43 [RC]
bZIP48 [RC]
GBF6
GBF5
bZIP3
bZIP44
bZIP53
B
DREB26
DREB19
DREB2
DREB
1e-11
1e-08
1e-05
1e-02
C
CBF4
CBF3
CBF1
CBF2
CBF
1e-06
1e-04
1e-02
CBF3 [RC]
CBF1
CBF2 [RC]

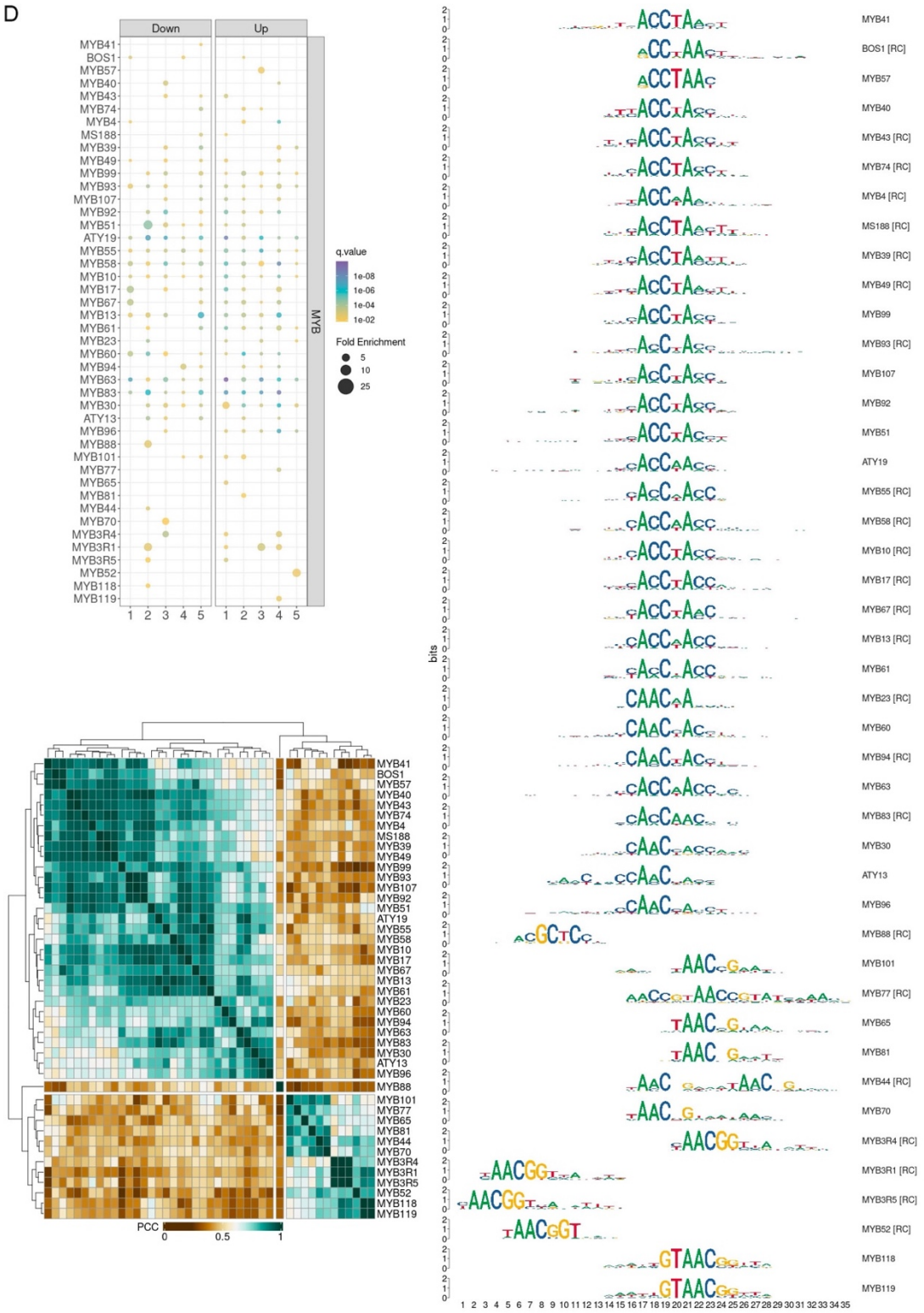
D
Down
Up
MYB41
BOS1
MYB57
MYB40
MYB43
MYB74
MYB4
MS188
MYB39
MYB49
MYB99
MYB93
MYB107
MYB92
MYB51
ATY19
MYB55
MYB58
MYB10
MYB17
MYB67
MYB13
MYB61
MYB23
MYB60
MYB94
MYB63
MYB83
MYB30
ATY13
MYB96
MYB88
MYB101
MYB77
MYB65
MYB81
MYB44
MYB70
MYB3R4
MYB3R1
MYB3R5
MYB52
MYB118
MYB119
MYB
q.value
1e-08
1e-06
1e-04
1e-02
Fold Enrichment
5
10
25
1 2 3 4 5
PCC
0
0.5
1
bits
MYB41
BOS1 [RC]
MYB57
MYB40
MYB43 [RC]
MYB74 [RC]
MYB4 [RC]
MS188 [RC]
MYB39 [RC]
MYB49 [RC]
MYB99
MYB93 [RC]
MYB107
MYB92
MYB51
ATY19
MYB55 [RC]
MYB58 [RC]
MYB10 [RC]
MYB17 [RC]
MYB67 [RC]
MYB13 [RC]
MYB61
MYB23 [RC]
MYB60
MYB94 [RC]
MYB63
MYB83 [RC]
MYB30
ATY13
MYB96
MYB88 [RC]
MYB101
MYB77 [RC]
MYB65
MYB81
MYB44 [RC]
MYB70
MYB3R4 [RC]
MYB3R1 [RC]
MYB3R5 [RC]
MYB52 [RC]
MYB118
MYB119
1 2 3 4 5 6 7 8 9 10 11 12 13 14 15 16 17 18 19 20 21 22 23 24 25 26 27 28 29 30 31 32 33 34 35

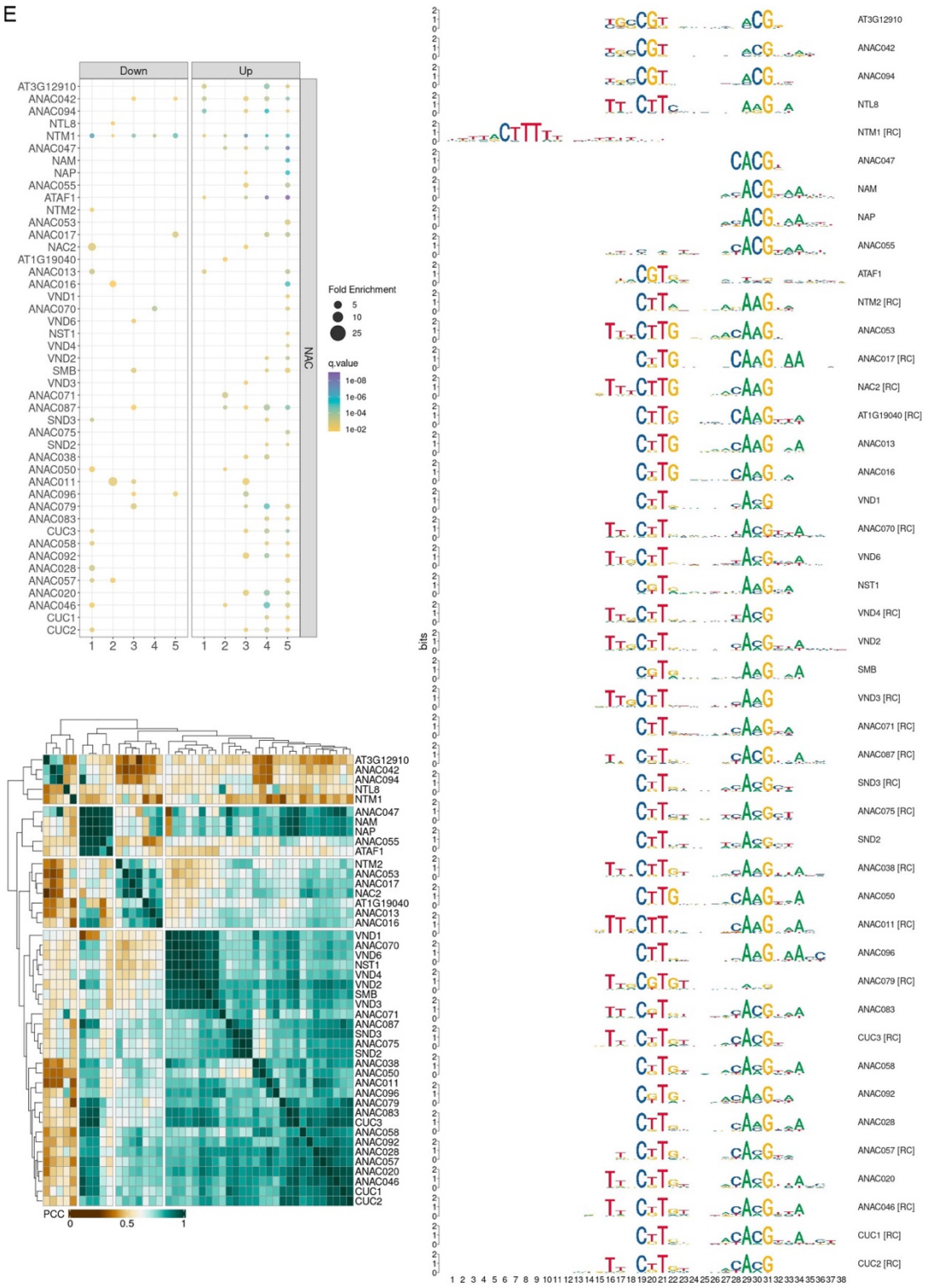
E
Down
Up
NAC
Fold Enrichment
5
10
25
q.value
1e-08
1e-06
1e-04
1e-02
PCC
0
0.5
1
bits

F

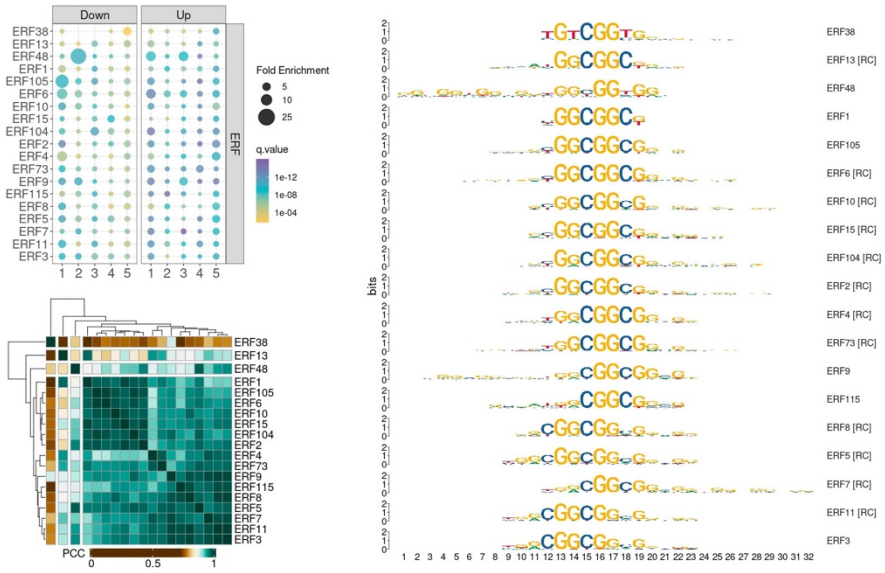
Down
Up
ERF
Fold Enrichment
5
10
25
q.value
1e-12
1e-08
1e-04
ERF38
ERF13
ERF48
ERF1
ERF105
ERF6
ERF10
ERF15
ERF104
ERF2
ERF4
ERF73
ERF9
ERF115
ERF8
ERF5
ERF7
ERF11
ERF3
PCC
0
0.5
1
bits
ERF38
ERF13 [RC]
ERF48
ERF1
ERF105
ERF6 [RC]
ERF10 [RC]
ERF15 [RC]
ERF104 [RC]
ERF2 [RC]
ERF4 [RC]
ERF73 [RC]
ERF9
ERF115
ERF8 [RC]
ERF5 [RC]
ERF7 [RC]
ERF11 [RC]
ERF3

G

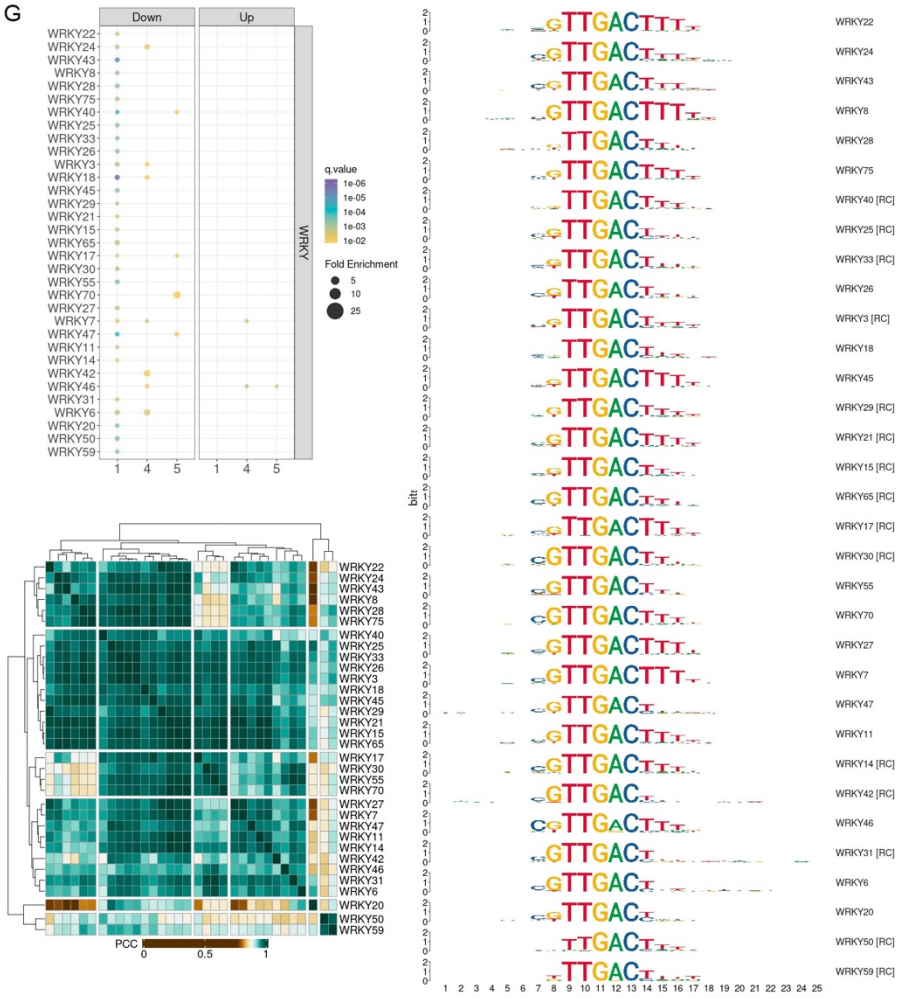
Down
Up
WRKY
q.value
1e-06
1e-05
1e-04
1e-03
1e-02
Fold Enrichment
5
10
25
WRKY22
WRKY24
WRKY43
WRKY8
WRKY28
WRKY75
WRKY40
WRKY25
WRKY33
WRKY26
WRKY3
WRKY18
WRKY45
WRKY29
WRKY21
WRKY15
WRKY65
WRKY17
WRKY30
WRKY55
WRKY70
WRKY27
WRKY7
WRKY47
WRKY11
WRKY14
WRKY42
WRKY46
WRKY31
WRKY6
WRKY20
WRKY50
WRKY59
PCC
0
0.5
1
bits
WRKY22
WRKY24
WRKY43
WRKY8
WRKY28
WRKY75
WRKY40 [RC]
WRKY25 [RC]
WRKY33 [RC]
WRKY26
WRKY3 [RC]
WRKY18
WRKY45
WRKY29 [RC]
WRKY21 [RC]
WRKY15 [RC]
WRKY65 [RC]
WRKY17 [RC]
WRKY30 [RC]
WRKY55
WRKY70
WRKY27
WRKY7
WRKY47
WRKY11
WRKY14 [RC]
WRKY42 [RC]
WRKY46
WRKY31 [RC]
WRKY6
WRKY20
WRKY50 [RC]
WRKY59 [RC]

Appendix Figure 3.2 Known motif enrichment analysis of different clusters of osmotic-stress responders (A-G) Motif enrichment results of different transcription factor families involved in osmotic stress. Each panel contains three plots. A dot plot indicated the enrichment of motif for specific TF listed on the left side. A heatmap presented the PCC (Pearson Correlation Coefficient) matrix showing the similarity between the enriched motifs. A sequence logo plot depicted the binding sites of the TFs listed on the right. The TFs in all three plots were arranged in the same order based on their similarity shown in the heatmap. **(A)** bZIP **(B)** DREB **(C)** CBF **(D)** MYB **(E)** NAC **(F)** ERF **(G)** WRKY